UNIVERSITY of CALIFORNIA

Santa Barbara

The Structure and Reactivity of Size-selected V_xO_y Clusters on the TiO_2 (110)-(1x1) Surface of Varying Oxidation State

A Dissertation submitted in partial satisfaction of the

requirements for the degree

Doctor of Philosophy

in

Chemistry

by

Joshua Woodbridge Buffon

Committee in charge:

Professor Steven Buratto, Chair
Professor Michael Bowers
Professor Horia Metiu
Professor Ram Seshadri

June 2017

The dissertation of Joshua Woodbridge Buffon is approved.

Professor Michael Bowers

Professor Horia Metiu

Professor Ram Seshadri

Professor Steven Buratto, Committee Chair

May 2017

The Structure and Reactivity of Size-selected V_xO_y Clusters on the TiO_2 (110)-(1x1) Surface of Varying Oxidation State

by

Joshua Woodbridge Buffon

Curriculum Vitæ

Joshua Woodbridge Buffon

Education

2012–2017	Ph.D. in Chemistry, University of California, Santa Barbara, CA, USA.
2008–2012	B.S. in Chemical Engineering, University of Nebraska Lincoln, Lincoln, NE, USA.

Publications and Presentations

5. **Joshua W. Buffon,** Jeremy C. Robins, Hunter L. Neilson, Horia Metiu, Michael T. Bowers and Steven K. Buratto, "The diverse catalytic reactions of methanol by size selected V_xO_y clusters on a TiO_2(110) surface," *in preparation*.

4. Jeremy C. Robins, Hunter L. Nielson, Xiao Tong, **Joshua W. Buffon**, Scott P. Price, Horia Metiu, Michael T. Bowers and Steven K. Buratto, "On the Role of Ti Interstitials in the Oxidative Dehydrogenation and Deoxygenation of Methanol on TiO_2 (110)-(1 x 1)," *in preparation*.

3. Xiao Tong, Scott P. Price, Jeremy C. Robins, **Joshua W. Buffon**, Claron Ridge, Hyun You Kim, Paul Kemper, Horia Metiu, Michael T. Bowers, and

Steven K. Buratto,"VO-Stabilized H_2O Adsorption on a TiO_2 (110) Surface at Room Temperature," *in preparation- Journal of Physical Chemistry C*.

2. **Joshua W. Buffon,** Jeremy C. Robins, Hunter L. Nielson, and Steven K. Buratto, "Size-selected vanadium oxide clusters on TiO_2(110)-(11) and their role in oxidative dehydrogenation of methanol: Every atom counts," *ACS National Meeting 2016, Talk; Pacifichem 2015 Conference, Poster.*.

1. Scott P. Price, Xiao Tong, Claron Ridge, Hunter L. Neilson, **Joshua W. Buffon**, Jeremy Robins, Horia Metiu, Michael T. Bowers, and Steven K. Buratto. "Catalytic Oxidation of Methanol to Formaldehyde by Mass-Selected Vanadium Oxide Clusters Supported on a TiO_2 (110) Surface," *The Journal of Physical Chemistry A,* **2014**, *114* (37), 8309-8313 [**doi**]

Awards and Honors

2014–2015	Partnership in Research & Education on Electron Chemistry & Catalysis at Interfaces *fellowship recipient*
2013	Outstanding Teaching Assistant Award, University of California Santa Barbara
2013	Phi Lambda Upsilon Award - National Honorary Chemical Society

Abstract

The Structure and Reactivity of Size-selected V_xO_y Clusters on the TiO_2 (110)-(1x1) Surface of Varying Oxidation State

by

Joshua Woodbridge Buffon

The study of the oxidative dehydrogenation of methanol to formaldehyde by vanadia/TiO_2 model catalysts has received a great deal of interest by the scientific community in recent years. However, due to the wide variety of catalyst preparation methods, there have been conflicting reports with formaldehyde production occurring anywhere from room temperature to 660 K. This is further complicated by the fact that the methods used often couple the oxidation state of the TiO_2 support to that of the vanadia, creating many structures on the surface with uncertain stoichiometries.

In order to overcome these challenges, we have studied the oxidation chemistry of mass-selected V_x and V_xO_y clusters deposited on TiO_2 (110) surfaces as a function of size and composition of the cluster as well as the oxidation state of the support. The cluster-decorated surface was characterized by scanning tun-

neling microscopy (STM) to determine the structure of the active catalyst and the chemistry was probed using temperature-programmed reaction (TPR). Density functional theory (DFT) was used to calculate the structure of the clusters on the surface and compared with experimental results.

We have shown that both V_2O_6 and V_3O_9 clusters are highly active in the oxidative dehydrogenation of methanol. V_2O_6 clusters catalyze the production of formaldehyde and methyl formate, the latter representing a previously undiscovered reaction path in the reaction of methanol and oxygen on supported-vanadia catalysts. Structural models from DFT and STM images have allowed us insight into the mechanism of this reaction. The models indicate that on a stoichiometric surface, the V_2O_6 cluster contains a peroxyl group that is active for the production of methyl formate.

TPR has revealed that the production of methyl formate is highly dependent on the oxidation state of the surface. For the case of V_2O_6 clusters on the reduced surface, only formaldehyde production is observed. STM results also show a variation in the cluster structure as a function of the oxidation state of the TiO_2, with the clusters on the reduced surface containing only vanadyl oxygen atoms due to the interaction with surface oxygen vacancies to dissociate the peroxyl group. The vanadyl oxygen has been previously shown to be active for production of formaldehyde by examining post-oxidized size selected VO

clusters. In addition, we show that oxidative dehydrogenation of methanol on V_3O_9-decorated TiO_2 surfaces results in methyl formate production at a lower temperature, and formaldehyde production with a significant increase in signal over that observed for V_2O_6 clusters.

Contents

List of Figures

List of Tables

Chapter 1

Introduction

The conversion of small molecules such as H_2O, CO_2, and CH_4 into such as H_2 and CH_3OH is of critical importance as we aim to produce energy from sustainable sources, instead of coal and oil. To do this require the use of a catalyst. As our understanding of the fundamentals of catalytic science has evolved, so has the productivity and efficiency. Going back over 100 years to the development of the of the Haber process for converting nitrogen and hydrogen into ammonia which began with an astronomically expensive osmium catalyst. This was quickly replaced with an iron catalyst supported on a variety of oxides and is still the basis for the catalysts used today to produce 450 million tons of nitrogen fertilizer. This reaction has been responsible for the four fold reduction

in land required for farming and led to the explosion in population since its widespread adoption after World War I.

Composition is not the only factor that controls the usefulness of a catalyst. Size, especially when considering nanoscale materials such as highly dispersed catalyst particles, plays an integral role on the catalytic chemistry[1, 2]. The classic example of this comes from the early work of Haruta where it was shown that small gold clusters (< 2 nm) are active for a variety of oxidation reactions[3–6] despite the fact that bulk gold is almost completely inert. Even a small increase in the cluster size causes a dramatic shift in the reactivity from producing propylene oxide with over 90% selectivity to only producing propane. While the nature of this reactivity is still an area of active exploration, most results indicate that the unique electronic structure and large number of under coordinated sites on the gold nanoparticle are the primary causes[6].

This has led to a wealth of studies designed to gain even finer control over particle size and to discover the reaction mechanisms at work at an atomistic level. The majority of these studies, including this one, aim to create size-selected model catalysts under ultra-high vacuum (UHV) conditions. In this approach, model catalysts are typically planar, well-characterized, single crystalline supports decorated with a single cluster species where all clusters have the same number of atoms. The effectiveness of these studies can be seen from

the initial work of Heiz and Landman who showed that for CO oxidation on MgO significant reactivity starts with Au_8 and peaks for Au_{18} clusters[7]. This same group has also found that for TiO_2 , Au_6 and Au_7 are the only active species for CO oxidation[8]. The reactivity trends with size are not always monotonic as Anderson *et al.* observed CO oxidation activity for Au and Pd on TiO_2 oscillates as atoms are added[9, 10]. These experiments showed that there is a direct relationship between electronic structure as observed by X-ray photoelectron spectroscopy (XPS) and the reactivity. These studies, and many more show that this method of model catalyst study is not only robust and versatile, but most importantly it provides unprecedented insight into the nature of chemistry taking place.

For our experiments we have chosen rutile TiO_2 (110)-(1x1) which has a well known, but still evolving, understanding of its surface chemistry and is used frequently in industrial catalysis settings. The apparatus used here, described in detail in Chapter 2, has the ability to prepare size selected metal or metal oxide nanoparticles of up to $\approx$ 30 atoms, perform catalytic investigations by temperature programmed desorption (TPD), and directly image the clusters on the surface by scanning tunneling microscopy (STM). The method also allows the support oxide to be prepared with a variety of oxidation states in a manner decoupled from that of the deposited catalyst. This is a concern often overlooked

in practical catalyst applications, but as this thesis will demonstrate, the nature of the support plays a critical role in controlling the activity.

Metal-oxide supported vanadia, the primary focus of these investigations, is one of the most studied transition metals in the catalysis literature and has been utilized in a wide range of industrial applications including the oxidation of SO_2 to SO_3, conversion of aromatic molecules to anhydrides, and reduction of NO_x by NH_3 [11]. This incredible versatility is attributed to the large variety of structures, both geometric and electronic, that have been observed for vanadia. It is therefore important to determine which of these structures are the most active for each reaction so that even more efficient and selective catalysts can be discovered and used industrially in the future. Clusters with a single vanadium atom have previously been explored by this apparatus [12, 12]; this work expands that to even larger clusters with two and three vanadium atoms.

$$\mathrm{CH_3OH} + \frac{1}{2}\,\mathrm{O_2} \longrightarrow \mathrm{CH_2O} + \mathrm{H_2O} \tag{1.1}$$

The oxidative dehydrogenation of methanol to formaldehyde, reaction shown above, is one of the most straight forward model reactions know to be catalyzed by bulk vanadia, gas-pahse vanadia clusters, and TiO_2 supported vanadia[13–15]. In the gas phase, this reaction is $150\ kJ/mol$ downhill and has

an activation barrier of $420\ kJ/mol$ without a catalyst [16, 17]. Typical vanadium oxide and molybdenum oxide catalysts reduce this barrier to between 65 and $85\ kJ/mol$ [14, 18]. Some of the first work on the subject by Deo and Wachs revealed that the choice of support has a major impact on the activity of the supported catalyst [19]. In these experiments monolayer and submonolayer coverages of vanadia were prepared by impregnating high surface area supports with a vanadium triiospropoxide precursor and calcination at 723 K. A common metric for catalytic activity the turnover frequency (TOF) is defined as the number of reactions occurring per catalytic site per unit time (typically seconds). Zirconia and titania supported vanadia demonstrated a TOF three orders of magnitude greater than for a silica support. Raman and IR spectroscopy revealed that the strength V−O−M bond, where M is the metal support atom, and thus the ease of reducibility of the vanadium atom was strongly correlated with activity.

It has been well established that the first mechanistic step is the dissociative adsorption of methanol to the vanadium atom to form a methoxy and a surface hydroxyl[11, 20, 21]. The next step of the mechanism and the site active for catalysis is somewhat controversial and many competing arguments have been put forward in the last few years and a summary of these results can be found in Table 1.1. The specific details of these mechanisms can be found in Chapter 4.

The general trend is that the most oxidized (V^{+5}) clusters are typically active in the monolayer to submonolayer regime, for this reason the industrial vanadia-titania catalysts are presumed to be bulk like V_2O_5.

Author	**Preparation Method**	**Techniques**	**Active Species**	**T_{max}**
Madix[22] (2002)	VO_3 hydrolysis	XPS, TPD	1.0/0.6 monolayer V^{5+}, deactivated to V^{3+}/V^{4+}	517/ 551 K
Vohs[23] (2001)	Vanadium evaporation, oxidized with $P(O_2) = 1 \times 10^{-6}$ Torr at 500 K	HREELS, TPD	1 monolayer V^{3+} presumed V_2O_3, multilayers inactive	660 K
Vohs[24] (2003)	Reactive evaporation, oxidized with $P(O_2) = 1 \times 10^{-3}$ Torr at 400 K	XPS, TPD	1 monolayer V^{5+} presumed V_2O_5	485 K
Netzer[25] (2004)	Post oxidation 2×10^{-7} mbar @ 473K and Reactive evaporation 1×10^{-8} mbar at 473 K	STM, LEED	Variety of morphologies, reactive evaporation creates a more ordered surface	-
Metiu[26] (2009)	Theory	DFT	VO_3 is most active of VO_x clusters	-
Granozzi [27] (2013)	Reactive evaporation 5×10^{-8} mbar at 300 K	STM, XPS, AR-PD, TPD, DFT	V_4O_6 is the only structure observed	300 K
Price[28] (2014)	Size selected V and VO_x clusters, post oxidized 2×10^{-6} Torr at 540 K	STM, TPD	VO_3	590 K
Bao[29] (2015)	Wet impregnation of anatase TiO_2 with NH_4VO_3	^{51}V NMR, microreactor	VO_3 and V_2O_x with a two oxygen bridge between V atoms	553 K*

Table 1.1. Literature summary of results for the oxidative dehydrogenation of methanol by vanadia on TiO_2 , where T_{max} is the temperature at which maximum formaldehyde desorption occurs from TPD experiments. *Active temperature in a fixed bed catalytic reactor.

Chapter 2

The Size-Selected Cluster Source Apparatus

The experiments detailed here were all conducted on a single-crystal rutile TiO_2 (110)-(1 x 1) sample in a chamber maintained at a base pressure below 3×10^{-10} Torr inside a home-built ultra-high vacuum (UHV) apparatus shown in Figure 2.1. The primary function of this instrument is to create and mass select small (1-20 atoms) metal or metal oxide clusters in the gas phase to be deposited on the TiO_2 for analysis of their catalytic properties. The apparatus is constructed of a series of custom UHV compatible steel chambers which in order of decreasing base pressure are: the source chamber, diffusion pump cham-

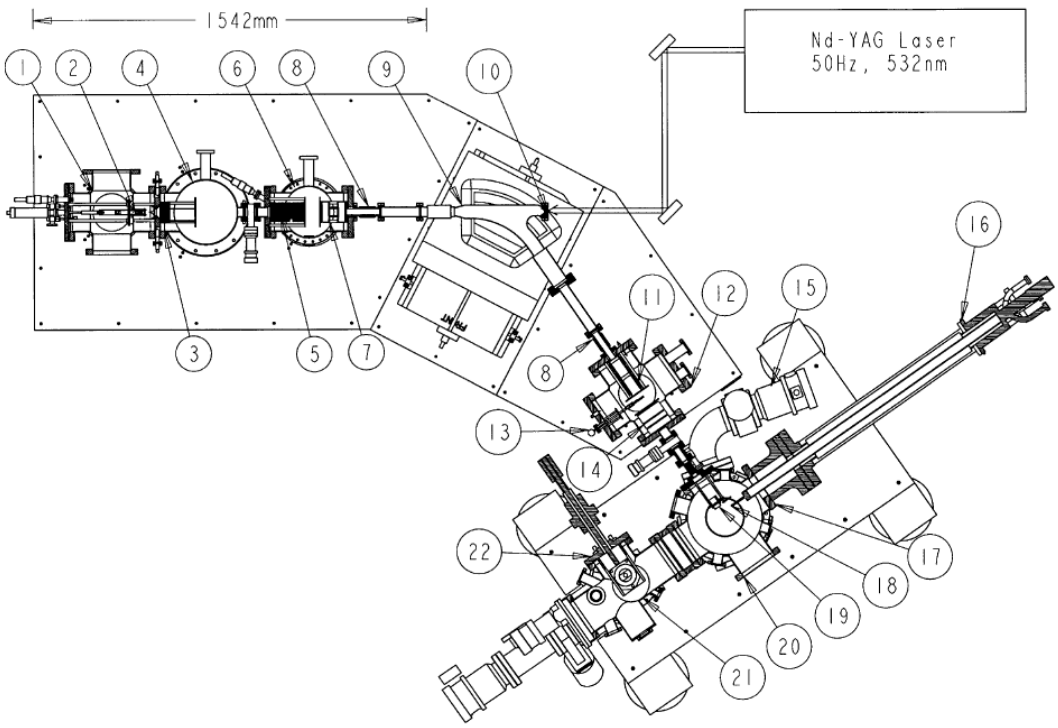

Figure 2.1. Overall view of instrument (drawn to scale). The absolute dimension of the laser vaporization source and associated pumping/expansion region is indicated: (1) source chamber; (2) cluster source (see Fig. 2); (3) first einzel/steering lens; (4) diffusion pump chamber; (5) second einzel/steering lens; (6) acceleration chamber; (7) acceleration/focus lens (see Fig. 3); (8) ceramic break; (9) magnet flight tube; (10) laser entrance window; (11) deceleration/y focus lens; (12) deceleration/collector chamber; (13) moveable detector; (14) z focus/steering lens; (15) turbo pump; (16) cryo-manipulator; (17) deposition and analysis chamber; (18) sample holder stage; (19) final focus lens; (20) Auger electron spectrometer; (21) STM chamber; (22) scanning tunneling microscope. Reproduced from [30]

ber, acceleration chamber, deceleration/collector chamber, UHV deposition and analysis chamber, and the STM chamber. [30]

To maintain the desired pressure these chambers must be continuously pumped by a three backing pumps, six turbomolecular pumps, and two ion pumps as detailed in Table 2.1. During cluster creation, the pressure in the source chamber can routinely reach 10^{-2} Torr and drops by over 8 decades over the cluster beam path to maintain a pressure of 5×10^{-10} Torr in the deposition chamber. To fully remove gases adsorbed to the walls of the chambers and reach the ultimate base pressure, the instrument must be baked-out periodically by wrapping heating tape along the exterior walls, insulating the entire chamber with aluminium foil, and heating to 200°C for 24 - 48 hours. Maintaining this low base pressure is important for two primary reasons: to keep the TiO_2 surface free from adsorbates during an experiment and to preserve the composition of the clusters in the gas phase.

$$F = \frac{P}{\sqrt{2\pi m k T}} \tag{2.1}$$

The flux of gas molecules incident on a surface (F) is given by Equation 2.1 where P is the pressure, m is the mass of the gas molecule, k is the Boltzmann constant, and T is the temperature. This gives 3×10^{23} $\frac{collisions}{cm^2 s}$ for atmospheric

Chamber	Pump Type	Backing Pump	Base Pressure (Torr)
Source	Osaka TS440 440 L/s helical grooved pump	Edwards E2M40 44 m^3/hr rotary pump	2×10^{-7}
Diffusion Pump	Edwards 250M 2400 L/s diffusion pump	Edwards E2M40	4×10^{-9}
Acceleration	Osaka TG1133 1100 L/s turbomolecular pump	Edwards E2M40	1×10^{-9}
Collector	Osaka TG413 430 L/s turbomolecular pump	Edwards E2M40	1×10^{-9}
Deposition & STM	Osaka TH261 235 L/s turbomolecular pump & Varian Valcon 300 L/s ion pump	Edwards E2M28 36 m^3/hr rotary pump	3×10^{-10} (Dep.) 5×10^{-11} (STM)

Table 2.1. Pumping and base pressure summary

conditions of 300 K, 760 Torr, and pure nitrogen gas. The crystalline sample has an exposed surface area of about 0.5 cm^2 corresponding to approximately 2.56×10^{14} binding sites available. This means that under atmospheric exposure the sample becomes covered in adsorbates in about 1 nanosecond. However, with a pressure of 3×10^{-10} the surface will reach saturation coverage on the order of 10^4 seconds, which is more than enough time to complete the desired experiments.

$$\lambda = \frac{kT}{\sigma P \sqrt{2}} \tag{2.2}$$

To ensure that clusters in the beam do not interact with other gas molecules we must consider the mean free path of a gas, given by Equation 2.2, where λ is the mean free path (the average distance traveled by a molecule before

collision) and σ is the collision cross-section of the molecule. During operation of the cluster source, the pressure in the acceleration chamber just before mass selection is regularly on the order of 10^{-6} Torr. Performing an approximate calculation with pure argon gas at this pressure gives a mean free path of about 20 m, ten times the length of the beam path, which is sufficient to be certain that the vast majority of clusters are not altered before being deposited on the sample. Knowing this, it is also clear that gases of interest on the sample surface can reach the mass spectrometer only a few centimeters away without interaction as well.

2.1 The cluster source

The cluster source used in these experiments is based on the Smalley type laser ablation source and only the most relevant details will be given here. Further details on the principles on which this cluster source is based can be found in the following references: [31–35]. The target used here is a 2.0 mm diameter vanadium wire (99.5%, Alfa Aesar) which is cut to 50 mm length and sanded to remove the oxide coating. The rod is mounted vertically in a "waiting room" ($\sim$1 cm^3), also known as the source body as listed in the schematic in Figure 2.2. The rod moves up and down while rotating at 30 rpm and completes its

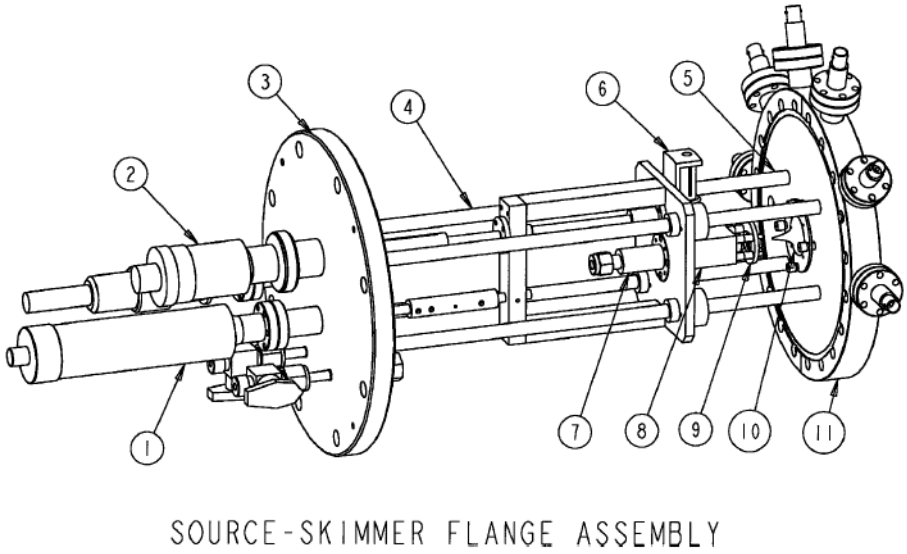

Figure 2.2. Ion source: (1) sample drive rotary motion feed through; (2) source linear position feed through; (3) ISO160 source mounting flange (all source connections are made here); (4) source linear position guide rods; (5) source locating posts (on skimmer flange); (6) rotation/translation mechanism; (7) pulsed valve; (8) source body; (9) focusing lens; (10) skimmer; (11) skimmer flange.

25 cm path in 5 minutes. In principle and in practice, nearly any metal rod can be used to generate clusters with this setup, such as the iron clusters that will be the next section. Immediately behind the rod is the gas pulse valve (General Valve, Series 9) which fills the waiting room to a pressure of about 1 Torr with argon for making metal clusters, and an argon/oxygen mixture for creating metal oxide clusters. The valve open duration, the delay between the gas and laser pulses, and the concentration of oxygen in the mixture (typically 20-30%) are critical parameters to optimize ion creation. The pulse delay time is the most sensitive adjustable parameter, a change of less than 5% can result in an order

of magnitude change in the ion current.

A frequency doubled Nd-YAG laser laser (Spectra Physics, Lab Pro 290) that emits 532 nm light with 500 mJ/pulse at 55 Hz is used with a beam splitter installed at the exit of the laser to modify the power incident on the rod, this is a critical adjustment. The beam is focused by a 1500 mm plano-convex lens to less than a 0.5 mm spot size on the rod. After the laser pulse, the hot ionized plasma expands into the source chamber, with the gas from the pulse valve, through a conical nozzle with variable orifice size and length. Typical nozzle dimensions are 1.5×20 mm, are only modified when working with other metals.

The whole of the source body-nozzle assembly is biased at ~ 500 V relative to chamber ground to extract only the positive ions. Just past the nozzle is the first in the series of ion control optics, the focus lens, it is biased -10 to -20 V below the source body, both voltages are critical adjustments. The beam is then confined by a grounded 3.0 mm skimmer before entering the diffusion pump chamber. A BNC lead connected to the skimmer allows for the first detection of the ion source intensity which is measured as a current of colliding cluster ions by an electrometer (Keithly 6517A) with sensitivity down to the pA scale.

Immediately following the skimmer is the diffusion pump chamber, the first stage in the differential pumping setup. The pressure drop between these two

chambers can be has high a 4 decades with pressures in the source chamber approaching 1×10^{-2} Torr. This chamber also contains the first einzel steering lens to further confine the ion beam which expands slightly over time due to coulombic repulsion.

2.2 Mass selection

Another set of ion optics further confine and steer the ion beam prior to mass selection. At this point, the optic system breaks from cylindrical symmetry to allow steering through the curved flight path that performs mass selection. The optics also serve to further accelerate the ions, increasing the mass resolution to allow for selection of clusters that differ by only one oxygen atom. This mass selection utilizes a VG-Micromass ZAB-2F variable field electromagnet to exert a force on the fast moving clusters according to Equation 2.3, where q is the charge, v is the velocity, and B is the applied magnetic field. The force causes the cluster to travel a circular path with radius r according to equation 2.4, where m is the mass of the cluster, that allows it to pass through the $42°$ curved flight path section. To calibrate the mass scale we must know all of the parameters in Equation 2.4. To determine the mass we use the following values: The radius is fixed and based on the geometry of the instrument, the charge of

the clusters has been shown previously to be +1, the velocity is assumed to be the sum of the source and acceleration voltages ($\sim$ 1200 V), and the field is measured by a hand held probe.

$$F = qvB \tag{2.3}$$

$$r = \frac{mv}{qB} \tag{2.4}$$

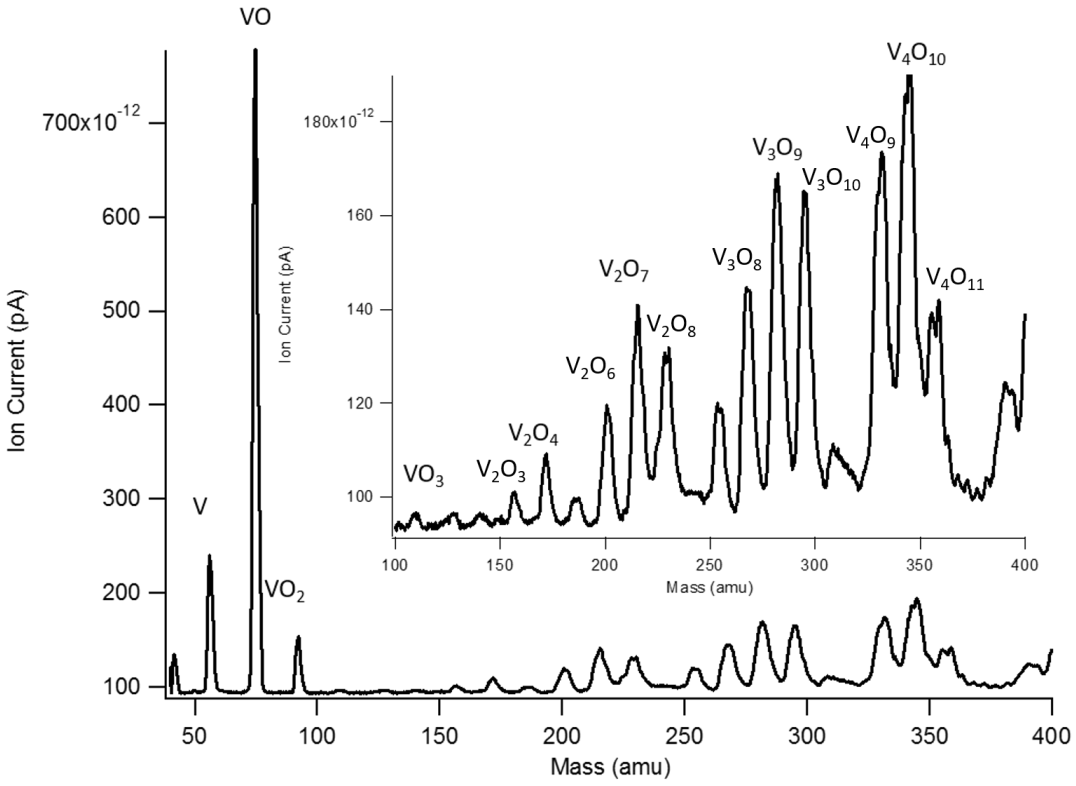

Figure 2.3. A mass spectrum of V_xO_y clusters created with 30% O_2 in Ar. The inset shows a reduced scale to more clearly show the intensity of the larger clusters.

Immediately following mass selection, another set of ion optics decelerate

and refocus the beam that now contains only one specific mass cluster. The signal of the cluster beam, in nA, is monitored by the Keithly electrometer connected to a 1 inch metal plate in the collection chamber while the magnetic field is varied to produce a mass spectrum. This detector is attached to the end of a linear translation rod with welded bellows to remove it from the beam path and allow deposition onto the sample surface. Here the ion signal can be optimized by adjusting the critical parameters listed above such as the laser power, pulse delay, extraction voltage, and ion optic steering voltages. A representative mass scan for vanadium oxide clusters is shown in Figure 2.3. This scan is optimized for VO cluster, and signal can be enhanced for the larger V_2 and V_3 clusters by modifying the steering and acceleration parameters. Approximately 100 pA of ion current is required to deposit 5% coverage on the TiO_2 sample before it becomes too contaminated by background gases, about 6 hours.

Figure 2.4 demonstrates the flexibility of this method to prepare a variety of cluster types, in this case, iron oxide. An interesting feature of this mass scan is that iron oxides are still present when pure argon gas is used. This is due to the difficulty of completely removing the oxide layer from the iron rod and the intensity of these peaks decay over time as the outermost layer of the rod is ablated away. Metal and metal oxide clusters have also been prepared by this system for aluminium, titanium, and tungsten for potential inverse catalyst

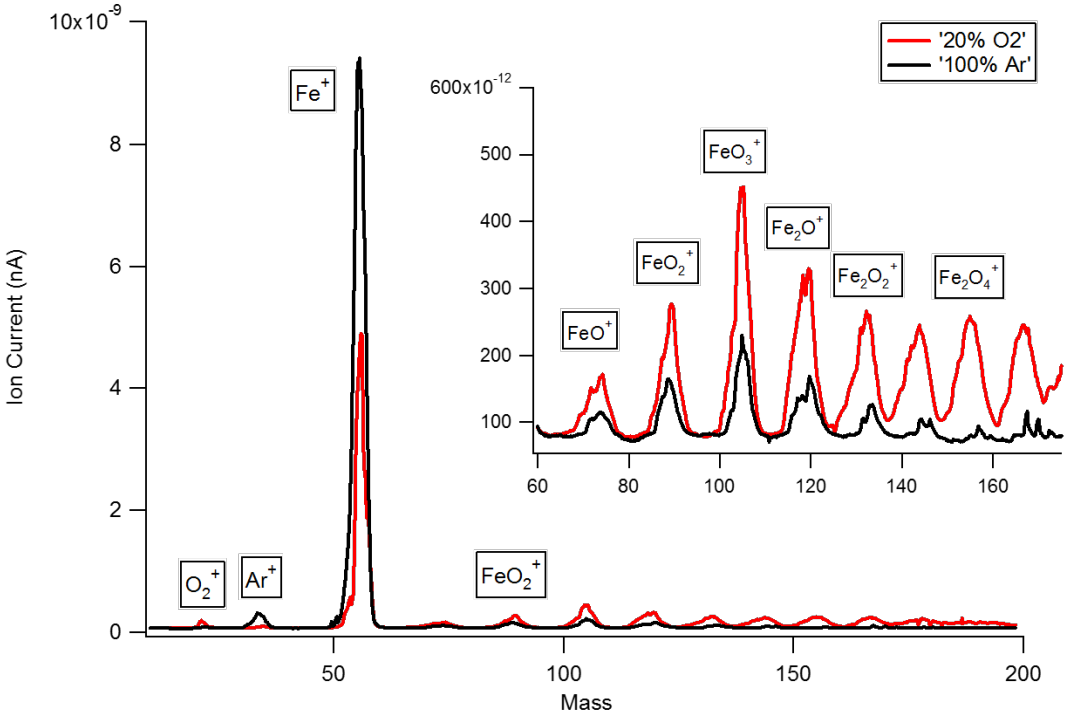

Figure 2.4. A mass scan comparison of of Fe_xO_y clusters created with 20% O_2 in Ar and pure Ar gas. The inset shows a reduced scale to more clearly show the intensity of the larger clusters.

studies on platinum that will not be discussed in this dissertation. Tungsten carbide clusters were also prepared from ethylene seeded argon gas.

Once the magnet is fixed on the cluster of interest and all relevant parameters have been optimized, a kinetic energy distribution of the clusters is measured. This is done by measuring the ion current at the detector as a function of a repelling bias applied to the detector. The repelling bias needed is proportional to the extraction voltage applied to the source body, but the various collisions each cluster undergoes upon expansion into vacuum generates a cluster beam

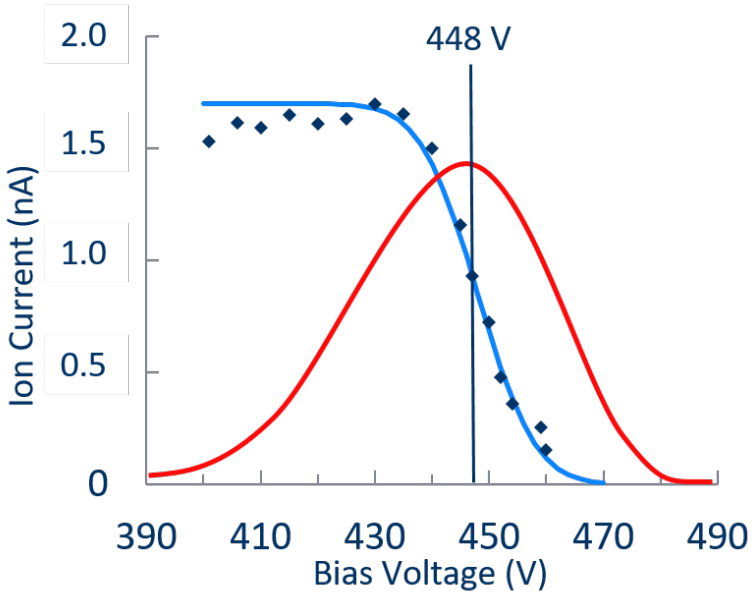

Figure 2.5. $V_2O_6^+$ ion current as a function of repelling bias applied to the moveable detector (blue diamonds), a fit with a normal distribution (blue trace), and a Gaussian distribution reflecting the fraction of clusters at each energy value (red trace).

with a Gaussian distribution around this energy. Figure 2.5 shows the kinetic energy distribution for $V_2O_6^+$ clusters as the black dots, a fit with a normal distribution in the blue trace, and a Gaussian distribution reflecting the fraction of clusters at each energy value in the red trace. Measuring this distribution is necessary as applying the repelling bias at the peak of the distribution maximizes signal while allowing soft-landing of the clusters on the TiO_2 support. Soft-landing is the regime where the average cluster lands with less energy than it would take to break the bonds in the cluster or on the surface, which are about 6.5 eV. When the bias is applied at the average cluster kinetic energy, 448 V in

this case, each atom has an energy given by $\frac{KE}{atom} = \frac{\sigma}{N\sqrt{\pi/2}}$. The standard deviation, σ, is 8 eV and the cluster has $N = 8$ atoms, gives a result of 0.8 eV/atom which is well below the V-O bond energy.

2.3 The surface science chamber

The surface science chamber houses the instrumentation for temperature programmed desorption/reaction (TPD/R) to analyze the catalytic activity of clusters on the TiO_2 surface, X-ray photoelectron spectroscopy (XPS) and Auger electron spectroscopy to observe electronic structure of the cluster decorated surface, and a 4 axis cryogenic manipulator to move the sample between techniques. This chamber is connected by a large gate valve to the STM chamber where the scanning tunneling microscope (STM) is housed. Both chambers are mounted on a 2 inch thick steel slab mounted on vibration isolating legs (Newport I200) and placed over a home-built sandbox to reduce vibrations to a level where atomic resolution can be achieved by STM.

A copper plate, known as the fork, is on the end of the manipulator where the sample holder can be securely placed and allows feed-through connections for resistively heating the sample, measuring the temperature by thermocouple, monitoring the ion current during a cluster deposition, and a cryostat for cooling

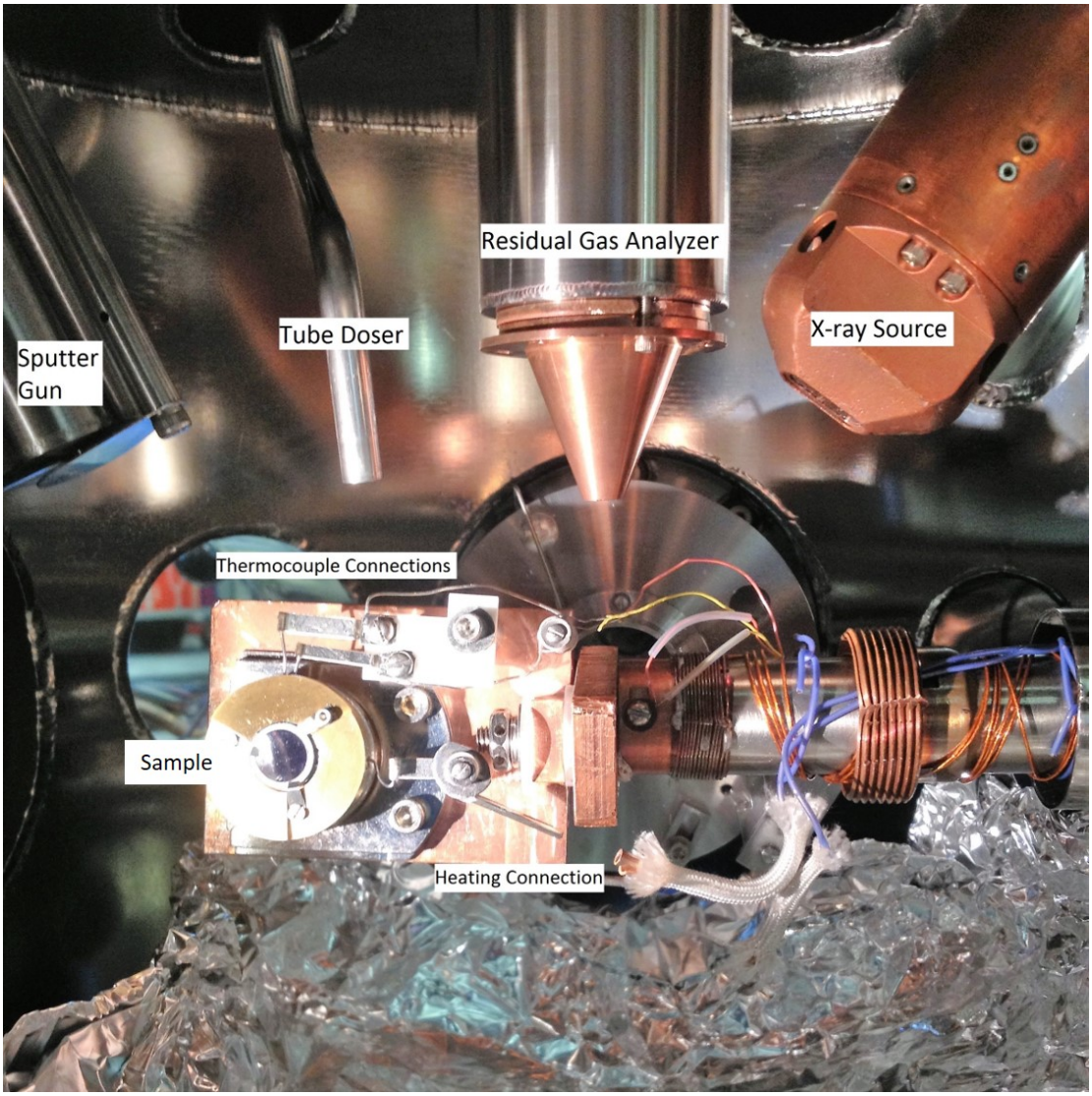

Figure 2.6. A view of the sample on the fork (rotated 90° relative to standard orientation) with relevant connections and instruments labeled. The flange through which this picture was taken is normally blocked by the XPS/AES detector.

the sample with liquid nitrogen or helium (VG Helitran 1000). The manipulator is equipped with manual micrometer motion controls for two linear directions and sample rotation. There is also a motorized control in the third lateral direction for moving the sample between analysis techniques and the ~ 60 cm to reach the STM chamber. A close up of the fork in Figure 2.6 shows the sample mounted in the sample holder, the thermocouple and heating connections, and the analysis instruments contained in this chamber. The sample holder itself is held in place by a stainless steel retaining plate that allows the sample to be slid in from the left side via the wobble stick in the STM chamber.

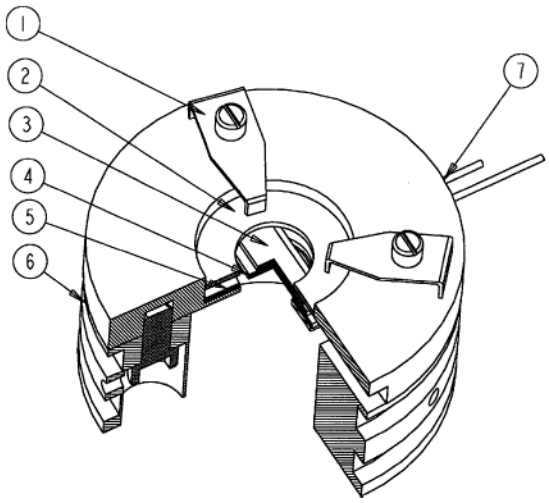

Figure 2.7. Cut away of the sample holder: (1) retainer clips; (2) sapphire washer; (3) sample substrate; (4) silicon heater; (5) sapphire washer; (6) sample holder body; (7) thermocouple connection. Reproduced from [30]

The TiO_2 sample and all necessary connections are contained in the copper

sample holder (RHK Technologies) as seen in the schematic in Figure 2.7. The view shown here is for the STM sample, but that differs from the TPD sample only in crystal dimensions. The STM sample ($10 \times 2 \times 0.5$ mm, Commercial Crystal Laboratories) and is held by a glass washer (10 mm O.D.; 6 mm I.D.; 0.5 mm thick; Mindrum Precision), while the TPD sample is a disk sample (10 mm diameter; 1.0 mm thick; Princeton Scientific) held in place by a sapphire washer (10 mm O.D.; 9 mm I.D.; 0.25 mm thick; Mindrum Precision). Both types of crystals are prepared by the manufacturer with extensive grinding and electro-polishing steps which produce a surface that is extremely flat, less than 0.1° slope, and with a surface roughness less than 10 Å, which is required for study by STM. The washer is held down by steel retaining clips mounted around the ramps that allow the STM to approach the surface. Directly below the sample is the chromel-alumel K-type thermocouple (Omega Engineering, with matching cold-junction compensator) which is electrically isolated from the sample holder by two small ceramic spacers. Because the thermocouple is on the bottom surface of the sample, a small temperature gradient can form between top and bottom of the sample. This leads to a slight overestimation of the surface temperature while heating during TPD experiments. This effect is compensated for by calibrating the observed temperature scale to well known desorption peaks on the clean, reduced TiO_2 surface. Below the thermocouple is a sapphire washer (10

mm O.D. 0.5 mm thick; Mindrum Precision) which provides electrical isolation from the heater and the fork. The tantalum heating wire is also isolated from the sample holder by ceramic spacers and has a tantalum flap spot welded to the end to make contact with the silicon resistive heater ($\sim 5\Omega$). When supplied with the feedthrough maximum of 5 A, the sample reaches a temperature between 900 and 1000 K depending on the specific resistance of the silicon. Finally, the tantalum flap on the bottom sapphire washer ensures connection to the sample holder on the opposite end of the silicon from the heating wire to complete the circuit.

2.3.1 Sample cleaning and preparation

Prior to conducting experiments, the as-received TiO_2 samples must be cleaned with multiple cycles of argon ion sputtering and vacuum annealing to create a flat well-ordered surface. When a new crystal is installed or repairs of the sample holder connections are required the sample must first be degased to remove adsorbates from exposure to the ambient pressure. For the degas procedure, the sample is heated overnight at 500K with the ion pump closed and only the turbo pump running. After that, the sample is annealed to 950 K repeatedly until the pressure rise in the chamber is minimal ($< 1 \times 10^{-9}$ Torr).

Once the degas procedure is complete, cycles of Ar^+ sputtering and annealing can begin. The sputter is carried out by the RBD Instruments IG2 2kV sputter gun package. In the sputtering process, high energy ions impact the sample and eject (sputter) away material from the top few atomic layers. This creates defects, such as oxygen vacancies and Ti^{3+} interstitials, which lead to an overall reduction in the crystal. As the sample becomes more reduced, its color changes from white to gray to blueish to black and its conductivity increases as a result of the accumulation of defects. To operate the sputter gun requires that the chamber is filled to a static pressure of 5×10^{-5} Torr argon. Inside the sputter gun, the gas is ionized by electron impact from the twin tungsten filament source. These ions are then accelerated up to 2kV and focused onto the TiO_2 sample. The ion current incident on the surface is measured through the thermocouple connections in the same manner as for cluster deposition. To align the required position for sputtering a piece of tantalum foil with 1000 Å tantalum oxide that reveals a strong blue color where the foil is being sputtered. Samples in this work were sputtered first with 2 kV ions at a current of 5 μA for 20 minutes until the crystal is sufficiently reduced. Once the crystal has reached a blue color and can be imaged by STM, the sputter voltage is reduced to 1 kV to allow finer control over the reduction of the sample.

After sputtering the sample is annealed twice to 850 - 950 K for 10 - 15 min-

utes depending on the desired level of reduction. This provides the energy for the rough surface generated by sputtering to rearrange into the (1 x 1) surface structure which is favorable due to its large terraces and relative flatness. Annealing also removes any gas that may have been implanted by the sputtering and allows common contaminants, such as calcium and carbon, to diffuse to the surface where they can be sputtered away in the next cleaning cycle. The majority of surface oxygen vacancies (O_v) are formed during the annealing step, which leads to further reduction of the crystal. After several (5+) cleaning cycles the surface is examined by XPS for well-defined titanium and oxygen peaks and a lack of contaminants. TPD and STM can also be used to interrogate the surface for the level of reduction and flatness.

2.3.2 Cluster deposition

Cluster deposition of the TiO_2 surface is carried out by rotating the sample 180° from its position in Figure 2.6 such that it is normal to the incoming ion beam. The detection chamber is connected to the surface science chamber via a manual gate valve to maintain pressure isolation and flexible bellows to accommodate the floating of the table by the vibration isolation legs. A final set of ion optics are used to maximized the ion signal on the sample as detected by

the thermocouple connections. The *x, y, z* position is also modified to increase the deposition current. The appropriate repelling bias, as determined on the detector used for the mass scan, is applied to the sample and cluster coverage, in monolayers, is calculated by Equation 2.5 where one monolayer is equal to one metal atom per TiO_2 unit cell, I_A is the ion current measured at the sample in Amps, t_D is the deposition time in seconds, N is the number of metal atoms in the cluster, A is the area of the surface in cm^2, s is the number of binding sites on the surface per unit area ($5.2 \times 10^{14}/cm^2$), and q is the charge of the cluster which is +1 for all clusters as determined from previous experiments. [30]

$$\Theta_{ML} = \frac{I_A \cdot t_D \cdot N}{A \cdot s \cdot q} \tag{2.5}$$

Cluster coverages between 0.05 and 0.25 ML was used for the majority of experiments in this work. During deposition, the ion current is continuously monitored and readings are taken every 30 minutes to determine the average current value of that time. Small adjustments will be to the critical parameters to compensate for the decreasing size of the rod as material is ablated away by the laser. For a typical cluster with an incident ion current of 250 pA on the sample, a coverage of 0.05 ML takes approximately 2.5 hours to complete. This system is inherently limited to clusters which have signal above 100 pA.

Clusters with lower signal, such as the elusive VO_3^+, would take an excess of 6 hours to deposit and, as the necessary current declines with decreasing rod size, this experiment is challenging to reliably complete.

2.3.3 Temperature programmed desorption

The surface science chamber also houses the primary chemical probe available in this system, temperature programmed desorption (TPD) and temperature programmed reaction (TPR). TPD is carried out by adsorbing a known quantity of a gas onto the TiO_2 surface and linearly increasing the temperature to a specified value. The gas desorbing from the surface is monitored by a mass spectrometer (SRS RGA 200) which can detect up to 10 species simultaneously as a function of the surface temperature. When only the adsorbed gas is monitored, this is referred to as TPD. If the gas undergoes a chemical reaction at the surface and the products are monitored, the technique is referred to as TPR. This method is used on the most basic level to determine if the cluster decorated surface is active for the oxidative dehydrogenation (ODH) of methanol to formaldehyde. However, it can also be used to obtain information about the reaction order and activation energy of desorbing species by varying the gas coverage and heating rate.

Each peak in the resulting plot of mass spectrometer response of a given species as a function of temperature is referred to as a desorption state. The peak area corresponds to the total amount of gas desorbing at that state which will be covered more detail below. The temperature at which the peak reaches its maximum corresponds to the maximum rate of desorption and is referred to as T_{max}. It has been shown by Redhead[36] that this value is related to activation energy of desorption by Equation 2.6 where E_a is the activation energy, R is the universal gas constant, n is the order of desorption, v is the pre-exponential factor, C is the coverage, and β is the heating rate (K s^{-1}).

$$\frac{E_a}{RT_{max}^2} = \frac{nvC^{n-1}}{\beta} Exp[\frac{-E_a}{RT_{max}}] \tag{2.6}$$

The order can be determined by the peak shape,[37] which is typically first order for most of these experiments. The pre-exponential factor is on the order of $10^8 - 10^{13}$ for this type of process, but is quite difficult to determine accurately. To determine this value one, must run several experiments at different heating rates using a constant value of cluster and gas coverage. The deposited catalysts typically become deactivated after the first TPD run so a new deposition would be needed for each heating rate. These types of experiments are time consuming, and due to the low ion current available for many clusters are often

impractical. While these experiments would be valuable, we can still determine if the catalyst is active for the chosen reaction and the selectivity can be found from the ratio of the product gas intensities.

The TPD set up used for these experiments is shown in Figure 2.8. Gas is adsorbed to the surface by the 14" stainless steel directional tube doser welded directly to a precision leak valve (MDC ULV-150). The leak valve allows control over the pressure of gas administered to the chamber down to 1×10^{-10} Torr with a range up to 1×10^{-4} Torr. The directional tube doser collimates the gas entering the chamber such that the flux on the sample placed at the opening is much higher than the pressure in the chamber. This allows for a lower overall pressure to be used and facilitates a quick return to UHV conditions prior to the TPD run.

The gases of interest are introduced to the leak valve through a gas manifold held at a base pressure of 5×10^{-6} Torr by an Osaka TG56 (50 L/s) turbomolecular pump and backed by an Edwards XSD 5 (5 m^3/s) scroll pump. The gas manifold has connections to 4 gas sources and three leak valves in the surface science and STM chambers. High purity compressed gas cylinders are used as received for dosing the sample with substances at exist as gases at room temperature. This system is also equipped with homebuilt liquid sources consisting of a large test tube welded to a stainless steel tube to interface directly with

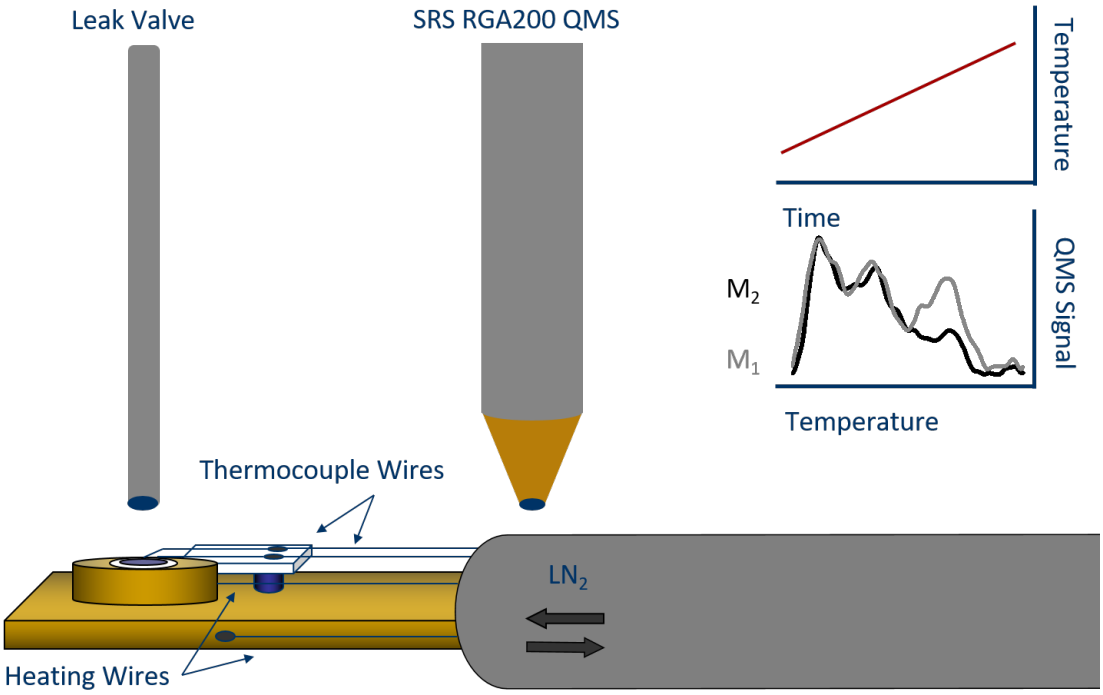

Figure 2.8. A schematic of the TPD/R experimental set up indicating the source of gas from the leak valve, the mass spectrometer, and a simplified depiction of the heating program and mass spectrometer response.

the manifold. The liquid sources are purified by submerging the sample tube in liquid nitrogen until liquid freezes and valve connected to the source is opened to the turbo pump to evacuate the gas above the frozen liquid. The source is then returned to room temperature and the process is repeated until there is no change in the manifold pressure when the valve to the frozen liquid is opened. High vapor pressure solid samples can also be used in this set up and are purified by the same freeze-pump-thaw method. To get a sufficient amount of gas into the line, the solid sample tube is often placed in a beaker of nearly boiling

water to further increase the vapor pressure.

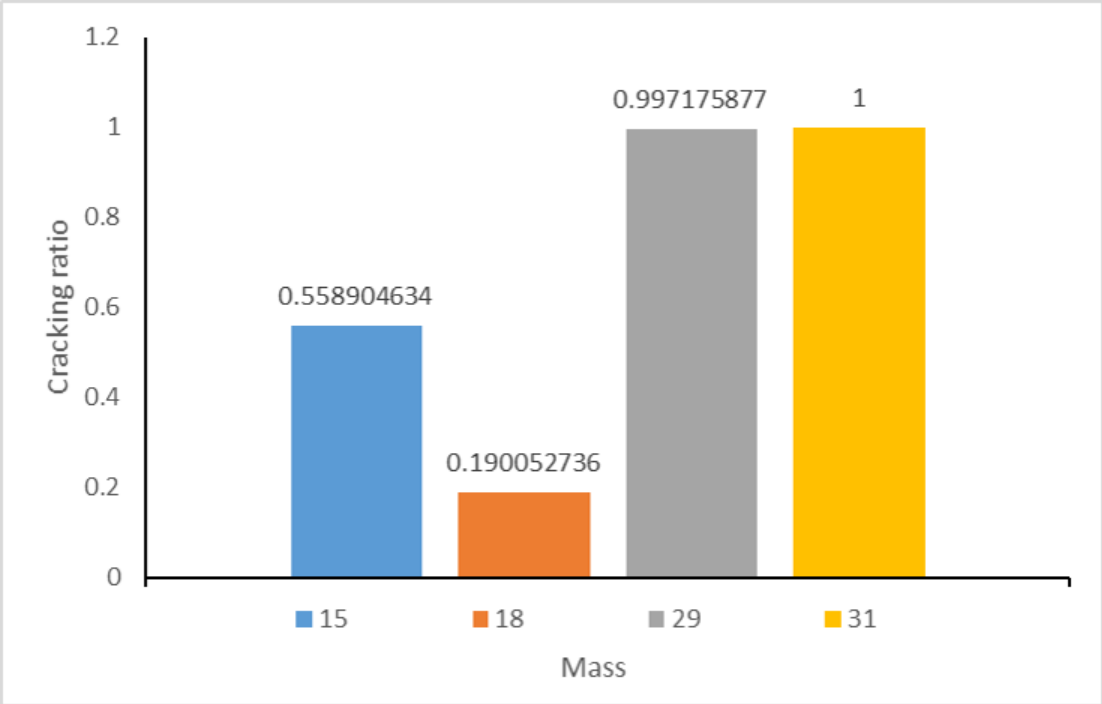

Figure 2.9. The intensity of the main mass cracking fragments for methanol in out mass spectrometer normalized to the most intense fragment m/z = 31

Once the TPD/TPR data has been collected by the Labview program, the interpretation is not necessarily trivial. For the RGA to separate the desorbing masses, they must first be ionized by the ionizer assembly in the mass spectrometer which fragmentation of these gas molecules. The ratio of the main fragmentation products are seen in Figure 2.9, where each is normalized to the mass 31 parent fragment. The other major gases of interest for this reaction system are methane (mass 15), water (mass 18), and formaldehyde (mass 29), all of which appear as cracking fragments of methanol. This leads to some ambigu-

ity when trying to determine how much of each mass come from a specific gas. For most of the data presented in this thesis, the cracking ratios are used analogously according to the following equation where I is the observed intensity by the RGA.

$$I_{formaldehyde} = I_{29} - CR_{29/31} * I_{31} \tag{2.7}$$

This method works well enough when there is only one species that contributes to the parent masses of the other species, but with methane that is not the case. Water and formaldehyde both crack to produce a signal at mass 15 which makes an accurate determination of the methane desorption difficult. Francisco Zaera has recently proposed a simple matrix algebra method[38] which allows for the deconvolution of TPD from the highly overlapping systems and for a more quantitative measure of the desorbing species. The method requires collecting the sensitivity factors, or response function, at each mass for all gas species of interest. This is done by filling the chamber with a range of pressures of each gas and monitoring the response at each pressure with the RGA. When plotted, the results will form a straight line with the slope corresponding to the sensitivity factor for that amu and gas species. This value allows one to convert between a certain pressure of a mass observed by the RGA to the true pressure value for that gas in the system. This is repeated for all gas species of interest until a square matrix of sensitivity factors can be built with one pri-

mary amu value for each species. This matrix is then inverted and multiplied by the TPD data (in vector form) at each temperature to give the quantitative deconvoluted data. A more detailed description of the procedure can be found in reference [38]. The response of the RGA and, thus the sensitivity factors change slowly over time and change quickly when routine maintenance such as ionizer filament replacement is performed. Because of this, unfortunately the method cannot be easily applied to data taken at different time, using different ionizer filaments.

2.4 The STM chamber

The final chamber in this apparatus contains the scanning tunneling microscope (STM), several "parking spaces" to hold extra samples, and a wobble stick manipulator to move samples from the fork to the parking spaces or the STM stage. The chamber is also connected, via a gate valve, to the load-lock chamber. The load-lock can be vented and pumped (by the same Osaka turbomolecular pump for the STM chamber) separately from the STM chamber. This allows the introduction of new samples or STM tips without having to expose the whole chamber to atmosphere which would require a bakeout. Samples are moved into the chamber by a magnetically coupled manual transfer arm and manipu-

lated from there by the wobble stick.

The STM was developed in 1981 by Binnig and Rohrer [39, 40] at IBM Zurich and the two later won a Nobel Prize in physics for this accomplishment. The instrument is used to acquire sub-nanometer resolution images of surfaces by using the quantum mechanical principle of tunneling to transport electrons from an extremely sharp metal tip to a metal or semiconductor sample across some finite barrier, in this case approximately 5 Å wide vacuum gap. At this distance the electronic wavefunctions of the tip overlap with those in the surface which is the required condition for tunneling to occur.

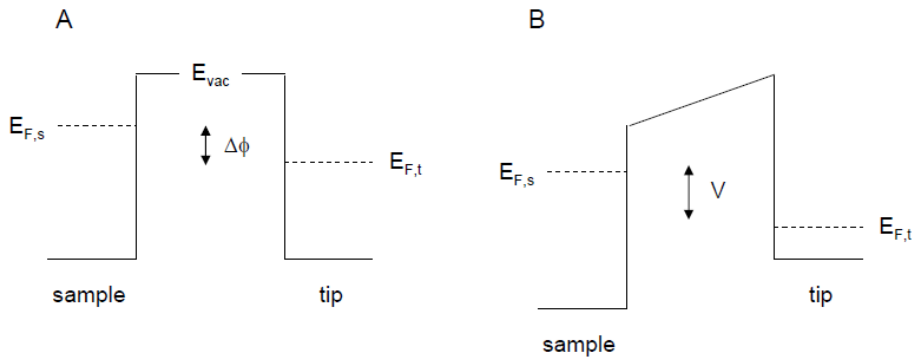

Figure 2.10. Potential energy schematic for two tunneling scenarios, (a) where no bias applied between the sample and the tip. (b) A positive bias V applied between the sample and tip. $E_{F,s}$ and $E_{F,t}$ are the Fermi levels of the sample and tip respectively, E_{vac} is the vacuum level, and $\Delta\phi$ is the tip-sample work function difference.

Because the tip and sample are rarely the same material, their Fermi energies will not align and a bias between the tip and sample must be applied to create a large enough tunneling probability that tunneling current (typically a few pA)

can be observed[41, 42]. Figure 2.10 shows STM conditions under no bias and a positive bias in which the valence band of the tip aligns with the conduction band of the surface causing electrons tunnel from the tip to the sample thereby probing the unoccupied states present. A negative bias can also be applied causing the opposite alignment of electronic states and tunneling from the sample to the tip which reveals information about the occupied states at the surface. For all experiments carried out here a positive bias is used.

$$I \propto \rho_{sa} V_b e^{-2\kappa d} \qquad \kappa \equiv \sqrt{2m_e(\Delta\phi - V_b)}/\hbar \tag{2.8}$$

The tip is raster scanned across the surface and an image is generated where the brightness at each pixel corresponds to value of the tunneling current. Equation 2.8 indicates the tunneling probability where I is the tunneling current, ρ_{sa} is the local density of states, V_b is the bias between the tip and sample, d is the tip-sample distance, m_e is the electron mass, $\Delta\phi$ is the tip-sample work function difference, and $\hbar$ is the reduced Planck constant[43]. From this equation, it is clear that the current will drop exponentially as the tip-sample distance increases. This effect is large enough that the tunneling current drops significantly in the small gaps between atoms on the surface, which makes atomic resolution imaging possible. For the experiments done here, all images were collected

using the constant-current imaging mode in which a feedback loop is used to maintain a constant tunneling current by modifying the voltages applied to the piezoelectric movement controls for the tip. Images taken with this method are a map of the height variation of the tip across the sample, corresponding to a surface map of constant charge density. STM can also be carried out in constant height mode where the bias voltage and tip height are fixed and the image corresponds to a map of the tunneling current.

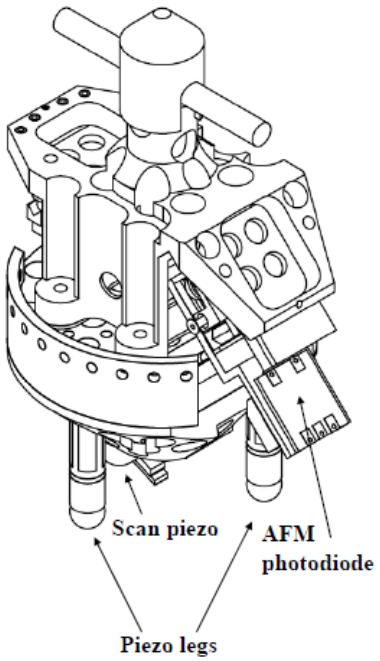

Figure 2.11. A schematic of the RHK walker type STM/AFM scan head. The piezoelectric legs allow automatic and precise approach of the STM tip to within a few angstroms of the surface.

The two microscopes used for these experiments are the RHK Technologies UHV 350 combination STM and AFM scan head and the UHV 300 STM only

only model. Both instruments are controlled by a common RHK 100 analog scan controller. These use a walker type mechanism to bring the tip within tunneling range of the surface. The walker consists of three legs that are placed on the ramps of the sample holder and a sawtooth wave is applied to the piezoelectric legs, which causes it to slowly "walk" down the ramps. Figure 2.11 shows the critical components of the STM/AFM scan head. The STM only scan head differs only in the removal of the AFM photodiode for a more rotationally symmetric instrument which experiences less vibrational noise. Because switching between these two instruments requires opening the chamber to atmosphere and a subsequent bakeout, most data was taken with the STM only model.

The STM stage, also produced by RHK, utilizes the same holding fork mechanism as on the sample manipulator to keep the sample secure during scanning. The stage itself is connected to the removable back flange by Viton ropes and O-rings to further reduce vibrational noise. Figure 2.12 shows the stage after removal from the chamber with a clear view of the electrical connections for thermocouple and sample heating indicated. The sample can be cooled by the installed cryostat by liquid nitrogen or helium and is thermally connected to the sample by a series of braided copper wires which serve also to reduce vibrations from the cryostat. Below the sample is a tungsten filament (0.25 mm diameter) with can be raised by a rotary motion feedthrough (MDC Vacuum Products) to

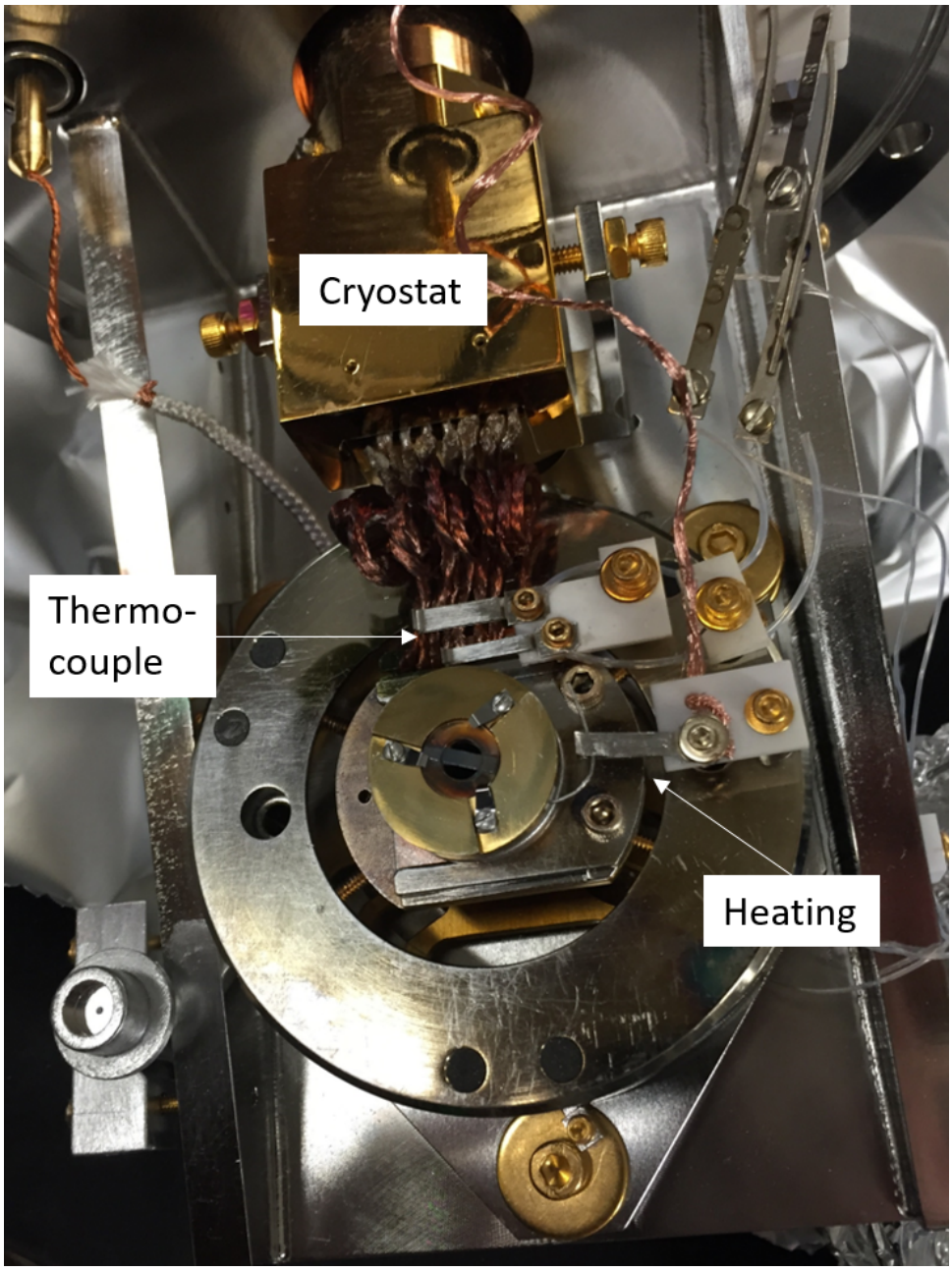

Figure 2.12. An image of the STM stage assembly after being removed from the vacuum chamber for adjustment with labels for relevant feedthrough connections.

radiatively heat the sample to 600 K. In combination, these allow the sample to be imaged at a wide range of temperatures allowing for the visualization of multiple steps along a reaction pathway.

2.4.1 STM tip etching

The STM tips used for these experiments are etched from tungsten wire (0.2 mm diameter, Alfa Aesar) by our Unisoku tip-etching apparatus. The wire is prepared for etching by being cut into ≈ 1.5 inch lengths, sanded to remove the oxide coating, and sonicated in methanol for 5 minutes to remove organic contaminants. The wire is mounted to a movable arm and inserted into the center of a platinum wire loop cathode which is resting on the meniscus of a 2.0 M sodium hydroxide solution. The wire is submerged 10 mm into the solution for a pre-etch step at 7 VDC to quickly remove the outer layers of the wire and assure a smooth starting surface. The wire is then raised until 5 mm remain in solution and the tip is etched at 2 - 3 V according to the following reaction:

$$\mathrm{W\,(s) + 2\,OH^-\,(aq) + 2\,H_2O \longrightarrow {WO_4}^{2-}\,(aq) + 3\,H_2\,(g)} \quad E^0 = -1.40V \quad (2.9)$$

Etching is stopped within 500 ns of the current dropping below a specified value (typically $1mA$) which occurs when the tip radius at the meniscus become small enough that the weight of the wire below causes it to break creating an atomi-

cally sharp tip. The tip is then rinsed with methanol and inspected by an optical microscope to verify a good, pencil-like tip shape. Any irregularities in shape, such as a rounded end or asymmetric profile will reduce the attainable image quality. Finally, the best tips are loaded into tip exchangers and introduced to the STM chamber via the load-lock. The tips are cleaned in vacuum by electron bombardment which removes the layer of oxide from the tip and improves scanning performance. The filament is raised to ≈ 1 mm from the tip, the whole stage and thus the tip itself is biased at $+500$ V relative to the filament, and 5-6 A are passed through the filaments while monitoring the electron bombardment current at the tip with an electrometer.

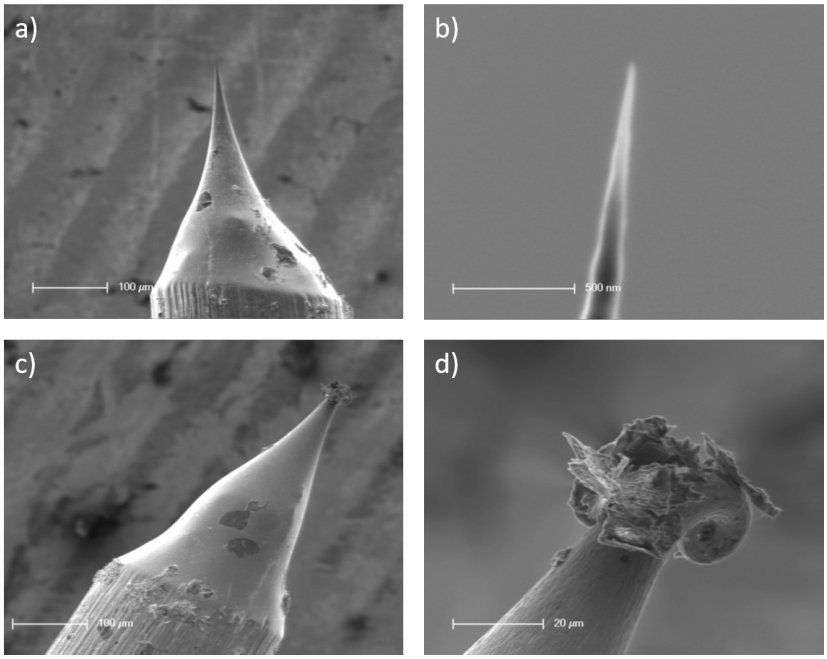

Figure 2.13. SEM images of etched, tungsten STM tips. (a-b) An ideal STM tip with zoom-in on the end. (c-d) A crashed STM tip with zoom-in on the end. Reproduced from [44]

Chapter 3

The Surface Science of Clean, Rutile TiO_2 (110) (1 x 1)

To fully understand the effect of the vanadium catalyst supported on the TiO_2 surface, we must first understand the structure and defects of the single crystal TiO_2 and how they interact with the molecules of interest such as methanol, formaldehyde, and water. This surface is one of the most studied and well-characterized oxide in the surface science literature. This chapter will present a quick overview of the relevant properties properties and is based heavily on the hallmark review by Diebold in 2003 [45], but will also include more recent work which has helped to illuminate the strong effect that Ti^{3+} interstitials play

on surface reactions.

3.1 The bulk structure of TiO_2

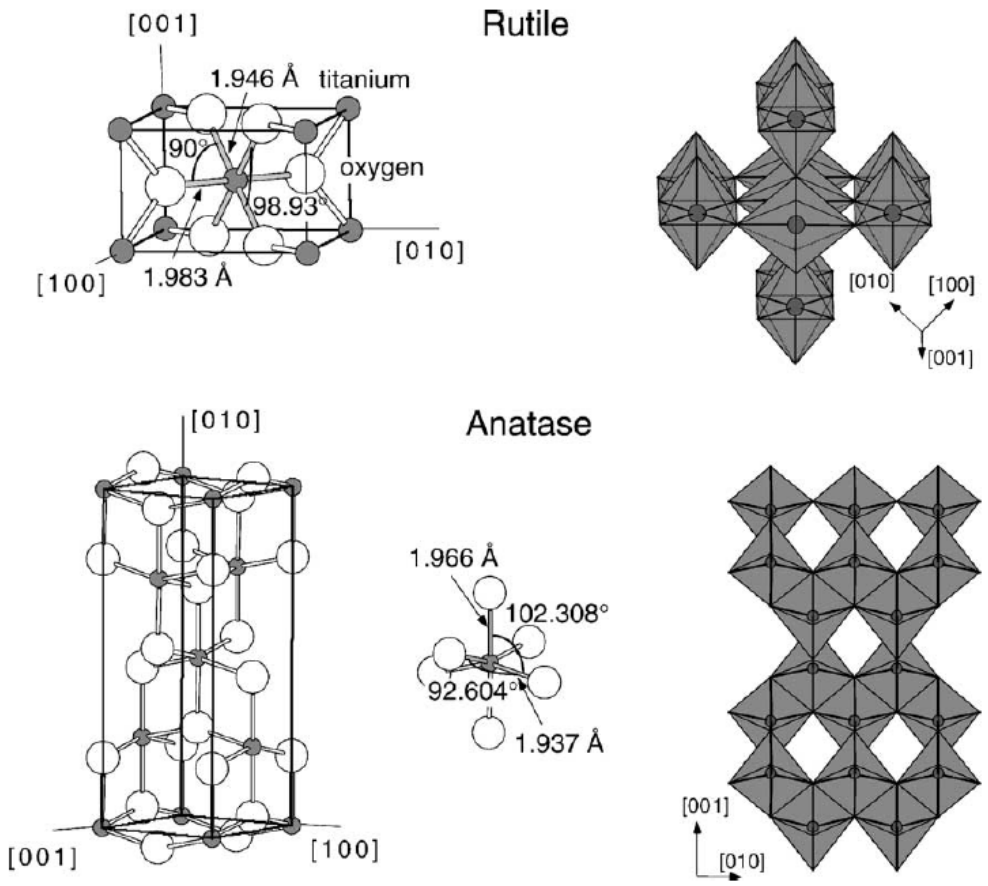

Figure 3.1. Bulk structures of rutile and anatase. The rutile unit cell has the dimensions $a = b = 4.587$ Å, $c = 2.953$ Åand for anatase is $a = b = 3.782$ Å, $c = 9.502$ Å. The bond lengths and angles are shown on the left and the distorted octahedral stacking is shown on the right for each phase. Reproduced from [45]

The bulk unit cell and octahedral representation of rutile and anatase TiO_2

are shown in 3.1 as these are the two most stable and studied structures in the literature. Both have distorted octahedral geometry with the anatase phase taking on the more distorted structure. This discussion will continue only with details about rutile, but it is important to see how these two structures differ for the sake of comparison. Of the low index faces for rutile, the (110), (001), and (100) planes have all been studied, with (110) being the most lowest energy by both measurement and calculation, and consequently, the best studied. Figure 3.2 shows how the bulk structure is cleaved to create the (110) surface.

In any surface science investigation, one must be aware of defects or contaminants in the bulk that may have some effect on the surface chemistry. In the case of out TiO_2 samples there is less than 25 ppm impurity metals such as iron, nickel, chromium, and calcium. These contaminants can be observed by XPS/AES when the crystals are new, but the signals disappear after a few cleaning cycles. This does not guarantee that the contaminants are entirely gone from the bulk, but that they are depleted in the near surface region; about the first 10-20 atomic layers. With such small starting concentrations, near-surface depletion, and reproducibility with samples from multiple manufacturers we believe that these contaminants have little to no impact on the surface chemistry. On the other hand, native defects of the TiO_2 crystal do play a large role in the surface chemistry.

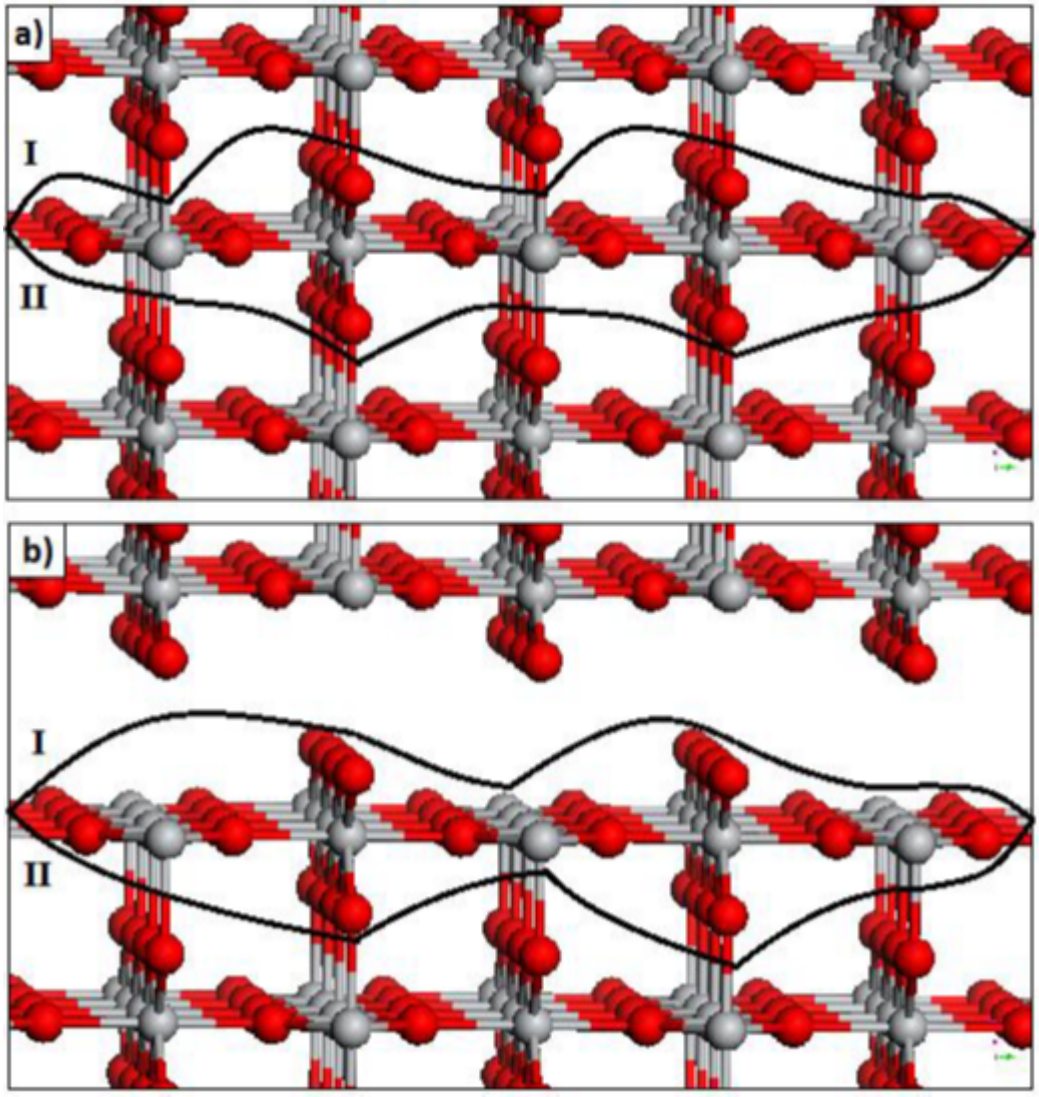

Figure 3.2. A ball and stick model of (a) bulk rutile TiO_2 with red balls indicating oxygen and grey indicating titanium. Cleaving along line I beaks an equal number of O $\longrightarrow$ Ti and Ti $\longrightarrow$ O bond which leads to the autocompensated (110) surface shown in (b). The two lines enclose a charge neutral repeating unit with no dipole moment. Reproduced from [45]

Figure 3.3. TiO_2 samples of increasing reduction, the color change is attributed to the accumulation of Ti^{3+} defects. The approximate number of cleaning cycles conducted on each sample from left to right is 0, 3, 12, 50 cycles.

The dominant native defects in bulk TiO_2 are Ti^{3+} interstitials and bulk oxygen vacancies that produce color centers. These defects are created as the sample becomes reduced by repeated cycles of Ar^+ sputtering and annealing in UHV. These Ti^{3+} interstitials and F-centers are responsible for producing the characteristic color change from a nearly transparent white crystal to a dark blue, nearly black color as seen in Figure 3.3. This also has the effect of reducing the bandgap from 3.05 eV and increasing the conductivity by nearly two orders of magnitude to a level more appropriate for imaging by STM. The creation of Ti^{3+} interstitial defects is only partially reversible by annealing the crystal in $\approx 5 \times 10^{-6}$ torr at 540 K or higher for an hour. This causes the Ti^{3+} atoms to diffuse to the surface and react with the adsorbed oxygen to form new TiO_2 layers and a variety of other structures. In addition, the defects have a significant impact on the reactivity of the surface by allowing charge transfer to adsorbates or clusters and will be discussed in the following sections.

It should be noted that the crystal also contains bulk oxygen defects that have a similar electronic effect on the sample as Ti^{3+} interstitials, as both effectively provide two excess electrons. XPS shows evidence of a titanium 3d state that is depleted by oxygen exposure at room temperature[46]. This does not conclusively show which defect is responsible for the 3d state observed. From here bulk defects will be referred to as Ti^{3+} interstitials, but actually represent any source of excess electrons provided to the crystal.

3.2 The surface structure of TiO_2

A ball and stick model with side and top down view can be seen in figure 3.4. This shows the alternating Ti-O row structure and several other key features that will be mentioned in this document, including the 5 and 6-fold coordinated Ti atoms (5c-Ti and 6c-Ti), the in-plane oxygen, bridging oxygen atoms (O_{br}), and an oxygen vacancy (O_v). Vacancies are formed by the repeated cycles of Ar^+ sputtering an annealing, are typically present in the 0.02-0.15ML range, depending on the level of reduction, and play an important role in the chemistry at the surface due to their high reactivity.

A large scale STM image with wide, flat terraces and well defined step edges is shown in figure 3.5. As mentioned above, this type of well defined surface is

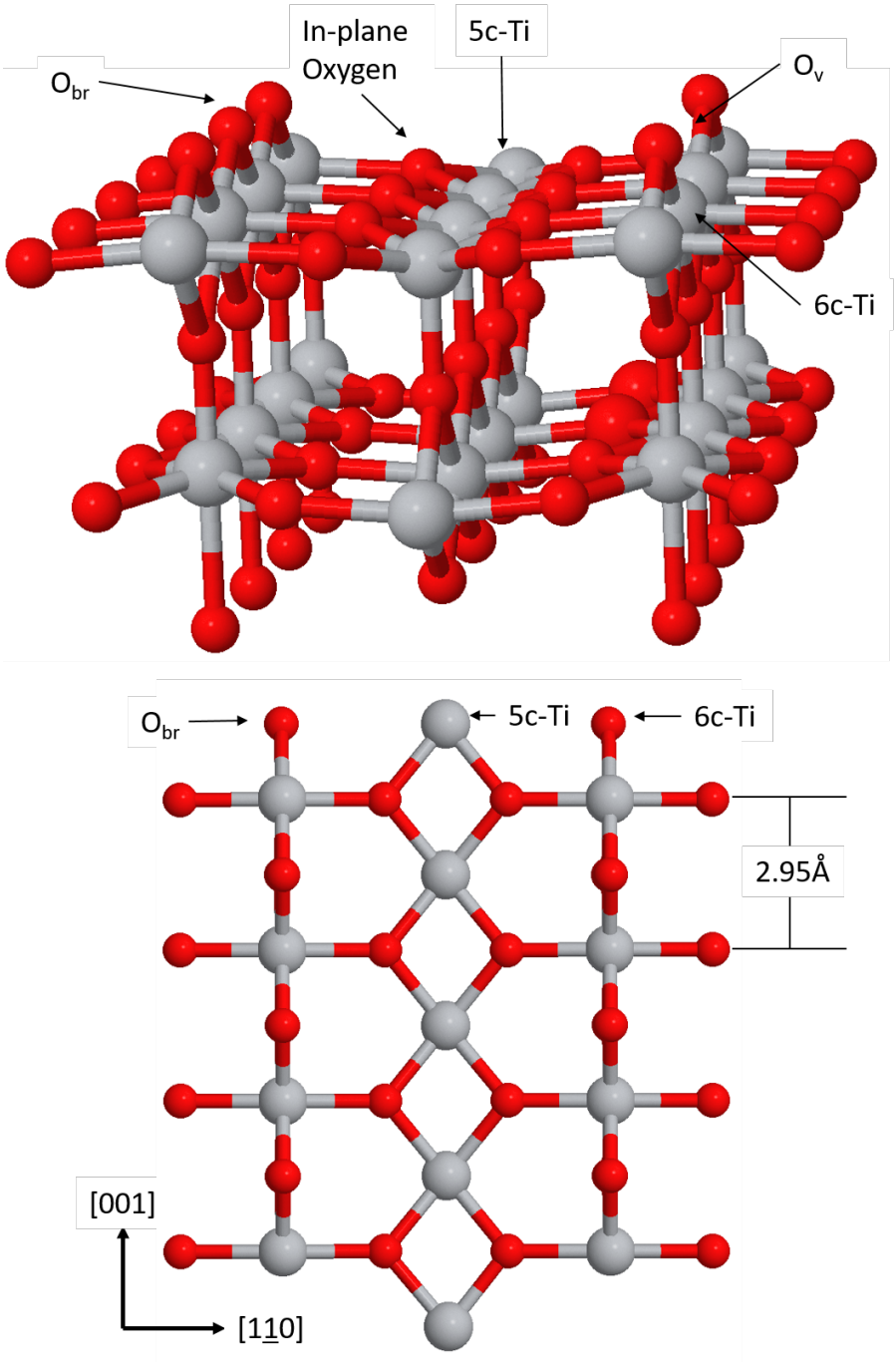

Figure 3.4. A side and top-down view ball and stick model of the rutile TiO_2 (110)(1x1) surface. Light grey spheres are titanium atoms and red spheres are oxygen atoms.

the product of multiple cycles of sputtering and annealing. The step height as observed by STM is 3.2 Å, the size of a single TiO_2 layer, is in good agreement with the literature[45]. The alternating Ti-O row structure can nearly be seen in this image and will be detailed below. The surface has edges running primarily in the [001] and [1$\underline{1}$1] directions parallel to the Ti rows and diagonally across the unit cell respectively. Most edges are smooth, but some have the jagged appearance, as indicated by the white box in the figure. This corresponds to only every fourth titanium atom along the edge being present. These edge defects, and other less common edge reconstructions can complicate interpretation of the surface chemistry as they represent binding sites with unique properties, but appear only in small quantities.

The atomic resolution STM image presented in figure 3.6 shows the characteristic row structure of the surface with an average row spacing of 6.3Å, the same distance observed in the bulk structure. The contrast observed here is somewhat counter-intuitive as the the taller bridging oxygen rows appear darker than the low lying bright titanium rows (indicated by the blue lines) with an average corrugation of 0.2Å. The titanium rows appear brighter because the STM images presented here are all acquired with a positive bias voltage which probes the unoccupied electronic states of the surface, for which the titanium atoms have a much higher density than the oxygen atoms. This is one of the

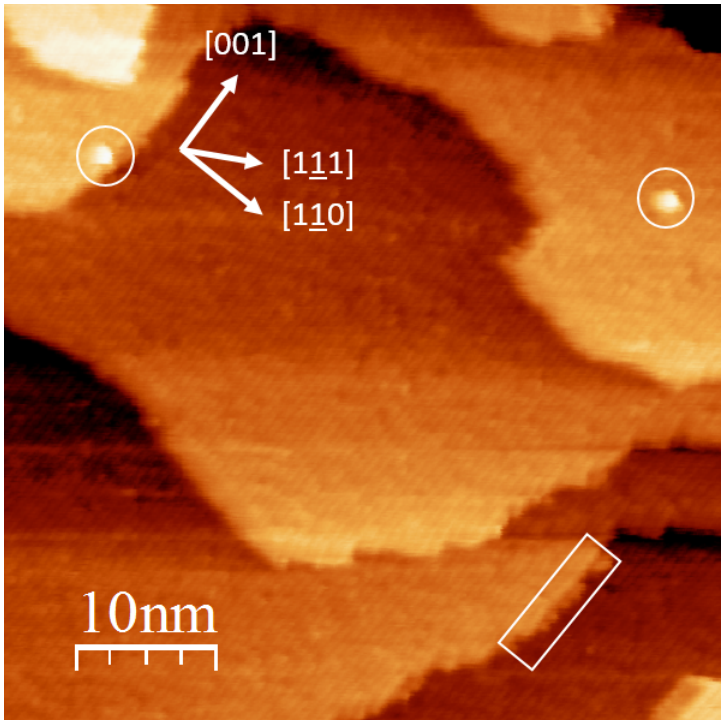

Figure 3.5. A large scale STM image depicting the terraced TiO_2 surface. The box indicates a jagged edge site and the circles indicate TiO_x islands.

clearest examples of STM contrast being controlled by electronic effects over the topography of the surface. This effect should be taken onto account when observing clusters on the surface as the apparent height as observed by STM may not exactly match that of theoretical calculations due to electronic effects of the oxygen atoms that typically lie above the vanadium atom in the cluster.

Oxygen vacancies appear as small bright protrusions in the dark bridging oxygen rows, as seen in the red circle in figure 3.6b [45]. These features appear bright because they expose the underlying titanium atoms. Both calcula-

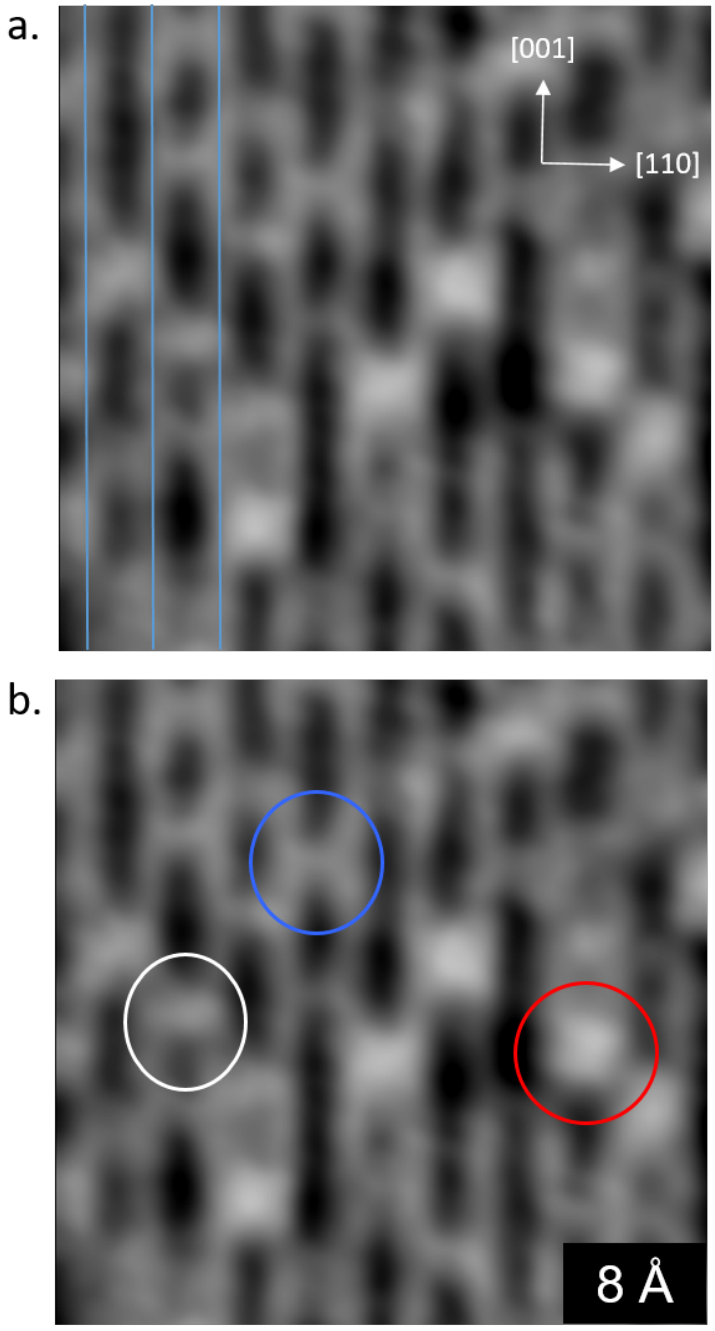

Figure 3.6. (a) STM image showing the row structure of the TiO_2 surface. Blue lines indicate the 5c-Ti rows. (b) The same image indicating the main surface defects: an oxygen vacancy in blue, a bridging hydroxyl in white, and a double hydroxyl in red.

tions and extensive experimental reports confirm that there is a large increase in charge density around these sites leading to the observed contrast [47]. The resulting extra two electrons delocalize to nearby 5c-Ti atoms, causing vacancies to be quite reactive towards the dissociative adsorption of many molecules of interest including water and methanol [48].

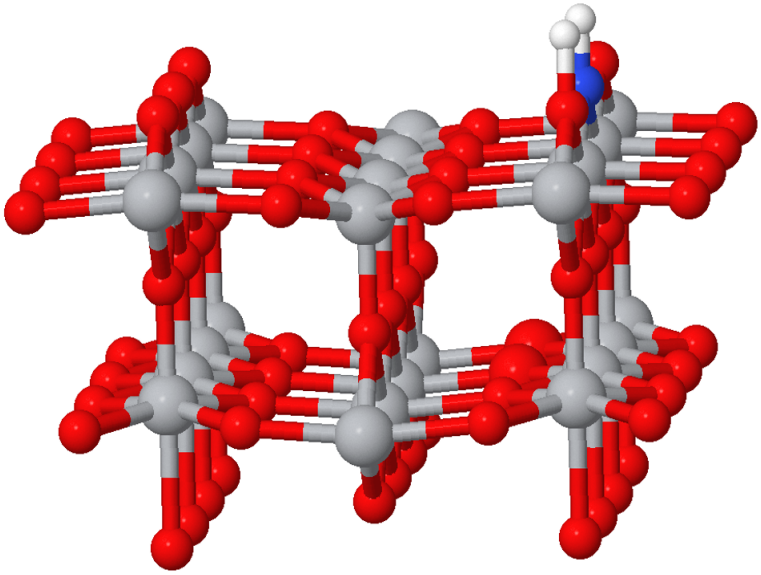

Figure 3.7. A ball and stick model of a double hydroxyl. The hydrogen atom appears in white and the blue atom is the oxygen atom from the water molecule that healed a vacancy.

Even under UHV conditions, water is always present in some small concentration of the background gases along with H_2, N_2, CO, and CO_2. Exposure to the background water causes the molecule to bind and dissociate at an O_v site to heal the vacancy and create two adjacent hydroxyls. This is referred to as a double hydroxyl ($d-OH_{br}$) and is shown schematically in 3.7. This feature appears

as a very bright spot centered over the bridging oxygen row and is elongated in the [001] direction and is indicted by the red circle in figure 3.6b. Single hydroxyls (OH_{br}) spots with intermediate brightness centered over the oxygen and more symmetric than the d-OH_{br} . These are represented by the white circle and form by diffusion of one of the two hydroxyl formed by the dissociation of water. Previous results from our group have shown that hydroxyls affect the adsorption of small gold clusters on the TiO_2 surface[49]. For this reason, they must be removed prior to cluster deposition by flash annealing the sample ($\sim$ 600K for 30s) which causes water recombination and desorption to leave behind O_v .

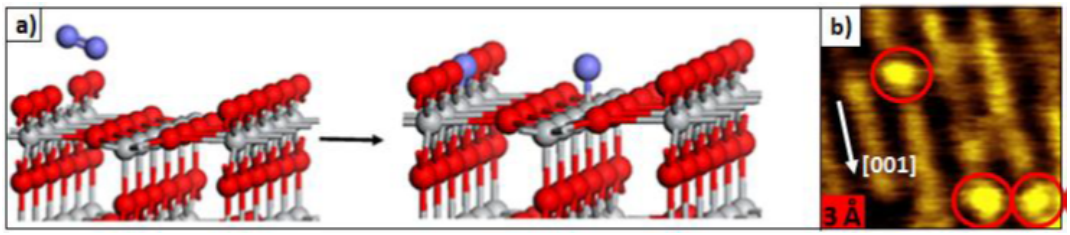

Figure 3.8. (a) Ball and stick representation for the reaction of molecular oxygen (purple) with a O_v to from an oxygen adatom (O_a) (b) STM image of O_a circled in red.

When the reduced TiO_2 surface is exposed to oxygen, the molecules can dissociatively adsorb at a O_v site to heal the vacancy and create an oxygen adataom (O_a) bound to the 5c-Ti row as seen in figure 3.8. We typically observe these features with a height of 0.25 Åby STM, in good agreement with the literature[48]. Oxygen can also to the 5c-Ti row and dissociate into a pair of O_a separated by a single Ti atom. It is believed that these structures are stabilized by excess elec-

trons from a nearby vacancy[50]. As expected, O_a can play a significant role in the chemistry that occurs on the surface.

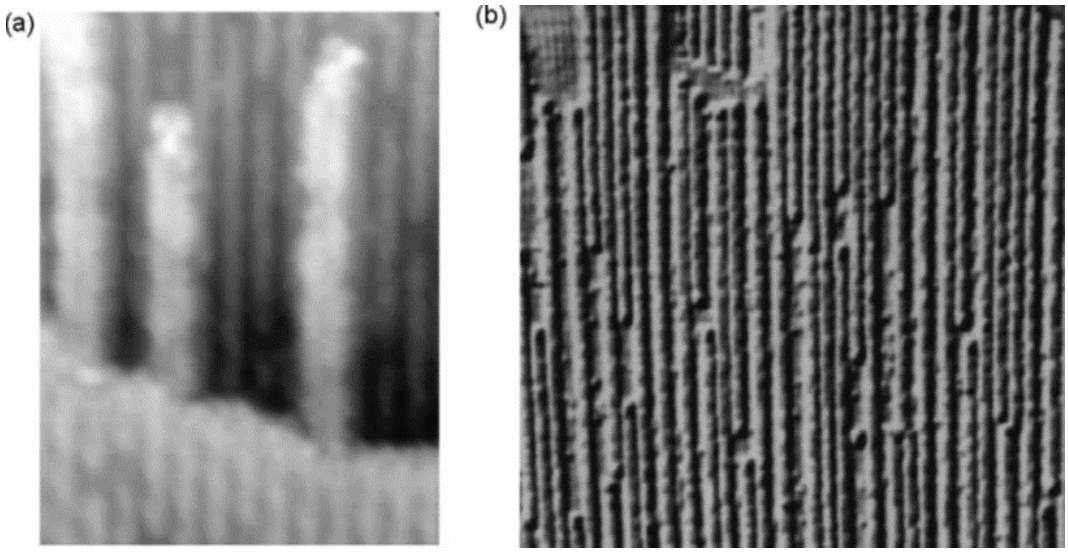

Figure 3.9. (a) STM image of the (1 x 2) reconstruction growing from the upper terrace (8.5 x 12.3 nm). (b) The fully reconstructed surface (70 x 70 nm). Reproduced from [51].

There are various reconstructions that can form on the TiO_2 surface, the smallest of which are TiO_x clusters. The white circles in figure 3.5 are these non-stoichiometric TiO_x islands which are formed when there are too few adsorbed oxygen atoms available to react with Ti^{3+} interstitials. Upon further heating of exceptionally reduced surfaces, the TiO_x islands can coalesce to form the (1×2) surface reconstruction which consists of long, alternating Ti_2O_3 strands forming along the [001] direction with regular TiO_2 rows in between. The precursor to this reconstruction can be seen in figure 3.9a and a fully reconstructed surface is presented in 3.9b. The (1×2) reconstruction can also form a cross-linked

structure running perpendicular to the strand growth direction. In these studies we only observe TiO_x islands and occasional (1×2) precursor strands which are always removed prior to cluster deposition by annealing in oxygen.

3.3 The surface chemistry of methanol and water on TiO_2

While the interaction of methanol with TiO_2 is often considered to be a well characterized model catalytic system, it is actually quite a complex system that depends sensitively on the variety of defects present in TiO_2 and continues to be an area of active investigation [52–65]. Much of the credit for the original interpretation of this system goes to the work of Madix and Henderson and this will form the basis of the introduction presented here[66, 67]. The details of the temperature programmed desorption (TPD) set up and analysis used for this study can be found above in section 2.3.3. The data presented in this section will be shown using the newer deconvolution method, but raw data will be shown later for the vanadium oxide cluster TPD as the sensitivity factors were not know at the time and change significantly when repairs are conducted on the RGA.

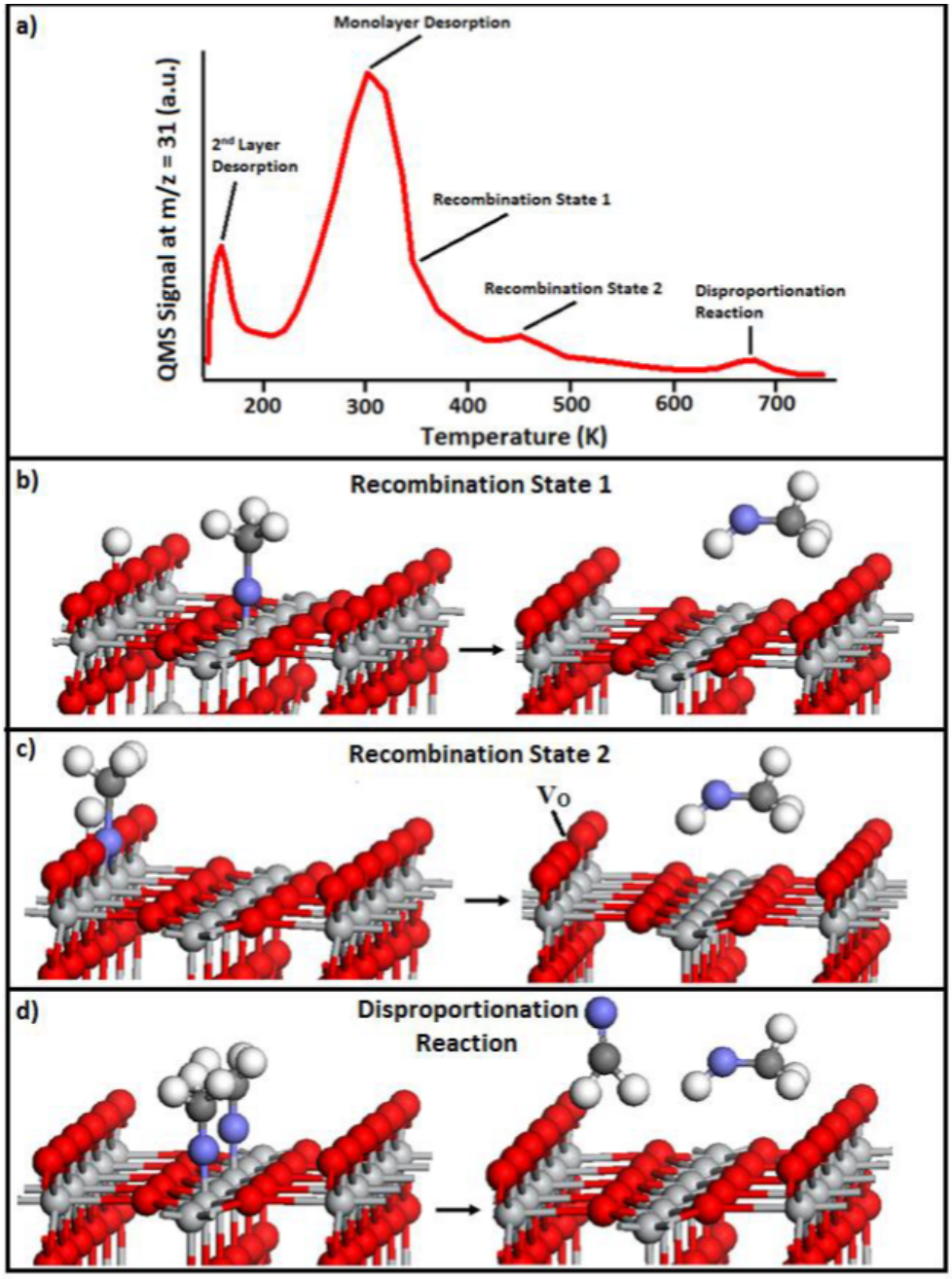

Figure 3.10. (a) A TPD spectrum of methanol (m/z = 31) dosed to 4.0L at 140 K, (b-d) reaction schematics for the various observed TPD peaks where the white, purple, and dark grey balls represent hydrogen, oxygen, and carbon respectively.

3.3.1 Methanol on the reduced surface

Figure 3.10 shows a methanol (m/z = 31) TPD spectrum for a reduced TiO_2 surface exposed to 4 L (Langmuirs, exposure to 1×10^{-6} Torr for 1 s) methanol at 140 K, referred to as cold-TPD. The sample was prepared with multiple cycles of sputtering and annealing to create a clean, reduced TiO_2 surface. The five peaks present here are the second layer desorption at 170 K, the monolayer desorption at 300 K, recombination state one (R_1) at 355 K, recombination state two (R_2) at 460 K, and the disproportionation reaction (D) at 660 K [52, 66, 67]. A recent combined DFT and experimental study has revealed that the nature of methanol binding in the first two peaks is strongly related to the amount of methanol on the surface [65]. They found that the maximum monolayer coverage is actually reached at 3/4 ML where about half of it exists as a dissociated methoxy with the CH_3O bound by the oxygen to a 5c-Ti and the hydrogen is transferred to the adjacent O_{br}, and molecular methanol with a hydrogen bond to the nearby O_{br}. This dissociated methanol state is also present in the R_1 and D reactions. However, when coverage is increased beyond this, the second layer on methanol favors binding with itself through hydrogen bonding and the fraction of dissociated methanol approaches zero when more than a second full layer is present, corresponding to 10 L dose. Due to the time of cooling the sample to cryogenic

temperature and lack of low temperature formaldehyde desorption, cold-TPD is only used occasionally as a means assessing the reduction of the surface and checking for low temperature catalytic activity, therefore the remainder of this discussion will cover TPD from room temperature.

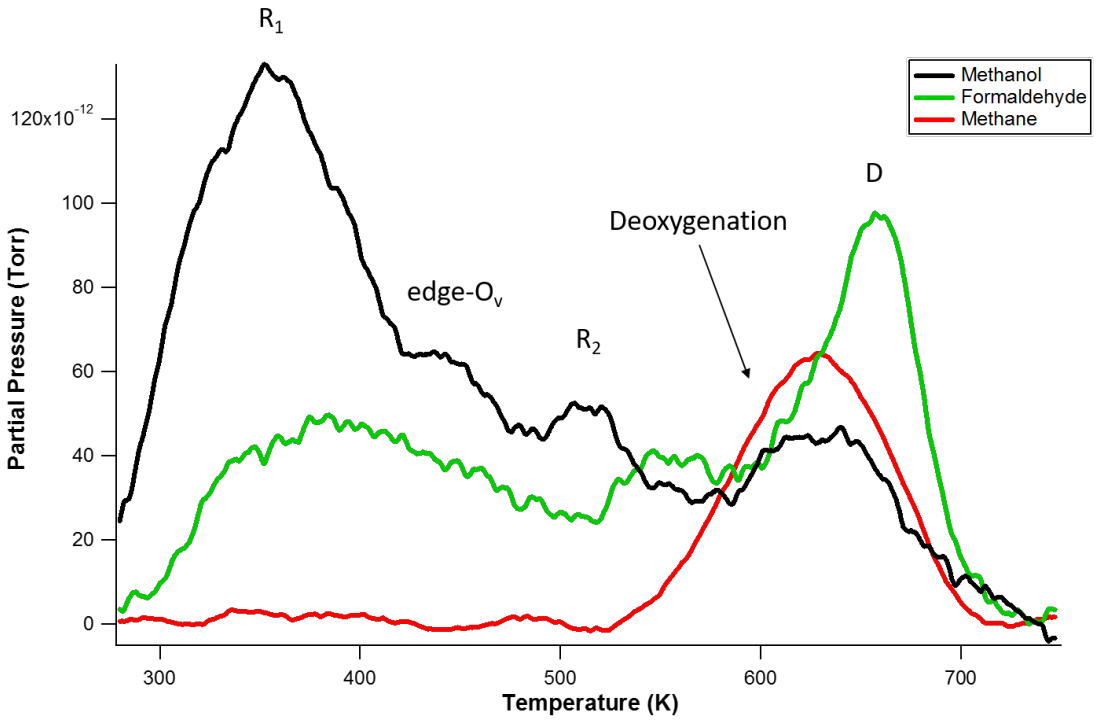

Figure 3.11. A deconvoluted TPR with a dose of 100 L methanol at room temperature on the clean, reduced surface.

The R_1 reaction also occurs on the surface when dosed with 100 L O_2 at room temperature, $\sim$ 290 K for these experiments. This reaction is depicted schematically in 3.10b, in which a 5c-Ti bound methoxy recombines with an

adjacent OH_{br} to reform methanol and desorb from the surface. Desorption of methanol molecularly bound to the 5c-Ti rows also contributes to this state. This desorption always observed and typically has the largest intensity as seen in the TPD spectrum in figure 3.11, which shows the deconvoluted values for methanol, formaldehyde, and methane generated from m/z = 31, 29, and 15 parent fragments respectively.

The Hammer group has shown by DFT that oxygen vacancies can form more readily on the step edge as compared to the terrace [61]. These vacancies (edge-O_v) can occur on every other oxygen atom along the edge and will strongly bind and dissociate both water, methanol and ethanol. Schematic representations of these reactions can be seen in References [61, 68]. Water TPD reveals an intermediate state associated with this edge vacancy binding [69]. This state occurs at a lower temperature than for recombination from terrace vacancies, but could not be resolved in these experiments due to the high background pressure of water in our system at the time. Thus, we attribute methanol recombination at these edge vacancies to the intermediate state appearing as a shoulder between the R_1 and R_2 state.

The next peak is the R_2 desorption state which corresponds to the recombination of a terrace vacancy bound methoxy and a nearby OH_{br} . As this state requires the presence of vacancies on the surface prior to dosing with methanol,

the intensity for this desorption can be used to approximate the vacancy concentration at the surface. We determine the vacancy concentration by taking the ratio of the areas of the R_1 and R_2 peaks which will be discussed in more detail in Chapter 4. For this surface the R_2/R_1 ratio is 0.45 and represents an O_v concentration of about 0.04 ML.

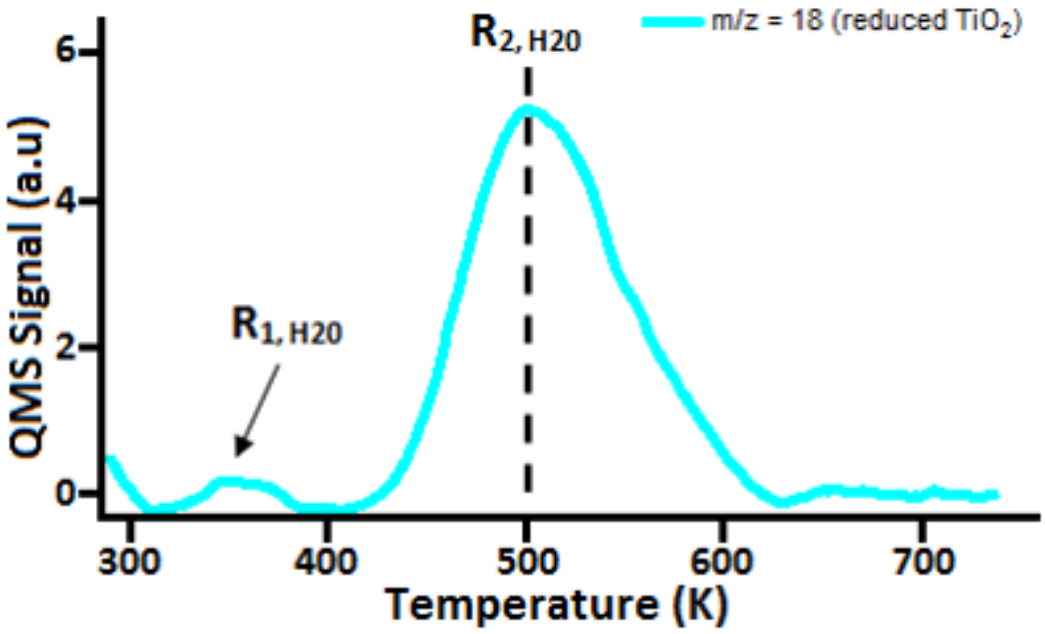

Figure 3.12. A raw data water TPR with a dose of 100 L methanol at room temperature on the clean, reduced surface.

It should be noted that the desorption of water also occurs, but the high background pressure of water in the system often masks any clear desorption states from appearing. Figure 3.12 shows the water desorption from the clean,

reduced TiO_2 surface after exposure to 100 L methanol. This data was collected with a slightly different surface state and mass spectrometer configuration, and thus is not a deconvoluted trace. Water TPD consists of two primary states that correspond to desorption from 5c-Ti bound water and recombination of OH_{br} at temperatures slightly higher than the R_1 and R_2 states for methanol respectively.

$$2\,(5\,\mathrm{c}{-}\mathrm{Ti}{-}\mathrm{OCH_3}) \longrightarrow \mathrm{CH_2O} + \mathrm{CH_3OH} \tag{3.1}$$

The last peak which shows desorption formaldehyde, methanol, and methane has long been attributed to the disproportionation reaction, shown in Figure 3.10d and Equation 3.1. In this reaction two stranded 5c-Ti bound methoxies react to form a methanol and formaldehyde in equal quantities. The methoxy groups that form the reactants are stranded due to the depletion of hydrogen adatoms that desorb at lower temperatures as either methanol or water. These stranded methoxy species are stabilized due to strong binding of methoxy pairs to 5c-Ti rows that cause a surface rearrangement where the Ti atom breaks its bond with the underlying oxygen atom [70]. Ti^{3+} interstitials also help to stabilize these species [46, 71]. This effect has been seen in other systems such as oxygen, ethanol, and benzaldehyde on highly reduced TiO_2 surfaces [68, 72, 73].

The disproportionation reaction as described by Henderson *et al.*[67] does

not completely explain the observed desorption products at this temperature. We observe that there is approximately double the amount of formaldehyde as methanol in conjunction with a broad methane desorption, which indicates there must be other reactions occurring here. Methane has been known to be produced by a TiO_2 surface reduced by electron bombardment, with desorption between 535 and 700 K for a heavily reduced (0.1 ML O_v) and lightly reduced (0.02 ML O_v) surface respectively [66]. It was proposed that this proceeds as a deoxygenation reaction at a vacancy site with a hydrogen adatom as seen in Equation 3.2. In this reaction the oxygen that is left behind heals a vacancy site.

We propose that Ti^{3+} defects are drawn to the surface due to binding of methanol. The accumulation of Ti^{3+} defects provides a binding site for stranded methoxy groups. Since the binding between the O-atom of a methoxy bound to a Ti^{3+} is stronger than the C−O bond, the disproportionation that includes this methoxy results in C−O bond scission. It is possible that a single methoxy stabilized by Ti^{3+} could produce methane by reacting with a hydrogen adatom as seen in Equation 3.3, but this reaction requires hydrogen bound to the surface above 600 K and hydrogen adatoms are not expected to be present at this temperature. This reaction is consistent with our data in Figure 3.11, but requires a reduced surface to produce methane. In addition, this reaction is in competition with the R_2 desorption that, according to theory, has a much lower

barrier. A more plausible explanation is that two stranded methoxies react to form formaldehyde and methane. This reaction leaves an oxygen atom behind that either heals a vacancy, Equation 3.4, or creates an oxygen adatom, Equation 3.5 Therefore, we propose that the production of methane is due to an additional disproportionation reaction between two methoxies to form methane, formaldehyde, oxygen. The combination of these last two reactions with the well known methanol/formaldehyde disproportionation faithfully account for the broad methane state which is likely the combination of two or more desorption states, and the excess formaldehyde produced in relation to methanol.

$$\mathrm{V_o{-}OCH_3 + H_a \longrightarrow CH_4 + O_{br}} \tag{3.2}$$

$$\mathrm{5\,c{-}Ti{-}OCH_3 + H_a \longrightarrow CH_4 + O_a} \tag{3.3}$$

$$\mathrm{V_o{-}OCH_3 + 5\,c{-}Ti{-}OCH_3 \longrightarrow CH_2O + CH_4 + O_{br}} \tag{3.4}$$

$$\mathrm{2\,(5\,c{-}Ti{-}OCH_3) \longrightarrow CH_2O + CH_4 + O_a} \tag{3.5}$$

The formaldehyde observed in the broad desorption state between 330 and 500 K has not been reported in the literature before and could come from a variety of sources. We suggest that this state is the result of a disproportionation of two edge vacancy bound methoxies to form methanol and formaldehyde. It cannot be entirely ruled out that this discrepancy is due to a poor calibration of the pressure response for certain gasses in our system, as methanol comes

from a liquid source and the formaldehyde is generated by sublimating solid paraformaldehyde. There is also some evidence to suggest that the fragmentation pattern of molecules can change as they are heated, and enter the mass spectrometer with a higher vibrational energy. Finally, this desorption state might be linked to a contaminant in the crystal such as calcium or iron which are present at parts per million (ppm) levels in TiO_2 but not observed by XPS. The exact nature of this state is not well understood, and the following experiments with a variety of surface states should shed some light on this.

3.3.2 Methanol on the stoichiometric surface

The stoichiometric TiO_2 surface is created by annealing the reduced sample in 5×10^{-6} Torr O_2 at 540 K for 30 minutes, followed by an anneal in UHV for 10 minutes at the same temperature to remove adsorbed oxygen. The process creates a surface with very few oxygen vacancies on the both terraces and edge sites while depleting the near surface region of most Ti^{3+} defects. As can be seen in figure 3.13, the R_1 state is not significantly effected as the annealing process has little effect on the terraces. Methanol desorption from the edge vacancy and R_2 states are diminished compared to the reduced surface but not completely eliminated as the UHV anneal allows for the formation of about 0.02 ML O_v on

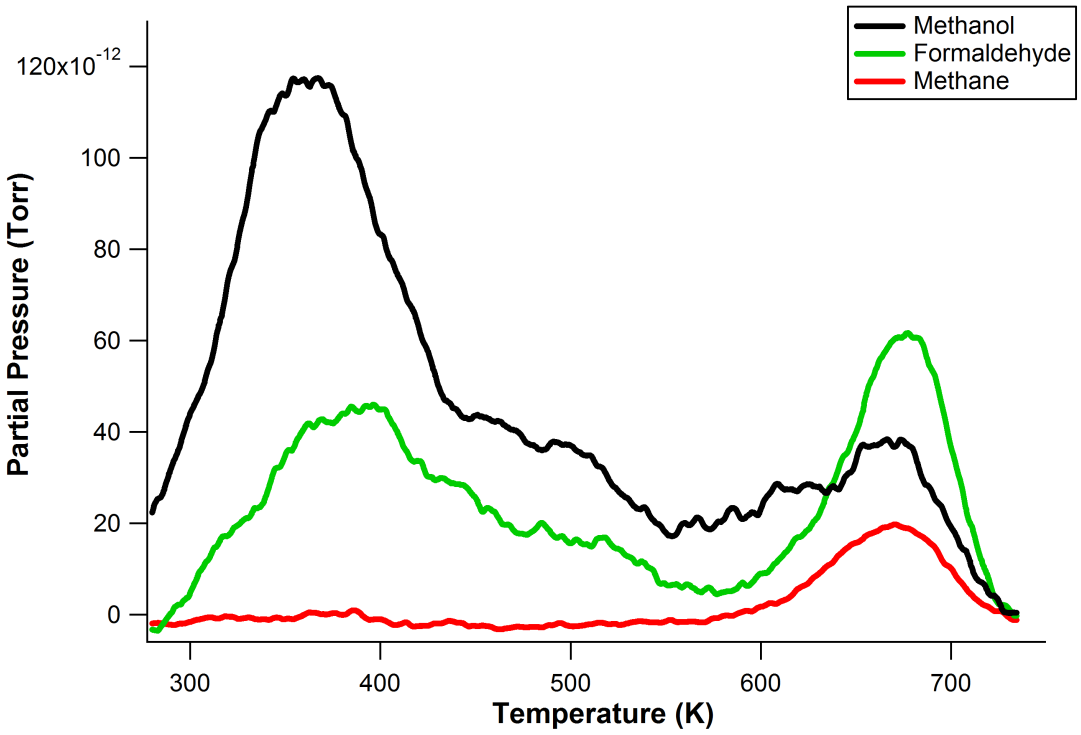

Figure 3.13. A deconvoluted TPR with a dose of 100 L methanol at room temperature on the stoichiometric surface.

the surface which are expected form more favorably at the edge sites[61]. The R_2 state is almost completely eliminated in this case due to the low concentration of O_v and the R_2/R_1 ratio for this surface is 0.28 ML.

At high temperature, there are significant changes to the desorption temperature and the distribution of products observed here. All three expected reactions are attenuated due to the lack of Ti^{3+} interstitials near the surface, indicating that fewer methoxies remain at this temperature. The corresponding

desorption temperatures for these reactions increased slightly as more energy is required for C–O bond scission in the absence of Ti^{3+} defects. The disproportionation reaction for methane is strongly affected, and the deoxygenation reaction to produce methane is eliminated, providing further evidence that Ti^{3+} interstitials are necessary for methane production.

3.3.3 Methanol on the oxidized surface

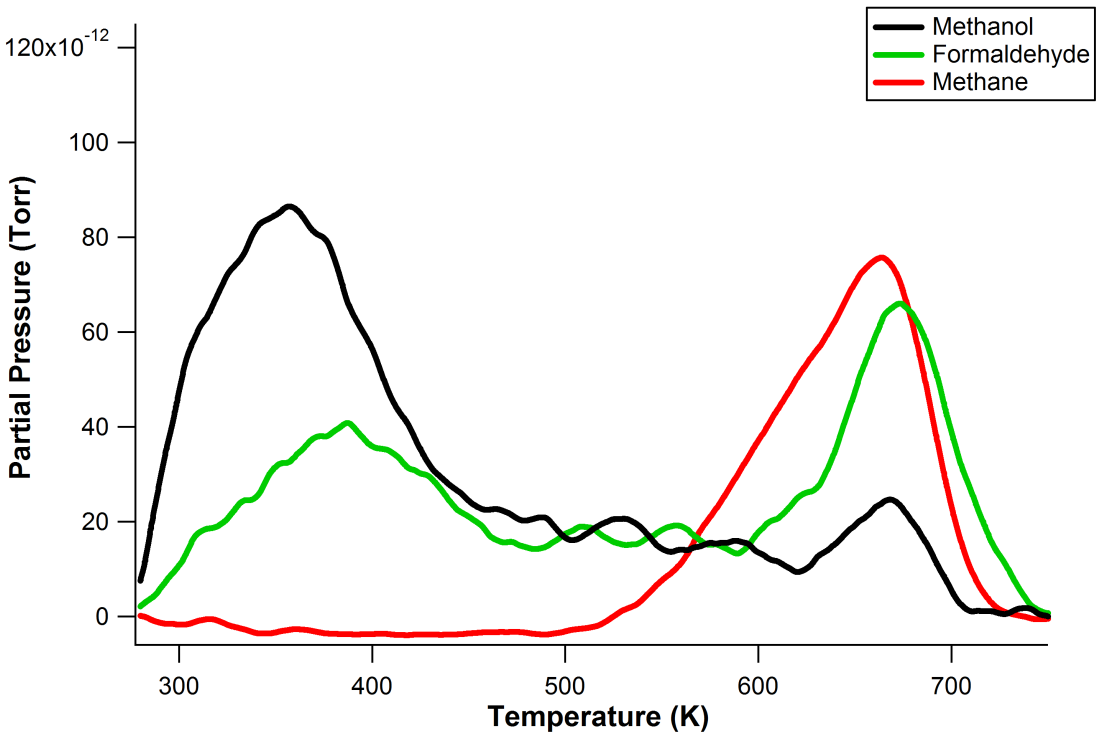

Figure 3.14. A deconvoluted TPR with a dose of 100 L methanol at room temperature on the oxidized surface.

The oxidized surface is created by exposing the reduced surface to 10 L O_2 at room temperature which fills all of the oxygen vacancies and leaves behind single and paired oxygen adatoms bound to the 5c-Ti rows. It should be noted that this low oxygen exposure has almost no effect on Ti^{3+} interstitials as observed by Besenbacher [46]. We observe a reduction in the intensity of the R_1 peak due to O_a blocking available 5c-Ti for methanol adsorption, as seen in Figure 3.14. The R_2 and edge-O_v states do not appear, as expected with no vacancies on the surface. Yet again, the products observed at high temperature change sensitively with the oxidation state of the surface. With O_a impeding diffusion of methoxies, many more become stranded, resulting in the higher desorption intensity observed here. The methanol-formaldehyde disproportionation reaction is reduced at the expense of methane production which provides further evidence that Ti^{3+} interstitials, and not O_v, are the driving force behind these reactions. This also indicates that O_a play some role in the deoxygenation reaction, likely by supplying higher mobility to the available H atoms by increased proton hopping.

3.3.4 Methanol on the hydroxylated surface

The hydroxylated surface is created by exposing the reduced surface to 10 L H_2O at room temperature which fills all of the oxygen vacancies to form single and paired hydroxyls on the bridging oxygen rows, and does not change the concentration of Ti^{3+} interstitials. The results here are very similar the oxidized surface as seen in Figure 3.15 as expected the R_1 state has mostly unaffected and the R_2 state does not appear as there are no available vacancies on the surface. The increase in methanol deoxygenation to methane is also expected as the reaction requires the presence of both hydrogen and Ti^{3+} interstitials which are abundant here.

From the collection of these experiments, it is clear that the surface state has almost no effect on the intensity, shape, or desorption temperature of the low temperature formaldehyde state between 300 and 500 K, which means that it has no physical relationship to the surface chemistry. As this peak strongly resembles the methanol desorption, we conclude that this peak is not truly a reaction product, but that this data artifact is most likely due to vibrational energy provided to methanol when it desorbs from the surface as compared to the free expansion of methanol into the chamber during sensitivity factor testing. Even with this issue, the data is valuable as it provides the best understanding of the

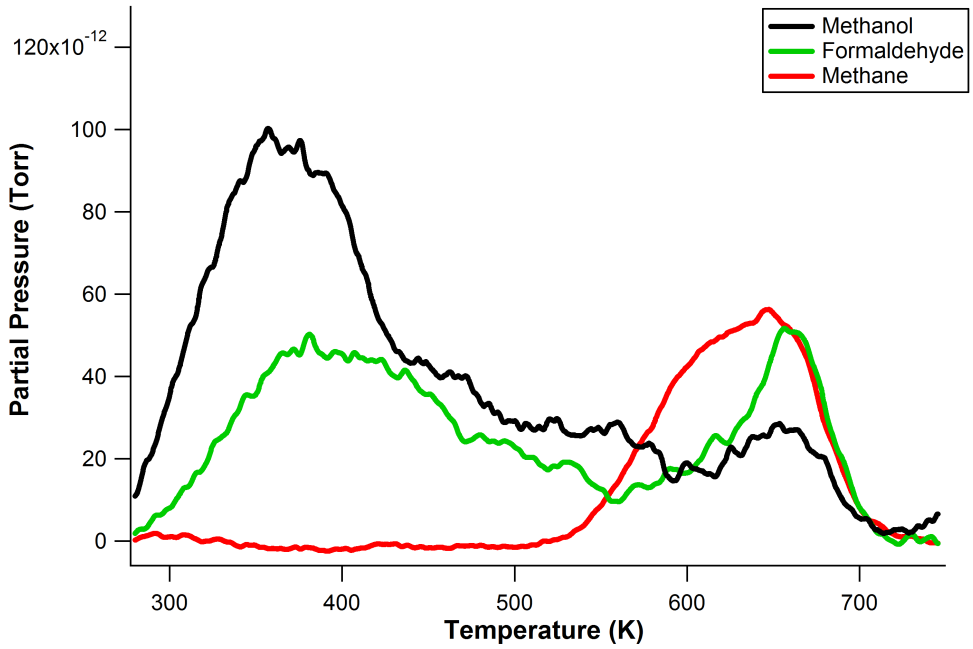

Figure 3.15. A deconvoluted TPR with a dose of 100 L methanol at room temperature on the hyroxylated surface.

high temperature reactivity of methanol on the TiO_2 surface by clearly demonstrating the ratio of desorption products and the presence of two methane desorption states. Due to changes in the mass spectrometer over time and a lack of prior data, this deconvolution method will not be used for the remainder of this dissertation. The observed cracking ratios will be used as in described by equation 2.7.

Chapter 4

The Structure and Reactivity of V_2O_6 Clusters on the TiO_2 Surface

Vanadium oxide films supported on a second metal oxide have been shown to be extremely versatile catalysts [74]. In particular, vanadia sub-monolayer films supported on TiO_2 are known to catalyze numerous reactions, including but not limited to, the ammoxidation of alkyl aromatics [75, 76], the selective reduction of NO_x by NH_3 [77, 78], and the selective oxidative dehydrogenation (ODH) of methanol to formaldehyde [19, 22, 26–28, 79, 80], dimethoxymethane and methyl formate [81, 82]. An enormous amount of model catalyst investigations, conducted in UHV, as well as theoretical studies have probed the activity of

the vanadia/TiO_2 (110) system for the oxidative dehydrogenation (ODH) of methanol to formaldehyde.

Previous studies have shown that for submonolayer to monolayer coverage of vanadium oxide on TiO_2 a variety of species are found on the surface and under different conditions the vanadium +3, +4, and +5 oxidation states can all be active for methanol ODH as seen in Table 1.1. The early work of Madix [22] prepared vanadia films of various coverages by $VOCl_3$ hydrolysis on TiO_2 (110) single crystal support follwed by an oxygen anneal at 600 K. The films prepared at a single monolayer and submonolayer coverages were found by XPS to contain vanadium in the 5+ oxidation state and were the most active for methanol dehydrogenation at the disproportionation reaction temperature as discussed in Chapter 3. Production of formaldehyde steadily decreased with increasing vanadia coverage while the desorption temperature decreased to a minimum of 517 K for a coverage of 1 monolayer (ML). The catalyst was found to be deactivated after the first run and the vanadium was observed to be in a mixture of the 3+ and 4+ oxidation states.

Vohs prepared vanadium films of varying thickness on TiO_2 by evaporation of vanadium on to the surface followed by annealing in oxygen at a pressure of 1×10^{-6} Torr at 500 K[23]. High resolution electron energy loss spectroscopy showed vanadium in the 3+ state, and formaldehyde production was maxi-

mized for 1 ML with desorption at 660 K. After one run, the catalyst was no longer active but could be regenerated by annealing under the same conditions. Further investigation of this system was conducted by annealing the films in a higher pressure (1×10^{-3} torr) of oxygen, this created a more active catalyst with more vanadium in the 5+ state [24]. This produced simultaneous desorption of methanol and formaldehyde at 485 K, a sharp reduction from previous experiments.

The structure of vanadia clusters was examined by Netzer with STM of isolated clusters prepared by reactive evaporation of vanadium in an oxygen environment [25]. It was discovered that this process creates a variety of cluster morphologies on the surface and that reactive evaporation creates a more well ordered surface than post-oxidation of vanadium. Catalytic and oxidation state of the vanadium was not investigated in this work.

More recently, Artiglia and co-workers prepared vanadium oxide submonolayer films on TiO_2 by reactive evaporation [27]. They found the dominant oxidation state of vanadium before reaction with methanol to be +3, and the stoichiometry was found to be exclusively V_4O_6 as determined by angle-resolved photoelectron diffraction. The clusters produced formaldehyde at an unprecedented low temperature of 300 K following adsorption of methanol at 130 K. Bao and co-workers prepared TiO_2 nanorod supported vanadia catalysts

by wet chemical methods, and found by ^{51}V NMR that VO_3 and vanadium dimer clusters connected by two bridging oxygen atoms are active for methanol ODH.

These studies have all used preparation methods that couple the creation of the vanadium oxide to the oxidation of the supporting TiO_2. In an attempt to unambiguously determine the identity of catalytically active vanadium oxide for the ODH of methanol to formaldehyde, our group has utilized methods to produce and deposit size selected V_x, VO_y and V_xO_y clusters on a TiO_2 (110) support of various oxidation states. We have previously investigated the structure and catalytic activity of vanadium monomer clusters: V_1, V_2, VO, and VO_2 [12, 28]. In combination with theoretical contributions from our collaborators [21, 26], we have shown that only VO clusters oxidized in 2×10^{-6} Torr oxygen at 540 K are active for methanol ODH as seen in Figure 4.1. As shown by STM, these clusters take on a VO_3 structure with out of plane vanadyl oxygen that is likely responsible for this activity. This activity is absent in a subsequent TPR experiment and can only be partially recovered by re-oxidation under the same conditions. This shows that the cluster or surface is irreversibly modified by the TPR/oxidation process and this is not likely to be the active species in the bulk catalyst. Due to experimental limitations, VO_3 cannot be deposited directly so this work will investigate larger clusters with a similar stoichiometry, namely V_2O_5, V_2O_6, V_2O_7 and V_3O_9 on TiO_2 surfaces with a variety of oxidation states.

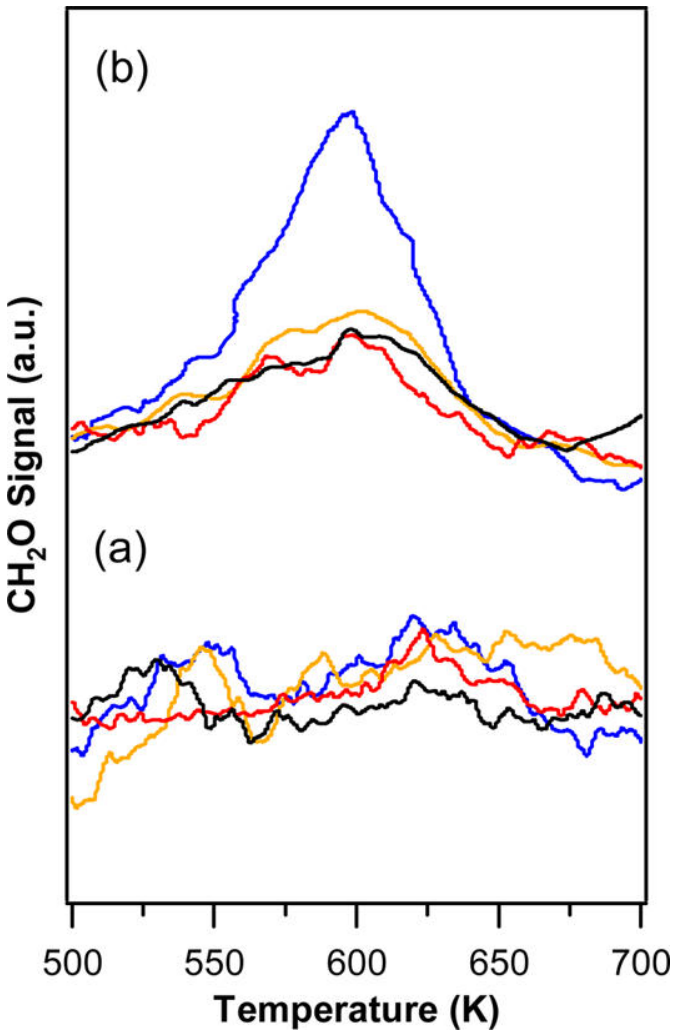

Figure 4.1. a. Formaldehyde TPR of the bare (black), V (orange), VO (blue), and VO_2 (red) cluster decorated reduced surface. b. Formaldehyde TPR of the same surfaces following oxidation on 2×10^{-6} torr O_2 at 540 K for 1 hour. All are shown on the same y scale. Reproduced from [28].

4.1 The reactivity of V_2O_6 on the highly reduced surface

The highly reduced surface is created after many cycles of argon bombardment and annealing in UHV until the crystal is dark blue to black in color. The surface is characterized by reaching the maximum concentration of oxygen vacancies 0.10 ML and many Ti^{3+} interstitial defects that give the crystal its color and facilitate STM imaging. The surface reduction state is quantified by the ratio R_2/R_1, the first two desorption states in RT methanol TPD from a clean TiO_2 surface. The values range from 0.1 to 1.2, indicating our most oxidized and most reduced surfaces respectively. The ratio R_2/R_1 was determined to 0.84 before 0.10 ML V_2O_6 was deposited on the surface. Immediately following the deposition, the cluster decorated exposed to 100 L methanol by a directed dose for TPR. After the surface had cooled back to RT from the first TPR experiment, the surface was dosed again for a "2nd run" experiment. Finally, a "re-oxidized run" was carried out by exposing the surface to 10 L O_2 before a third exposure to 100 L methanol.

The results can be seen in Figure 4.2, where a) shows the methanol TPR data from the clean surface just before cluster deposition. The traces for methanol, simply the data from m/z = 31, and for m/z = 29 are shown to demonstrate

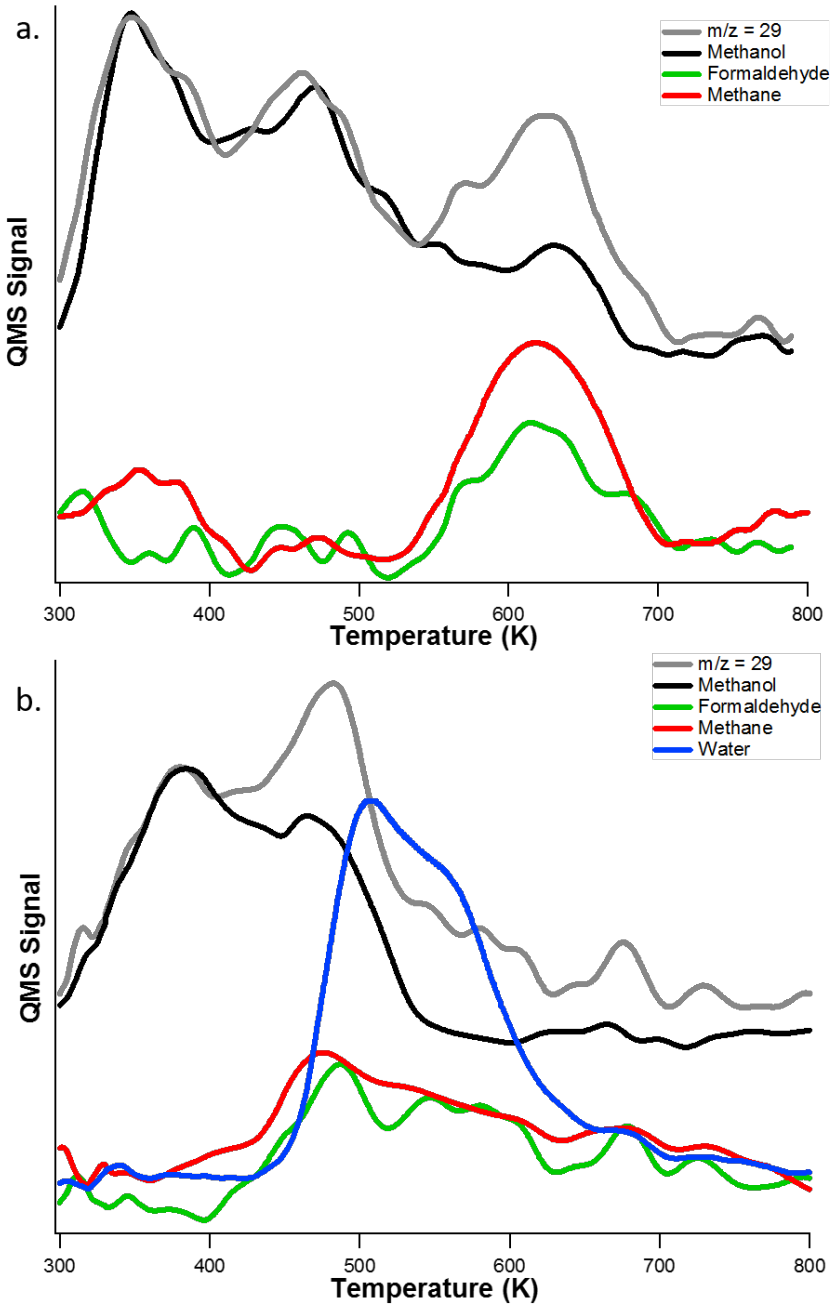

Figure 4.2. a. Methanol TPR of the clean, highly reduced TiO_2 surface just before cluster deposition. The m/z = 29 and methanol traces are shown offset from the formaldehyde and methane traces for clarity. b. Methanol TPR of V_2O_6 cluster on the highly reduced surface, the water trace is scaled down by one half, and other traces offset for clarity.

that in our mass spectrometer methanol fragments into m/z = 29 and 31 in a ratio near unity, thus the formaldehyde signal can be found by subtracting the two TPD traces. The formaldehyde and methane traces are then found by using their respective cracking ratios from methanol. Methane (m/z = 15) is also a cracking fragment of formaldehyde and the contribution to m/z = 15 from formaldehyde should be about 3.9% of the m/z=29, which is variable and not included when calculating the methane signal. Therefore, the amount of methane shown might slightly overestimate actual production. We observe the same qualitative results as described in Chapter 3 when using this method as compared to the deconvoluted TPR.

The results of the methanol TPR from the cluster decorated surface are shown in Figure 4.2b. The slightly elevated temperature of the R_1 state demonstrates the stabilizing nature of these clusters, and this small shift is consistent across other active V_xO_y catalysts which will be discussed later. The peak desorption of formaldehyde occurs around 480 K and no formaldehyde desorption is observed here on the clean surface, thus the V_2O_6 cluster is active for selective oxidation of methanol and represents a decrease in desorption temperature by 120 K compared to the VO_3 decorated surface. This result also represents the lowest temperature for formaldehyde production from a reduced surface. This is quite similar to the results of Vohs [24] who observed desorption at 485 K

from a full monolayer of vanadium heated in oxygen to create a vanadia film. The model catalyst here produces slightly less formaldehyde than the result in the literature with only one tenth the amount of vanadium on a reduced surface.

Methane desorbs simultaneously with formaldehyde indicating that these are likely produced in the same reaction. This is most likely similar to the disproportionation reaction presented in section 3.3.1 where two stranded methoxy groups react around 620 K to form methane and formaldehyde in a 1 to 1 ratio. In this instance, one of the methoxy groups is bound to a vanadia cluster and the other to a nearby oxygen vacancy as in Equation 4.1. Methanol desorption is also observed at this temperature from the recombination of a vacancy bound methoxy and adjacent hydroxyl. We believe that the high concentration of Ti^{3+} defects play an important role in this reaction as they are both associated with the production of methane on the clean surface. It remains unclear exactly how this interaction takes place but could help stabilize methoxy groups bound on or near the V_2O_6 cluster. A STM and theoretical investigation of the binding of methanol to the cluster decorated surface could elucidate further details about the nature of this reaction and its connection to defects in the support.

$$V_2O_6H{-}OCH_3 + V_o{-}OCH_3 \longrightarrow V_2O_6H + CH_2O + CH_4 \tag{4.1}$$

At this temperature, vacancy bound hydroxyls recombine to form water and

a larger than usual state desorption state was observed with a peak shoulder near the next formaldehyde desorption. This new state most likely comes from the H atom bound to the cluster recombining with with another nearby hydroxyl to remove one oxygen atom from the surface. It is uncertain if the oxygen atom comes from the cluster to create a V_2O_5 cluster or from a bridging oxygen to form an oxygen vacancy. The second run below sheds some light on this, but understanding could be improved by an oxygen isotopic labeling experiment.

Formaldehyde desorption continues with another peak centered around 545 K, which lacks a clearly defined peak in either the methane or methanol desorption. This state instead shows a simultaneous water desorption, indicating another cluster mediated reaction that produces water and formaldehyde similar to the reaction that occurs on post oxidized VO. We propose that the H atom transferred to the cluster during dissociative adsorption of methanol reacts with the cluster bound methoxy to form water, formaldehyde, and remove one oxygen from the cluster. The reduction of the cluster by this reaction is why the second run TPR shows that the catalyst becomes inactive for methanol ODH.

Finally, a reaction that resembles the disproportionation reaction occurs at an elevated 675 K. While the exact position of this peak does vary some on the clean TiO_2 surface based on the relative level of reduction, this peak occurs nearly 45 K above the temperature observed directly before cluster deposition

and we take this to be a significant shift. It is known that the clusters themselves reduce the mobility of stranded methoxy groups on the surface by limiting diffusion along the 5c-Ti troughs. This could occur by the cluster blocking movement along the path, or by stabilizing nearby methoxy groups due to its strong electronic effect on the surface. Alternatively, this peak may indicate another cluster mediated reaction and not the usual disproportionation reaction. This desorption temperature matches that observed by Vohs [23] for a full monolayer of vanadia, thus we conclude that both disproportionation reactions are possible on the surface as indicated below.

$$\mathrm{V_2O_6H{-}OCH_3 + 5\,c{-}Ti{-}OCH_3 \longrightarrow V_2O_6H + CH_2O + CH_4} \tag{4.2}$$

$$\mathrm{V_2O_6H{-}OCH_3 + 5\,c{-}Ti{-}OCH_3 \longrightarrow V_2O_6H + CH_2O + CH_3OH} \tag{4.3}$$

Immediately following the first TPR experiment, a second run was performed by dosing the surface with 100L methanol and running a standard TPR as soon the surface had returned to room temperature. Figure 4.3 shows the results of this run, in which the R_1 and R_2 states have returned to the expected temperature and intensity on the clean TiO_2 surface. The ratio of R_2/R_1 is now 1.04, indicating that the surface became more reduced and contains a higher concentration of oxygen vacancies than before the first run. The surface however shows no observable water desorption this time, likely due to the much

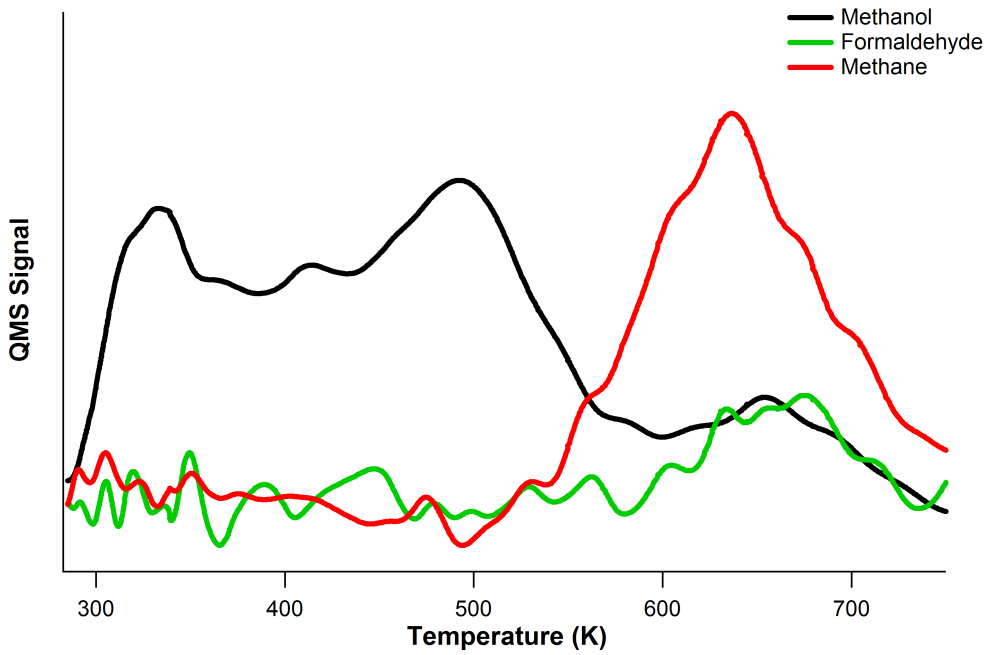

Figure 4.3. Second run methanol TPR of V_2O_6 clusters on the highly reduced surface.

shorter background exposure of 45 min, as compared to 6 hours before the initial TPD experiment. The previously observed methane and formaldehyde desorption states in this temperature range are no longer present, indicating that V_2O_6 has been deactivated for the oxidation of methanol, a common result among this type of experiment in our lab and the literature in general. This loss of activity is attributed to reduction of the cluster to V_2O_5 by the removal of an oxygen atom to form water following the production of formaldehyde at 480 K. At the disproportionation temperature there is only a small formaldehyde desorption similar to the clean surface. However, there is an exceptionally large methane state here, nearly twice what would be expected based on the

amount of formaldehyde. This indicates that after a single run, the surface now favors the deoxygenation of methanol to methane instead of the formaldehyde-methane disproportionation.

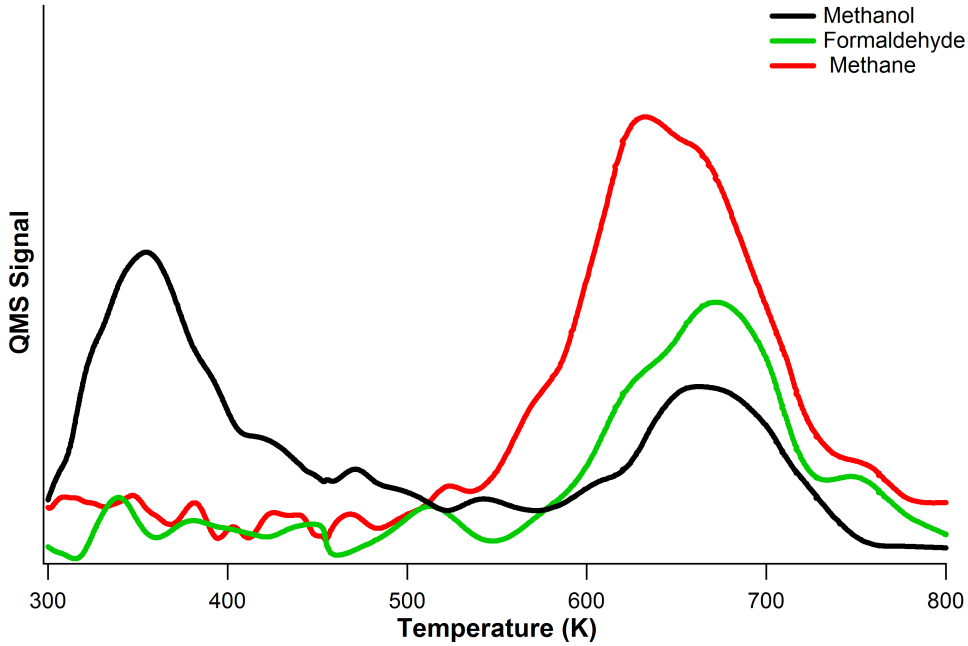

Figure 4.4. Re-oxidized methanol TPR of V_2O_6 clusters on the highly reduced surface.

To see if the activity of the clusters could be regenerated, the cluster decorated surface was exposed to 10 L oxygen prior to the standard dose of 100 L methanol for the re-oxidized run immediately after the sample had returned to room temperature following the second run. As expected, this leads to a R_2/R_1 of around 0.1, indicating that the O_2 was sufficient to heal the surface oxygen vacancies. Neither of the two low temperature formaldehyde or methane states are present as seen in Figure 4.4, clearly demonstrating that the active V_2O_6

cluster cannot be regenerated in this way. This result is in contrast to the work of Vohs where a similar treatment of vanadia with oxygen shows that an active catalyst can be regenerated. The work reported there varies in a few ways, first that experiment see the amount of formaldehyde increases and the desorption temperature decreases with increasing oxygen exposure which is at least four orders of magnitude greater than the dose in this experiment. Additionally, their work was for a full monolayer of vanadia in which reoxidation of clusters does not compete with the healing of TiO_2 vacancies.

Above 600 K there is a broad formaldehyde and methane desorption state that can be deconvoluted in two separate peaks, one centered around 625 K and the other at 675 K. The 625 K state shows all of the characteristics of the clean surface disproportionation reaction from an oxygen exposed surface. The 675K peak likely follows a similar reaction pathway but cluster bound methoxys. No water is observed in conjunction with either desorption state.

4.2 The structure of V_2O_6 on the highly reduced surface

There have only been a few STM of vanadia submonolayer films and isolated clusters on the TiO_2 surface and those results will be summarized briefly here. Madix and co-workers prepared submonolayer films by deposition of vanadium in an oxygen environment on a highly reduced, reconstructed surface [83] at room temperature and was observed to bind atop the Ti_2O_3 added row structure to maximize coordination with oxygen. A more complete study of vanadium and vanadia clusters on a stoichiometric surface by vapor deposition of vanadium in a 5×10^{-8} Torr oxygen environment with the surface heated to 473 K [25]. They found three distinct cluster shapes for vanadium on the surface: single features bound over the 5c-Ti rows or in the upper three-fold hollow site - that is vanadium bound between two bridging oxygen atoms and an in plane oxygen - and as pairs elongated in the [1$\underline{1}$0] direction above the 5c-Ti rows. Our group has shown by STM of size selected vanadium monomers and dimers that these structures correspond to V_2 clusters, V atoms and V pairs respectively [12].

At low vanadium oxide concentration, Netzer observed 2.5 Å double lobed structures bound over the 5c-Ti rows elongated in the [001] direction that become a uniform film of such structures at coverages beyond 2 ML [25]. Our

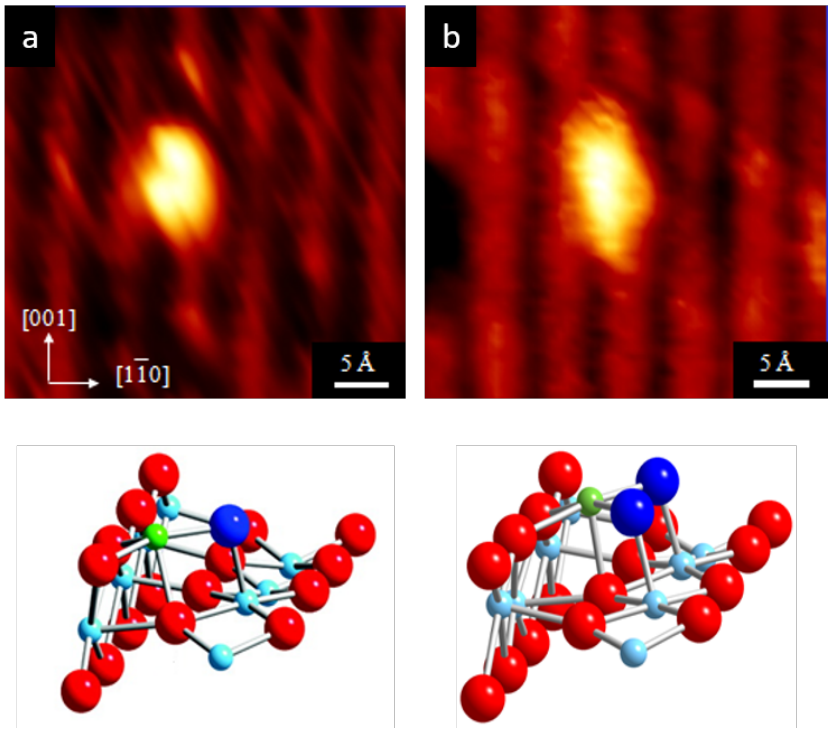

Figure 4.5. STM and corresponding ball-and-stick model representing the lowest energy DFT structure of size selected VO (a) and VO_2 (b) clusters on the reduced surface. Light blue - Ti, red - surface oxygen, dark blue - cluster oxygen, and green - V

group also deposited VO and VO_2 is the report above and found them to be 1.7 Å tall and bound asymmetrically over the Ti rows. This indicates that the vanadium sits in the three-fold upper hollow site, matching the accompanying DFT as seen in Figure 4.5. Post oxidation of VO clusters yields the structures seen marked by the squares in Figure 4.6b have been assigned to VO_3 clusters are 2.3 Å in height due to an out of plane vandyl oxygen. This structure resembles a single unit of the double lobed structures observed by Netzer [25].

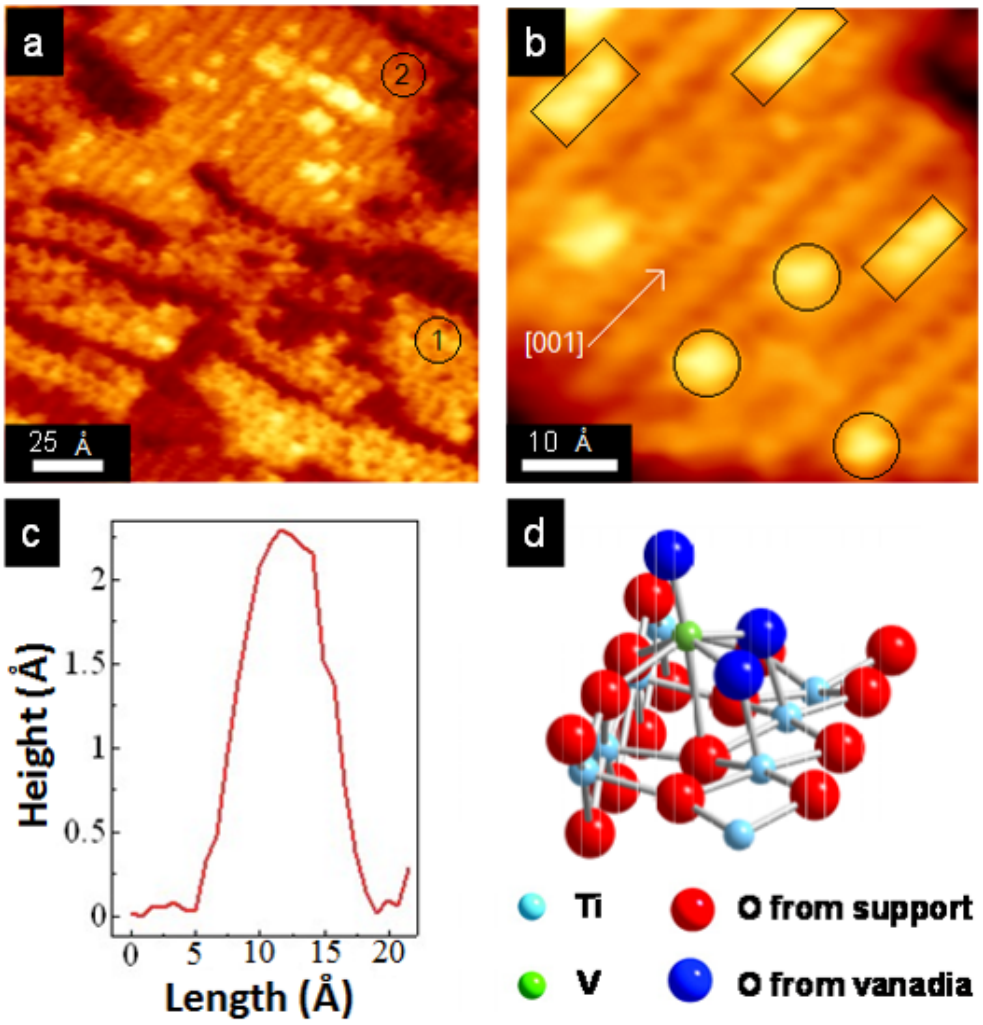

Figure 4.6. (a) Large-area and (b) high-resolution STM images of the VO-decorated TiO_2 surface following oxidation in 2×10^{-6} Torr O_2 at 600 K for 10 min. Numbers 1 and 2 indicate the rosette and characteristic atomic structure with vanadia clusters, respectively. Features marked with a circle are oxygen adatoms, while features marked with a square are vanadia clusters. (c) Line scan in the [001] direction along a vanadia cluster. (d) Proposed structural model for a VO_3 cluster supported on the TiO_2 surface. Reproduced from [28].

A combined STM and DFT study in collaboration with Dr. Kristoffersen and Professor Metiu was employed to understand the structure of isolated vanadium dimeric species on a TiO_2 surface of varying oxidation state. The results presented here highlight the key findings as related to the observed reactivity and further details can be found in [84, 85]. V_2O_5 was chosen for this study as it is still considered the most relevant species for industrial catalysis applications, additionally, we believe that these results can be seen as analogous to those expected for V_2O_6 when combined with the calculated structures for that cluster. For V_2O_5, these authors found that on a stoichiometric surface the cluster should remain intact with both vanadium atoms in the 5+ oxidation state, while on the reduced surface the cluster will dissociate into a VO_3 and a VO_2 group on adjacent 5c-Ti rows as modeled in Figure 4.7. Upon oxygen exposure to the clusters on a reduced surface, the dissociated clusters will each take on the VO_3 stoichiometry and exist in the 5+ oxidation state. The results show that these clusters are highly sensitive to the oxygen vacancies, defects in the substrate, and adsorption of water and oxygen, all of which would be present under steady state reaction conditions.

A large scale STM image of 0.02 ML V_2O_6 deposited on the highly reduced surface is shown in Figure 4.8. Immediately following deposition, the clusters were imaged with a bias of 1.8 V at a constant tunneling current of 0.6 nA. Here

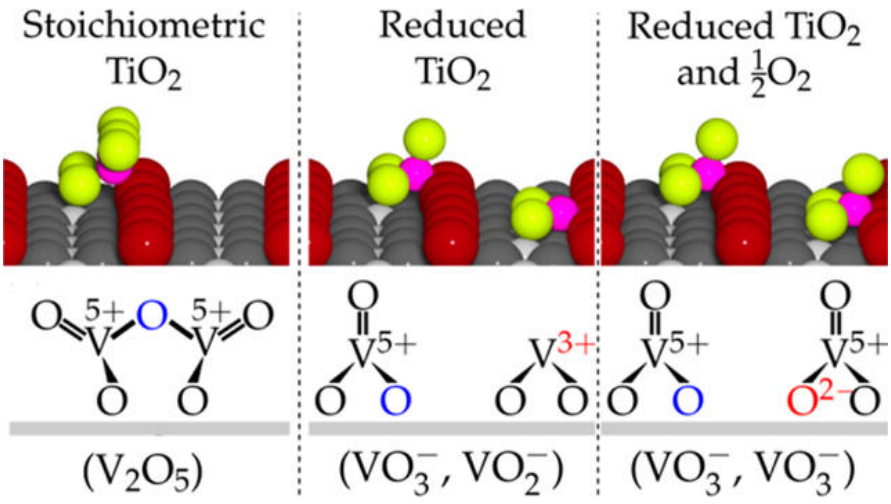

Figure 4.7. Calculated lowest energy structures for an isolated V_2O_5 cluster on a stoichiometric TiO_2 surface, reduced surface, and a reduced surface after exposure to oxygen at room temperature with reaction schematic and assigned oxidation state. Light grey - Ti, dark grey - surface oxygen, red - bridging oxygen, pink - Vanadium, and yellow - cluster oxygen. Reproduced from [85].

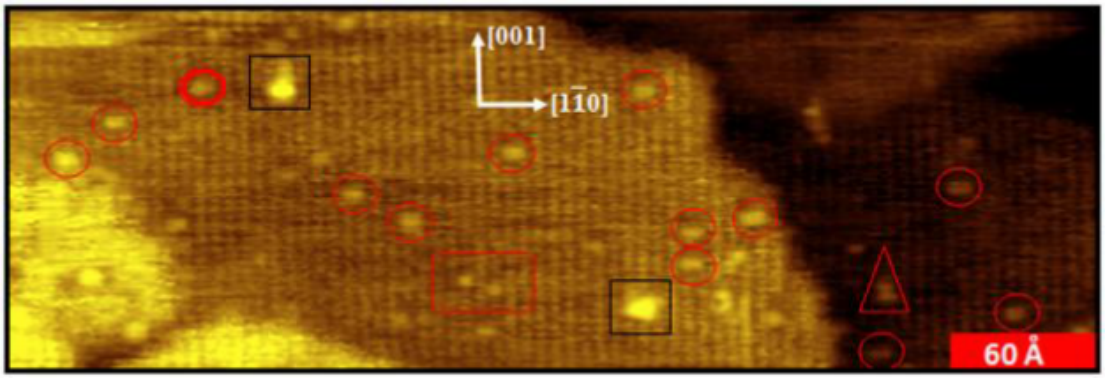

Figure 4.8. A large scale STM image of 0.2 ML V_2O_6 clusters deposited on the reduced TiO_2 surface. Red circles and triangles indicate V_2O_6 clusters, the red rectangle indicates a dissociated cluster and the black squares are assigned to TiO_x islands. Reproduced from [84].

we observe a variety of clusters, about 80% of which are the ones indicated by the thin red circles in the STM image. Clusters of this type have been assigned to the structure seen in Figure 4.9b which consists of two VO_3 units across the bridging oxygen row. The STM line cuts reveal that the lobes these clusters are approximately 2.3 Å in height and are slightly asymmetric due to a different electronic environment for each side of the cluster. This height corresponds to a vanadyl oxygen as observed for post-oxidized VO clusters which were active for ODH of methanol to formaldehyde. As this is the primary cluster type observed on this surface, we believe that this is the structure responsible for the observed activity.

The remainder of the clusters observed in this experiment constitute less than 20% of species on the surface, considering the sensitivity of our TPR method we do not believe that a desorption from these would be discernible from the other states observed. One key finding is that there are very few structures corresponding to the reduction of a V_2O_6 cluster to V_2O_5 and a filled vacancy as was expected. While this process is energetically favored, it is kinetically limited on this surface, indicating that at room temperature movement of clusters across the surface is inhibited by strong binding of the cluster to the surface. Additionally, we observe clusters elongated in the [1$\underline{1}$0] direction in contrast to the typically [001] elongation seen for clusters prepared by re-

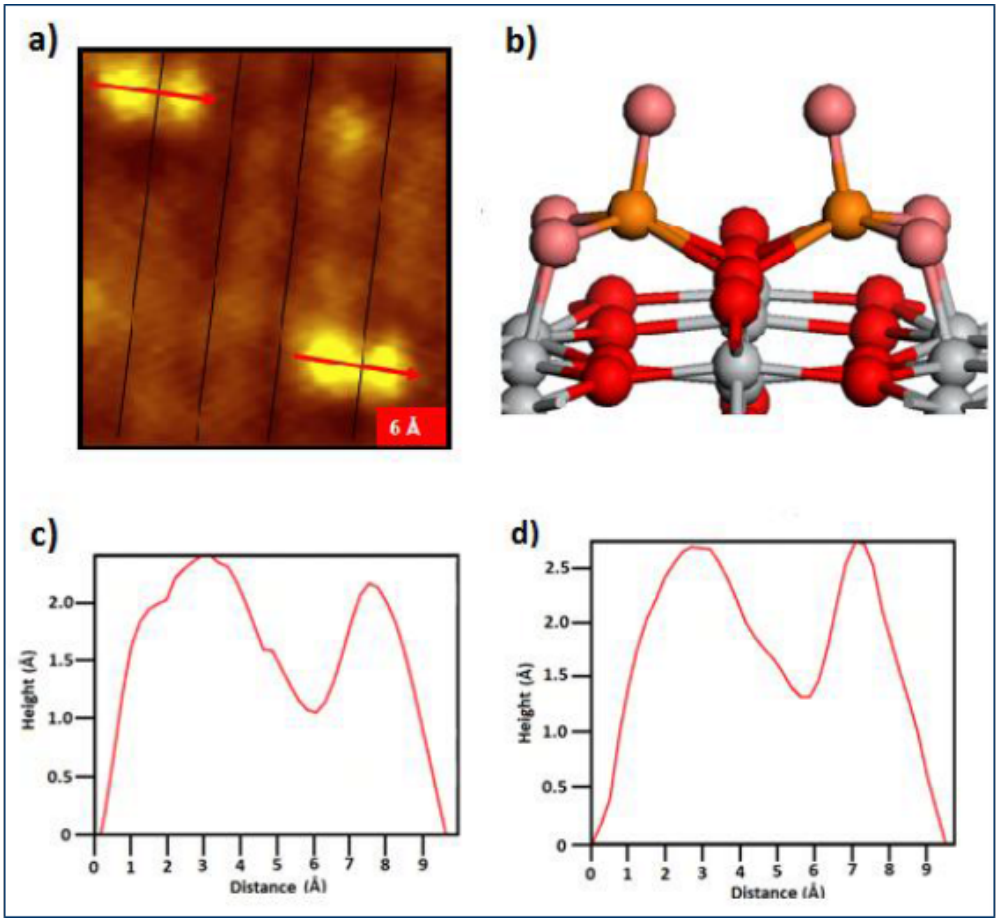

Figure 4.9. (a) A high resolution STM image of 0.2 ML V_2O_6 clusters deposited on the reduced TiO_2 surface, (b) the lowest energy structure for clusters of this type, (c-d) STM line cuts (red lines in a) to support this assignment. Reproduced from [84].

active evaporation. STM of the clusters after the first TPR experiment would provide insight into the structure of the deactivated clusters which may take on the structure observed by others in the literature. A more detailed discussion of each cluster type can be found in [84].

4.3 The reactivity of V_2O_6 on the stoichiometric surface

The lightly reduced surface in created by annealing the highly reduced crystal in 1×10^{-6} torr O_2 for 30 min at 540 K. This creates a nearly stoichiometric surface with around 0.01 ML oxygen vacancies and depletes the near surface region of Ti^{3+} interstitial defects while the bulk of the crystal remains reduced. Treatment in this manner alters the ratio of the R_2/R_1 peaks observed from the clean surface methanol TPD from 0.84 to 0.48 for this less reduced case. Not following the oxygen anneal with a short UHV anneal leaves the surface rougher due to TiO_x islands, but keeps the crystal from becoming more reduced.

For this oxidation, state the R_1 peak has shifted to a maximum at 390 K from 340 K indicating that V_2O_6 is stabilizing Ti-bound methoxy groups. A new methanol and formaldehyde state has emerged between R_1 and R_2 on this run centered around 435 K which comes at the expense of methane desorption. Since these two products are observed simultaneously, this peak is assigned to a cluster mediated disproportionation reaction. The smaller R_2 peak in both the methanol and water on this surface further corroborate that this is an intermediate level of reduction. Finally, very little formaldehyde and no methane is observed over the very broad disproportionation range in this experiment in-

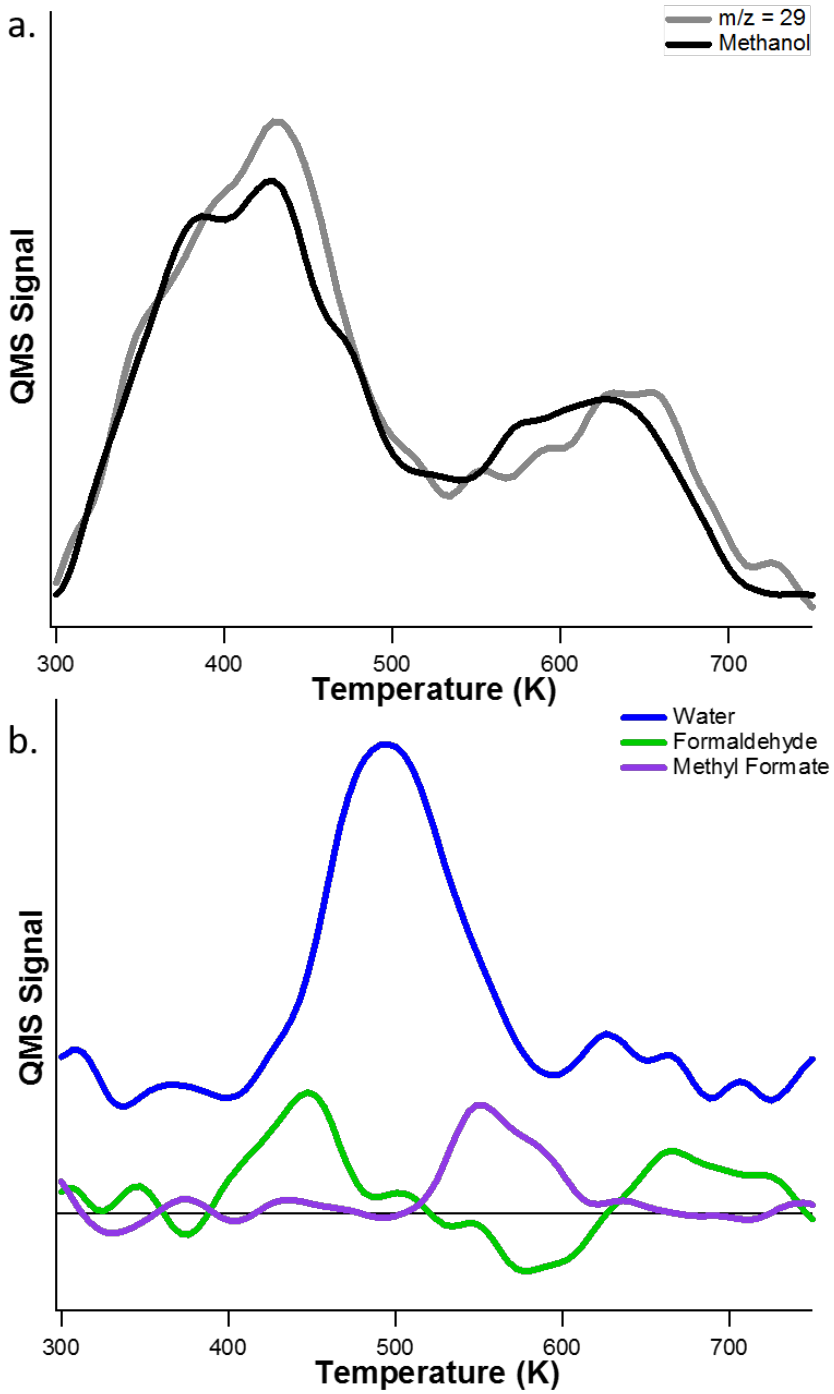

Figure 4.10. Methanol TPR of V_2O_6 clusters on the stoichiometric surface. Water is shown offset for clarity in b.

dicating that it has either been consumed entirely or is producing some other catalytic product.

A further investigation of the negative formaldehyde signal in this region led to the conclusion that the production of methyl formate ($HCOOCH_3$) was responsible for this deviation. To the best of our knowledge this is the first reported production of methyl formate from a vanadia *model* catalyst. There is some evidence to show that V_2O_5/TiO_2 mixed oxide catalysts [81, 86] can produce methyl format and that it can be made photocatalytically on the TiO_2 surface [87]. There are two separate peaks in the methyl formate desorption at 540 and 570 K before formaldehyde returns at the disproportionation reaction. This desorption pattern suggest that some critical amount of formaldehyde must be present on the surface before it can combine with an adjacent methoxy to form methyl formate. This occurs with likely one or both of these species bound to the V_2O_6 cluster as shown in the following reaction where X indicates an unknown binding site for the methoxy and H^* means we do not know the fate of the other hydrogen after reaction.

$$V_2O_6H{-}OCH_2 + X{-}OCH_3 \longrightarrow V_2O_6H + COOCH_3 + H^* \tag{4.4}$$

If water is produced in conjunction with methyl formate desorption, it cannot be easily differentiated from the R_2 water state desorbing at the same temper-

ature. Based on the reduced surface it could be expected that the H atoms left over from the production of methyl formate could react to form water and remove an oxygen from the cluster. Additionally, there are two new water states at 625 and 675 K. The first corresponds to the crossover from production of methyl formate to formaldehyde and the second to the peak of formaldehyde desorption at high temperature. Water is not typically observed from the disproportionation reaction of the clean surface and was not seen with V_2O_6 on the highly reduced surface. From this, we conclude that this water likely comes from cluster bound hydroxyls formed during the production of methyl formate. We were unable to complete an STM investigation of these clusters due to surface roughness introduced by the oxygen annealing process.

4.4 The reactivity of V_2O_6 on the oxidized surface

The oxidized surface is created when the highly reduced surface is exposed to an additional 10 L of O_2 at room temperature to heal the remaining vacancies and create oxygen adatoms on the surface via the dissociative adsorption of molecular oxygen. Treatment in this manner has three primary effects on the deposited clusters: they cannot be reduced by landing near an oxygen vacancy and donating and oxygen atom to heal it, the cluster can potentially react with

the oxygen adatoms to form a more oxidized cluster, or it can simply land near an oxygen adatom which has the potential to facilitate other reaction pathways. This method is most similar to that used by other groups, but the sample is not heated prior to examining the catalytic activity. By not heating the sample or exposing to an extreme excess of oxygen (>100L), bulk defects such as Ti^{3+} interstitials will remain and may influence the reaction.

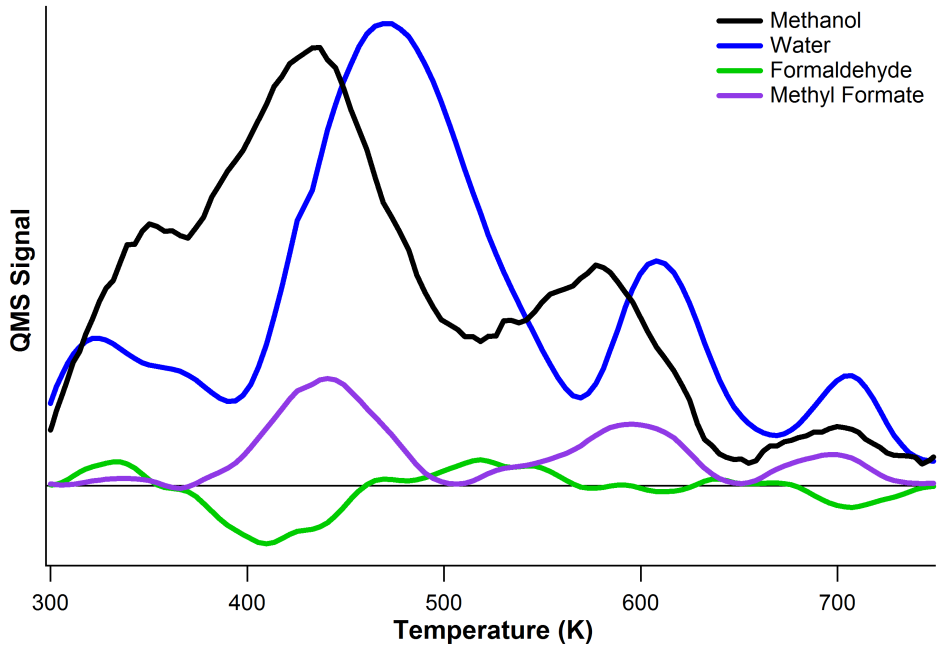

Figure 4.11. Methanol TPR of V_2O_6 clusters on the oxidized surface.

Figure 4.11 shows the first run methanol TPD for the deposition of 0.05 ML soft-landed V_2O_6 on the oxidized surface. It should be noted that this is half the cluster coverage from the experiments preformed on the reduced surface and that should be taken into account when comparing relative magnitudes in

TPD spectra. Methanol desorption shows the R_1 state is present at 355 K as expected for a clean surface. The second major peak occurs at 440 K and is preceded by a small shoulder. The shoulder matches the temperature of the R_1 state observed for a V_2O_6 cluster decorated reduced surface and the peak is consistent with desorption of cluster bound methoxies. The coexistence of these two states indicate that 5c-Ti bound methoxy groups are not saturated by clusters on the surface giving rise to two separate peaks here.

As expected, there is no clear R_2 state due to the absence of oxygen vacancies after oxidizing the surface. The cluster mediated state at 575 K also appears on this surface, but the disproportionation reaction either doesn't appear or is shifted to nearly 700 K which would again implicate strong interaction between the cluster and methoxy groups. In all of these desorption states there is no significant deviation of 29 from 31, with little to no formaldehyde being produced in this experiment. There are three methyl formate peaks observed from this surface, all of which correspond cluster bound methanol desorption states.

4.5 The structure of V_2O_6 on the oxidized surface

A representative large scale STM image of 0.02 ML V_2O_6 clusters on the oxidized surface is shown in Figure 4.12. The asymmetric structure seen here

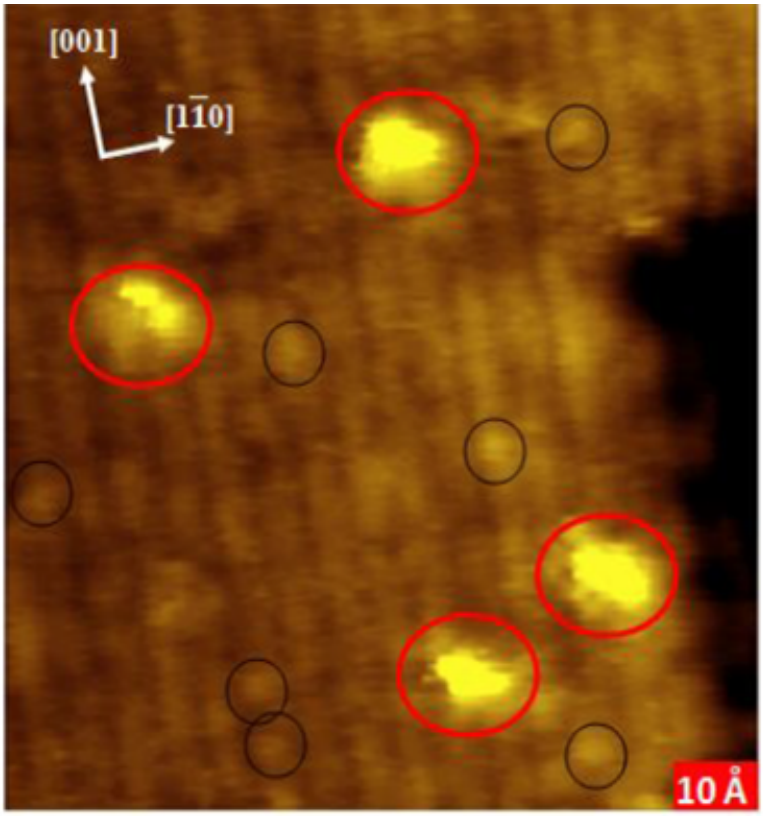

Figure 4.12. STM image of V_2O_6 clusters on the oxidized surface. Red and black circles indicate clusters and oxygen adatoms respectively. Reproduced from [84].

accounts for approximately 90% of cluster in the images taken on this surface. The clusters almost always appear blurry or distorted while the row structure and oxygen adatoms appear clearly which could indicate a unique electronic effect in these clusters. If this was simply due to a bad STM tip or an oxygen molecule attached to the end of the tip the poor resolution would impact the entire image, thus there some real effect as the tip passes over the cluster. To understand what could cause this, one must look to the gas phase struc-

ture of the V_2O_6 cluster, as seen in Figure 4.13 where each vanadium had one vanadyl bound oxygen and is connected to the other by an asymmetric two oxygen bridge. Additionally, one vanadium atom contains a highly reactive peroxyl (O_2^-) group. It is unclear if this moiety could survive deposition as there have been no reports in the literature indicating a peroxyl group of any type on the TiO_2 surface.

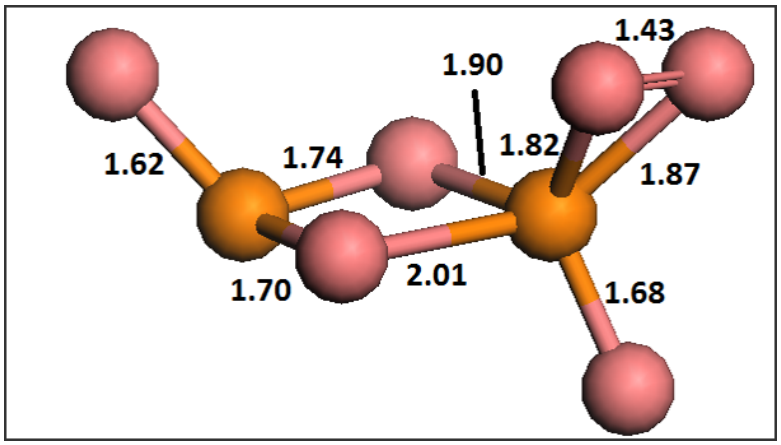

Figure 4.13. DFT calculated gas phase structure of $V_2O_6^+$ with bond lengths in Å. Orange and pink balls represent vanadium and oxygen atoms respectively.

Figure 4.14a-b shows a high resolution STM image of a single cluster with the corresponding line cut across it indicated by the red line. The height of the taller lobe is 2.3 Å which is consistent with a VO_3-like structure with a vanadyl oxygen, while the smaller lobe is only about 1.3 Å tall. This height is shorter than any observed for vanadium or vanadium oxide cluster by our group, even V monomers were observed to be 1.7 Å tall. It is important to remember that

apparent height in STM depends not only on the topography of the surface, but also on the ability to tunnel electrons into the surface. It should be clear that a peroxyl group has a low density of available states, thus would appear much shorter than its topography would suggest. Therefore, we assign this cluster to the structure seen in Figure 4.14c and propose that the peroxyl group unique to this system is responsible for the production of methyl formate. Further DFT investigation would be required to determine a specific mechanism for the coupling of two methoxy groups to complete this reaction.

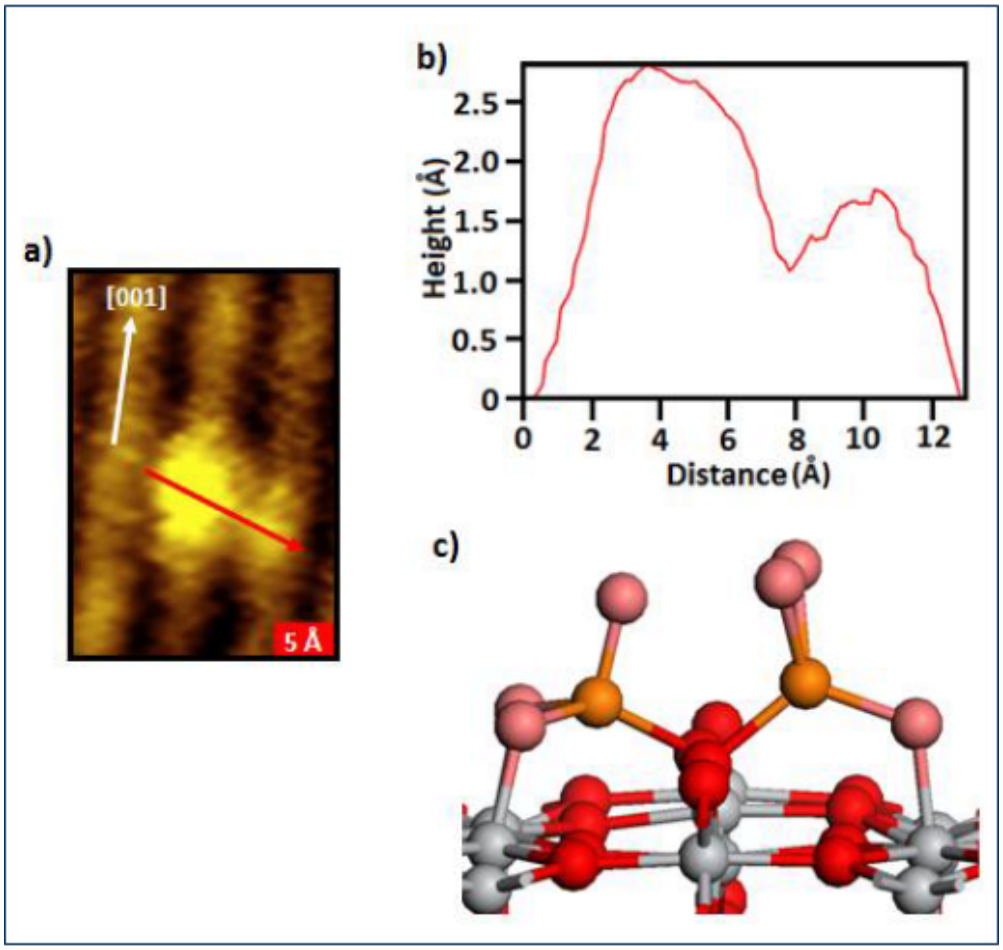

Figure 4.14. (a) High resolution STM image of a single V_2O_6 cluster on the oxidized surface. (b) height line cut of the cluster as indicated by the red line in (a). (c) Assigned DFT structural model of the cluster, grey - titanium, red - surface oxygen, pink - cluster oxygen, orange - vanadium. Reproduced from [84].

Chapter 5

The Structure and Reactivity of Other V_2O_x and V_3O_9 Clusters on the TiO_2 Surface

5.1 The reactivity of V_2O_5 on the stoichiometric surface

V_2O_5 was investigated as this species is presumed to be the active bulk catalyst for the conversion of methanol to formaldehyde. This assignment is made using the detected 5+ oxidation state observed by XPS but other evidence has

not yet been put forth to support this claim. The results presented here also suggest that the V_2O_6 cluster is reduced to V_2O_5 either upon landing on the reduced surface and one oxygen being used to heal a nearby O_v or upon reaction with methanol to form formaldehyde or methyl formate and subsequently water. Thus, if V_2O_5 is deposited on a nearly stoichiometric surface it should not lose an oxygen to a O_v and resemble the activity of the second run for V_2O_6.

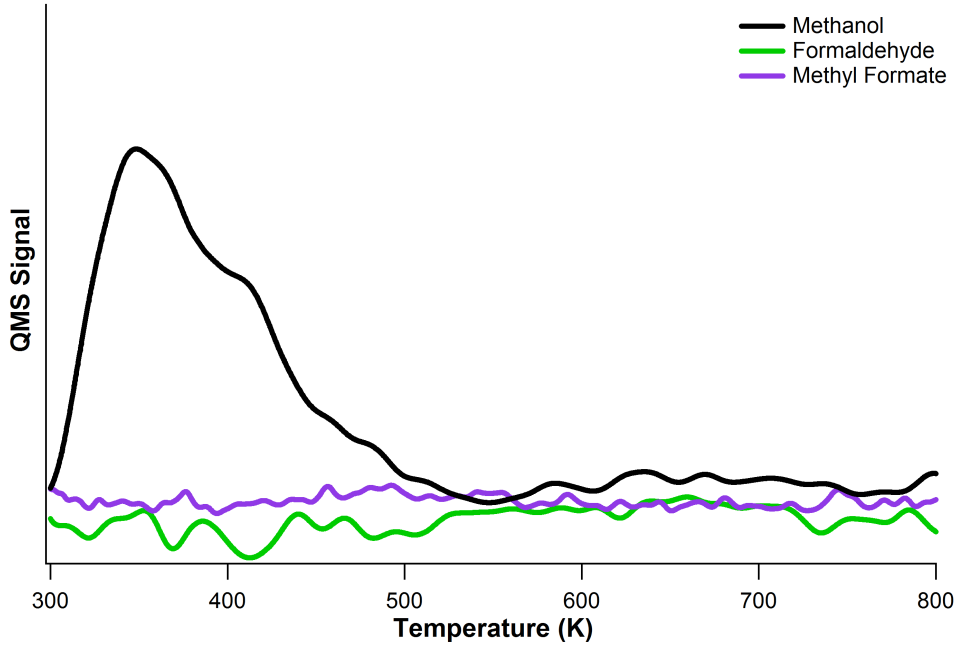

Figure 5.1. Methanol TPR of V_2O_5 clusters on the stoichiometric surface.

The stoichiometric surface in created by annealing the moderately reduced reduced crystal in 1×10^{-6} Torr O_2 for 30 min at 840 K followed by a 10 minute anneal in UHV at the same temperature to flatten the surface. This creates a nearly stoichiometric surface with less than 0.01 ML oxygen vacancies and

depletes the near surface region of Ti^{3+} interstitial defects while the bulk of the crystal remains somewhat reduced. Figure 5.1 shows the results for the first run methanol TPR of the stoichiometric TiO_2 surface decorated with 0.05 ML V_2O_5 clusters. The methanol desorption resembles that of the clean surface with a broad R_1 state with a tail extending to nearly 500 K and a lack of a discernible R_2 state. In contrast to the clean surface, there is no disproportionation state occurring on this surface. This is likely due to this crystal being less reduced before annealing than the comparable clean surface, which would result in a lack of Ti^{3+} interstitials near the surface that methoxies could interact with to produce this state. The V_2O_5 clusters could be bound strongly to the few defects present, further reducing defect interaction with methanol at the surface.

Additionally there is no formaldehyde, methyl formate, or methane desorption observed, indicating that V_2O_5 clusters are not responsible for the observed catalytic activity of this system. This leads to the conclusion that the methane and formaldehyde observed for the second run V_2O_6 TPR is due only to the reduced support and not to the deactivated clusters. These results are in contrast to the work of Madix and Vohs [22, 24] who claim that V_2O_5 is responsible for the oxidative dehydrogenation of methanol to formaldehyde. In their work, the clusters were prepared by annealing in oxygen at pressures up to 1×10^{-3} Torr and lower temperatures that used in this investigation. Thus, with the observed

sensitivity of these cluster to the surface oxidation state, it may be possible that V_2O_5 clusters on a highly oxidized surface are active for this reaction.

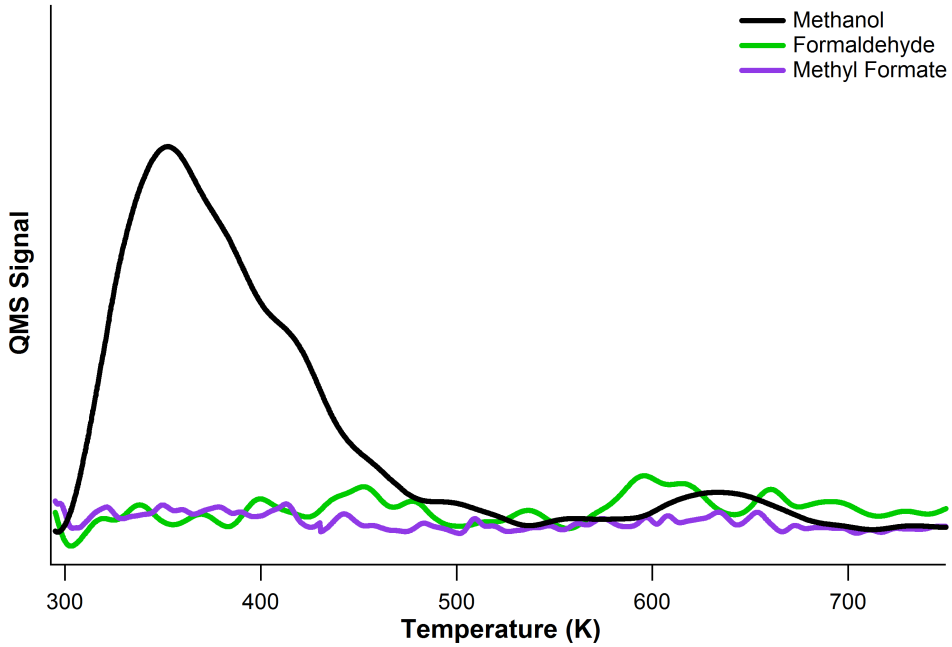

Figure 5.2. Methanol TPR of re-oxidized V_2O_5 clusters on the stoichiometric surface.

In an attempt to activate these cluster by oxidation, the cluster decorated surface was exposed to 10 L O_2 at room temperature following the first run TPR. The results shown in 5.2 are nearly identical to the previous run, indicating that this treatment was insufficient to create an active catalyst. There is a small hint of the disproportionation reaction in this experiment due to the stabilizing nature oxygen atoms have on adsorbed methanol.

5.2 The reactivity of V_2O_7 on the reduced surface

In a similar attempt to create another V_2O_6 like structure, V_2O_7 clusters were deposited on a reduced surface with the goal that the cluster would be reduced upon healing an O_v. The methanol TPR spectra for 0.05 ML V_2O_7 on a highly reduced surface (R_2/R_1 = 0.81 before deposition) is shown in Figure 5.3. This experiment yields much greater changes to the surface chemistry than was observed for V_2O_5 clusters. Across the entire temperature range, there are no clear water or methyl formate desorption states observed for this cluster decorated surface. There is a clear enhancement of the methanol R_1 desorption state due to increased adsorption of methanol on the surface induced by the presence of these clusters. The observed R_2/R_1 ratio decreased sharply to 0.50, attributed to both the increase in the R_1 state intensity and by V_2O_7 clusters healing a significant fraction of O_v on the surface. As seen with V_2O_6, there is a methanol desorption state centered at 450 K between the two recombination states with a small corresponding formaldehyde desorption peak. This is attributed to a disproportionation reaction between a cluster bound and vacancy bound methoxy with the decreased intensity assigned to either the lower concentration of O_v on this surface or to the lower affinity for this cluster to facilitate the reaction.

The ratio of products observed around 630 K is quite similar to that of a

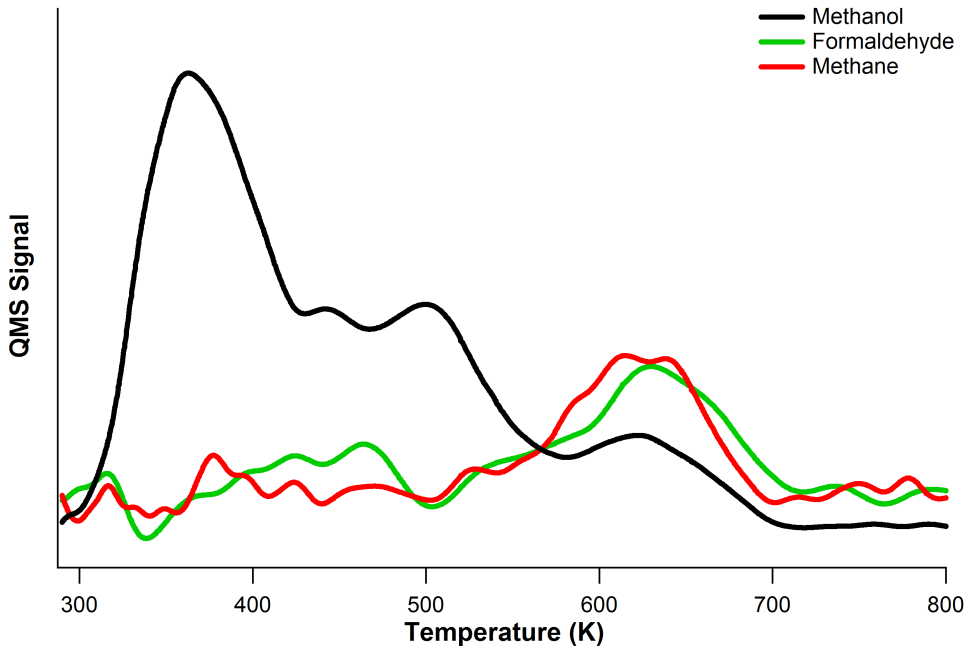

Figure 5.3. Methanol TPR of V_2O_7 clusters on the highly reduced surface.

clean, reduced surface. In this case there is more formaldehyde than expected indicating a shift in the ratio of the two disproportionation reactions and the deoxygenation reactions. It is possible that favoring the methanol-formaldehyde reaction is caused by the cluster, but could simply be an effect of the TiO_2 having a slightly different oxidation state than before the deposition.

Upon a second run of methanol TPR, the V_2O_7 decorated surface was deactivated and showed a desorption spectrum indistinguishable from the clean, reduced surface. A subsequent re-oxidized run was performed by exposing the cluster decorated surface to 10 L O_2 at room temperature following the second run and the results are shown in Figure 5.4. Here the R_1 methanol state has

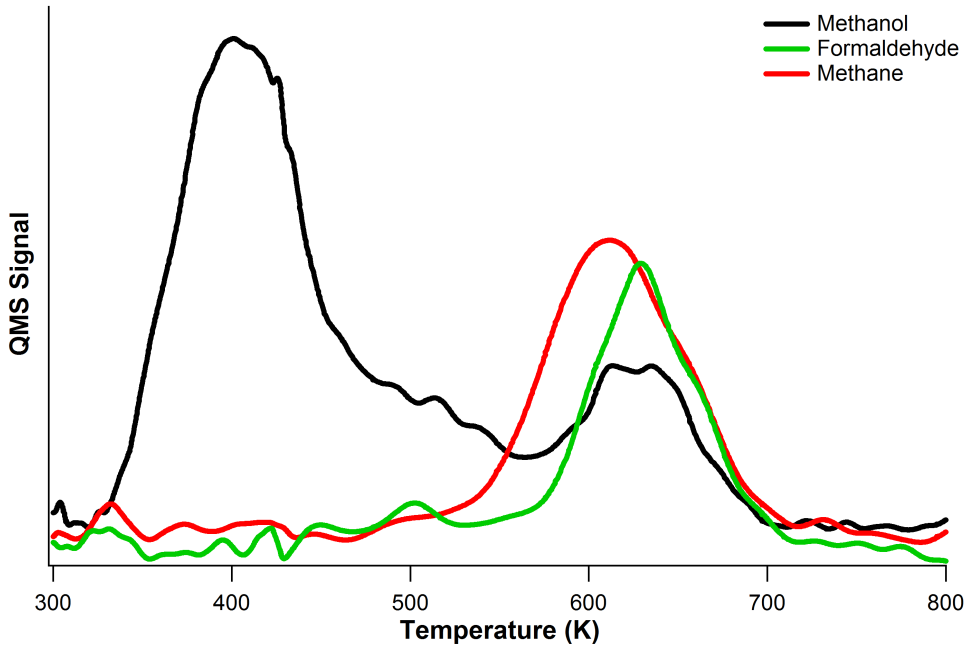

Figure 5.4. Re-oxidized methanol TPR of V_2O_7 clusters on the highly reduced surface.

shifted nearly 40 K higher to be centered around 400 K due to strong binding of methoxies by the oxygen activated cluster. There is an intense desorption of methane, formaldehyde, and methanol between 600 and 700 K that is much larger than would be expected for a clean surface oxidized in the same manner. This is the most significant change observed for a cluster decorated surface. These results imply that the V_2O_7 undergoes reduction upon landing to a modified V_2O_6 structure or cluster decomposition into two VO_3 groups. Given that this matches the observed activity for VO_3 cluster produced by post-oxidation of VO [28], we conclude that that both of these cluster modifications occur simultaneously and can be partially reversed by this light oxidation procedure.

5.3 The reactivity of V_3O_9 on the reduced surface

As show the the previous experiments, methanol ODH is highly sensitive to the cluster composition and structure on the surface. While VO_3 and V_2O_6 are both highly active for this reaction, V_2O_5 is completely inactive and V_2O_7 shows only moderate activity. Here we investigate the deposition of 0.05 ML V_3O_9 on the highly reduced surface, which should also be highly active if it maintains a vanadyl or peroxyl group upon landing. Figure 5.5 shows the methanol TPR results for 100 L methanol dosed at room temperature. The methanol trace shows the R_1 , R_2 , and disproportionation reactions occurring within 10 K of the values observed on the clean surface and a small desorption state at 440 K which has previously be attributed to recombinative desorption of methanol from the cluster. The R_2/R_1 ratio observed is about 0.50, a sharp reduction from 0.81 observed before cluster deposition. This change is likely due to reduction of the V_3O_9 cluster to heal oxygen vacancies. The change in the R_2/R_1 ratio is much larger than for other clusters on the highly reduced surface, indicating that the cluster is less stable and more likely to dissociate than V_2O_6 clusters.

On this surface we observe methyl formate desorption a 360 K, the lowest temperature desorption state of any methanol ODH product reported in this work. The low intensity observed here indicates that there may be a wide dis-

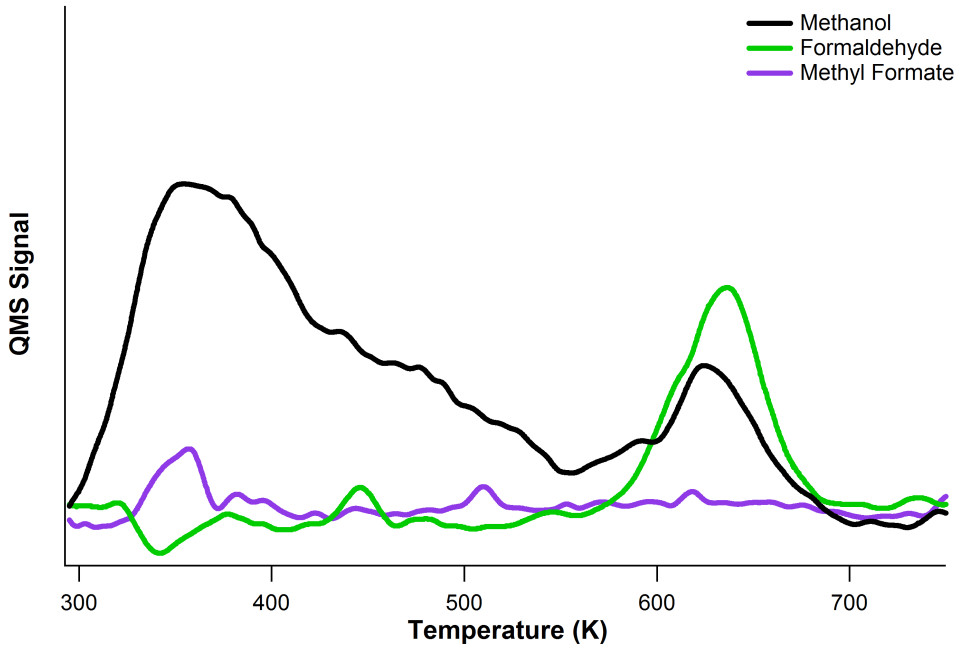

Figure 5.5. Methanol TPR of V_3O_9 clusters on the highly reduced surface.

tribution of cluster stoichiometries present on the surface and this state comes from only a small fraction of clusters capable of carrying out this reaction. The lack of any higher temperature desorption peaks for methyl formate, as seen on V_2O_6, helps corroborate the notion that these clusters are less stable than others investigated and that the structure changes as the sample is heated allowing it to reach an equilibrium configuration with a barrier too large to overcome at room temperature.

There is a small formaldehyde desorption state coinciding with methanol at 440 K, giving further evidence to a cluster mediated disproportionation occurring with vacancy bound methoxys. Again the small intensity of this peak

furthers the idea that there is a variety of cluster types present on the surface. At high temperature, there is an intense formaldehyde desorption, roughly comparable to that for post-oxidize VO clusters, implying that some V_3O_9 contains a vanadyl group. Interestingly, the center of the formaldehyde peak is about 15 K higher than the one for methanol, where for other clusters formaldehyde precedes methanol due to the reaction to form methane and formaldehyde. There was an error in collecting the methane signal in this case, but it would likely be observed between 600 and 700 K as on similar systems.

We would have liked to investigate this cluster further with multiple runs on the same surface and with other surface oxidation states. However, due to technical difficulties with the instrument and irreversible contamination (addressed in the Appendix) of the TiO_2 substrate these experiments were not possible, but should be examined in future work.

5.4 The structure of V_3O_9 on the reduced surface

The lowest energy gas phase structure of $V_3O_9^+$ as determined by DFT is shown in Figure 5.6 where each vanadium atom is in the 5+ oxidation state and the cluster contains four bridging oxygen atoms, one vanadyl group, and two peroxyl groups[88]. Studies of neutral clusters on the gas phase has shown

that this cluster is much more likely to decompose than V_2O_6 upon collision with other molecules [89]. Thus it is possible that not all clusters on the surface represent a true V_3O_9 stoichiometry due to these collisions, but based on our experimental set up this should not be a major effect.

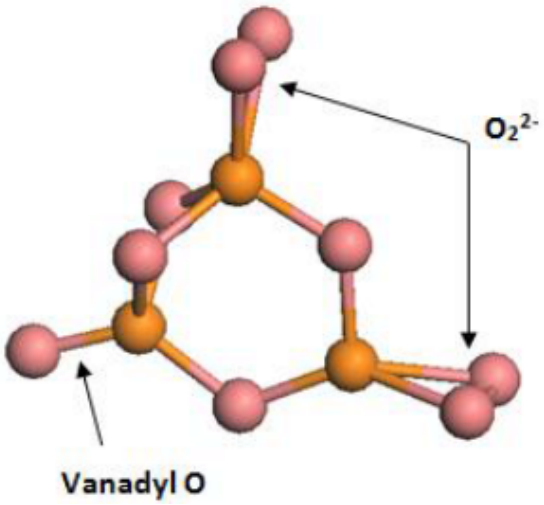

Figure 5.6. Gas-phase structure of $V_3O_9^+$ as determined by DFT from [88].

Figure 5.7 shows a large scale STM of 0.02 ML with similar cluster types marked with the same shape. The density of clusters observed on the surface appears to be much higher than the estimated 0.02ML that was deposited. This discrepancy is likely due to the fact that the cluster beam is evenly distributed across the surface, and images from other locations on the sample do in fact show a lower density of clusters.

We observe four distinct cluster geometries on the surface with none clearly in the majority as observed with other cluster types. A high-resolution STM im-

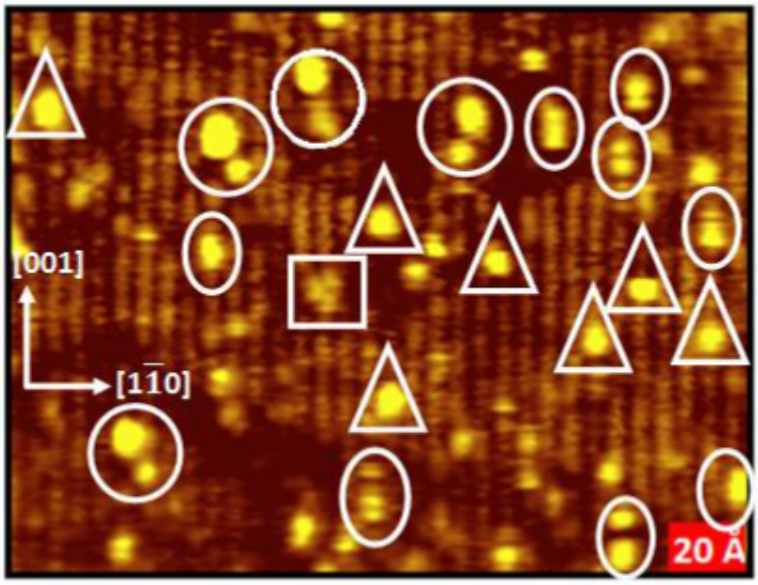

Figure 5.7. Large scale STM image of V_3O_9 on the reduced surface, similar clusters are marked with the same shape. Reproduced from [84].

age of the clusters marked with the circle consists of one large lobe and a smaller one which appears in the adjacent row offset by one unit cell is shown in Figure 5.8 with the indicated height profile. The height of the larger lobe is 6.5 Å and the smaller lobe is 3.5 Å , both of which are taller than any structure observed for V_2O_6 clusters. Without DFT calculations of the cluster on the surface it is impossible to make a definitive structural assignment based on STM alone, yet we predict, based on the gas-phase structure that this cluster type could correspond to it adsorbing with the orientation shown in Figure 5.6. It is likely that such an arrangement would cause a ring opening leaving a V_2O_5 on one side of the bridging oxygen row in which a vanadium atom sits on top of the row and VO_4

on the other which could account for the larger than expected height from the smaller lobe.

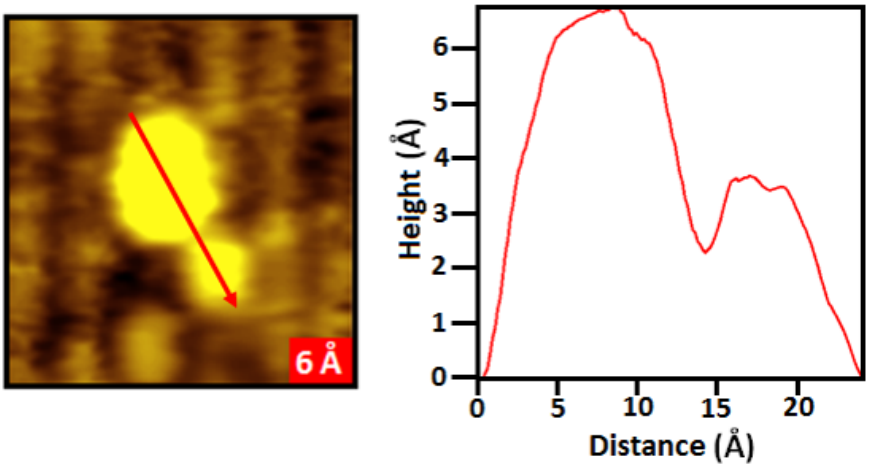

Figure 5.8. High-resolution STM image of the V_3O_9 marked with a circle in figure 5.7 on the reduced surface. Reproduced from [84].

The length and height of the clusters marked with an oval corresponds well to one of the less frequently (5%) observed V_2O_6 clusters on the reduced surface where the cluster binds intact to the 5c-Ti row and maintains the bridging oxygen rin structure with two vanadyl oxygen atom creating the observed two lobe structure. The clusters marked with a triangle correspond to the size of the smaller lobe observed for the circle clusters, providing strong evidence for the dissociation of V_3O_9 upon landing on the surface as the two components of the larger cluster have been accounted for. The last cluster type, marked with a square, appears as three short lobes in a roughly triangular shape each with a height of 2.5 Å . This could be the V_3O_9 landing intact with its 6-membered

ring lying parallel to the surface, but might also be three adjacent VO_3 members interacting to cause a slight increase in height compared to isolated vanadyl containing groups.

From these results, we conclude that the low temperature methyl formate production is most likely due to the clusters marked by the square as that structure does not occur with other clusters and its low concentration is compatible with the small desorption intensity. We also attribute the high temperature formaldehyde production to the wealth of vanadyl structures observed on the surface.

Chapter 6

Conclusions and Future Directions

We have shown the catalytic activity and selectivity of size-selected V_xO_y clusters on the TiO_2 surface depend sensitively on cluster stoichiometry and the oxidation state of the surface which controls the structure of the cluster. For V_2O_6 clusters on the reduced surface, there was a broad multi-state desorption of methane and formaldehyde attributed to the vanadyl groups present in the cluster. On the oxidized surface, V_2O_6 clusters were active for formaldehyde and methyl formate production. This is the first report of methyl formate production from a vanadia/titania system, and we attribute this reactivity to the peroxyl groups in the cluster which are not formed by other methods. The presumed active species for bulk catalysis, V_2O_5, was not active for methanol ODH on the

stoichiometric surface, indicating the the species we have deposited is not the one present in other reports of vanadia/titania catalysts. V_2O_7 clusters on the reduced surface underwent the largest change upon landing, but showed only a slight enhancement in formaldehyde production. The cluster was reduced by loss of an oxygen and healed a significant number of oxygen vacancies. V_3O_9 clusters on the reduced surface were active for methyl formate production just above room temperature and for increased formaldehyde production at high temperature. This activity was attributed to the presence of two types of clusters, one containing a vanadyl oxygen and another contain a peroxyl group.

We believe that there results demonstrate a correlation between the vanadyl and peroxyl moieties in clusters with $(VO_3)_n$ stoichiometry and particular reaction pathways for the oxidation of methanol. I propose that the following experiments should be conducted to further explore the generality of this phenomenon. First, we should investigate the structure and reactivity of V_3O_9 clusters on stoichiometric and oxidized surface to see if methyl formate production is enhanced due to the survival of more peroxyl groups as was seen with V_2O_6. However, it is possible that with a cluster this large some rearrangement on the surface is inevitable and could lead to other unique oxidation products. Second, the structure of V_2O_5 and V_2O_7 should also be investigated to better understand their lack of activity. V_2O_5 clusters should also be prepared with an oxygen an-

neal following deposition in an attempt to recreate the catalyst made by reactive evaporation of vanadium. Finally, this method can be extended to larger clusters of $(VO_3)_n$ stoichiometry such as V_4O_{12}. DFT becomes more difficult with clusters this large as more structures are possible, but it becomes more critical as tool for interpreting the results from STM.

Bibliography

[1] M Boudard. Size dependence in catalysis. *Advances in Catalysis*, 20(153), 1966.

[2] Helmut Poppa. Model studies in catalysis with UHV-deposited metal particles and clusters. *Vacuum*, 34(12):1081–1095, 1984.

[3] Masatake Haruta. Size- and support-dependency in the catalysis of gold. *Catalysis Today*, 36(1):153–166, 1997.

[4] M. Haruta, S. Tsubota, T. Kobayashi, H. Kageyama, M. J. Genet, and B. Delmon. Low-Temperature oxidation of CO over gold supported on TiO_2 , α-Fe_2O_3, and Co_3O_4. *Journal of Catalysis*, 144(1):175–192, 1993.

[5] Toshio Hayashi, Koji Tanaka, and Masatake Haruta. Selective vapor-phase epoxidation of propylene over Au/TiO_2 catalysts in the presence of oxygen and hydrogen. *Journal of Catalysis*, 178:566–575, 1998.

[6] Masatake Haruta. Gold as a novel catalyst in the 21st century: Preparation, working mechanism and applications. *Gold Bulletin*, 37(1-2):27–36, 2004.

[7] A. Sanchez, S. Abbet, U. Heiz, W.-D. Schneider, H. Hkkinen, R. N. Barnett, and Uzi Landman. When gold is not noble: Nanoscale gold catalysts. *The Journal of Physical Chemistry A*, 103(48):9573–9578, 1999.

[8] X. Tang, J. Schneider, A. Dollinger, Y. Luo, A. S. Wrz, K. Judai, S. Abbet, Y. D. Kim, G. F. Gantefr, D. H. Fairbrother, U. Heiz, K. H. Bowen, and S. Proch. Very small window of opportunity for generating CO oxidation-active Au_n on TiO_2 . *Physical Chemistry Chemical Physics*, 16(14):6735–6742, 2014. 36g.

[9] William E. Kaden, Tianpin Wu, William A. Kunkel, and Scott L. Anderson. Electronic structure controls reactivity of size-selected Pd clusters adsorbed on TiO_2 surfaces. *Science*, 326(5954):826–829, 2009.

[10] Sungsik Lee, Chaoyang Fan, Tianpin Wu, and Scott L. Anderson. Cluster size effects on CO oxidation activity, adsorbate affinity, and temporal behavior of model Au_n–TiO_2 catalysts. *The Journal of Chemical Physics*, 123(12):124710, 2005.

[11] Bert M. Weckhuysen and Daphne E. Keller. Chemistry, spectroscopy and the role of supported vanadium oxides in heterogeneous catalysis. *Catalysis Today*, 78(14):25–46, 2003.

[12] Scott P. Price, Xiao Tong, Claron Ridge, Vladimir Shapovalov, Zhenpeng Hu, Paul Kemper, Horia Metiu, Michael T. Bowers, and Steven K. Buratto. STM characterization of size-selected V_1, V_2, VO, and VO_2 clusters on a TiO_2 (110)-(1$\times$1) surface at room temperature. *Surface Science*, 605(910):972–976, 2011.

[13] Fred Roozeboom, Peter D. Cordingley, and Paul J. Gellings. Vanadium oxide monolayer catalysts: The vapor-phase oxidation of methanol. *Journal of Catalysis*, 68(2):464–472, 1981.

[14] Marianne Engeser, Detlef Schrder, and Helmut Schwarz. Gas-Phase dehydrogenation of methanol with mononuclear vanadium-oxide cations. *Chemistry A European Journal*, 11(20):5975–5987, 2005.

[15] Pio Forzatti, Enrico Tronconi, Ahmed S. Elmi, and Guido Busca. Methanol oxidation over vanadia-based catalysts. *Applied Catalysis A: General*, 157(12):387–408, 1997.

[16] Nist standard reference database 69: Nist chemistry webbook. 2016.

[17] Timothy J. Held and Frederick L. Dryer. A comprehensive mechanism for methanol oxidation. *International Journal of Chemical Kinetics*, 30(11):805–830, 1998.

[18] Janet N. Allison and William A. Goddard. Oxidative dehydrogenation of methanol to formaldehyde. *Journal of Catalysis*, 92(1):127–135, 1985.

[19] G. Deo and I. E. Wachs. Reactivity of supported vanadium oxide catalysts: The partial oxidation of methanol. *Journal of Catalysis*, 146(2):323–334, 1994.

[20] Israel E. Wachs. Recent conceptual advances in the catalysis science of mixed metal oxide catalytic materials. *Catalysis Today*, 100(12):79–94, 2005.

[21] Hyun You Kim, Hyuck Mo Lee, and Horia Metiu. Oxidative dehydrogenation of methanol to formaldehyde by a vanadium oxide cluster supported on rutile TiO_2 (110): Which oxygen is involved? *The Journal of Physical Chemistry C*, 114(32):13736–13738, 2010.

[22] Qinggen Wang and Robert J Madix. Partial oxidation of methanol to formaldehyde on a model supported monolayer vanadia catalyst: vanadia on TiO_2 (110). *Surface Science*, 496(12):51–63, 2002.

[23] G. S. Wong, D. D. Kragten, and J. M. Vohs. The oxidation of methanol to formaldehyde on TiO_2 (110)-supported vanadia films. *The Journal of Physical Chemistry B*, 105(7):1366–1373, 2001.

[24] G. S. Wong, M. R. Concepcion, and J. M. Vohs. Reactivity of monolayer V_2O_5 films on TiO_2 (110) produced via the oxidation of vapor-deposited vanadium. *Surface Science*, 526(3):211–218, 2003.

[25] S Agnoli, M Sambi, G Granozzi, C Castellarin-Cudia, S Surnev, M. G Ramsey, and F. P Netzer. The growth of ultrathin films of vanadium oxide on TiO_2 (110). *Surface Science*, 562(13):150–156, 2004.

[26] Hyun You Kim, Hyuck Mo Lee, Raj Ganesh S. Pala, and Horia Metiu. Oxidative dehydrogenation of methanol to formaldehyde by isolated vanadium, molybdenum, and chromium oxide clusters supported on rutile TiO_2 (110). *The Journal of Physical Chemistry C*, 113(36):16083–16093, 2009.

[27] Luca Artiglia, Stefano Agnoli, Andrea Vittadini, Alberto Verdini, Albano Cossaro, Luca Floreano, and Gaetano Granozzi. Atomic structure and special reactivity toward methanol oxidation of vanadia nanoclusters on TiO_2

(110). *Journal of the American Chemical Society*, 135(46):17331–17338, 2013.

[28] Scott P. Price, Xiao Tong, Claron Ridge, Hunter L. Neilson, Joshua W. Buffon, Jeremy Robins, Horia Metiu, Michael T. Bowers, and Steven K. Buratto. Catalytic oxidation of methanol to formaldehyde by mass-selected vanadium oxide clusters supported on a TiO_2 (110) surface. *The Journal of Physical Chemistry A*, 2014.

[29] Jian Zhi Hu, Suochang Xu, Wei-Zhen Li, Mary Y. Hu, Xuchu Deng, David A. Dixon, Monica Vasiliu, Raluca Craciun, Yong Wang, Xinhe Bao, and Charles H. F. Peden. Investigation of the structure and active sites of TiO_2 nanorod supported VO_x catalysts by high-field and fast-spinning ^{51}V MAS NMR. *ACS Catalysis*, 5(7):3945–3952, 2015.

[30] Paul Kemper, Andrei Kolmakov, Xiao Tong, Yigal Lilach, Lauren Benz, Manuel Manard, Horia Metiu, Steven K. Buratto, and Michael T. Bowers. Formation, deposition and examination of size selected metal clusters on semiconductor surfaces: An experimental setup. *International Journal of Mass Spectrometry*, 254(3):202–209, 2006.

[31] R. E. Smalley. Laser studies of metal cluster beams. *Laser Chemistry*, 2(3):167–184, 1983.

[32] Claude Phipps. *Laser Ablation and its Applications*. Springer, 2007.

[33] John Ready. *Effects of High-Power Laser Radiation*. Elsevier, 2012.

[34] M. Pellarin, B. Baguenard, M. Broyer, J. Lerm, J. L. Vialle, and A. Perez. Shell structure in photoionization spectra of large aluminum clusters. *The Journal of Chemical Physics*, 98(2):944–950, 1993.

[35] R. C. Bell, K. A. Zemski, D. R. Justes, and A. W. Castleman. Formation, structure and bond dissociation thresholds of gas-phase vanadium oxide cluster ions. *The Journal of Chemical Physics*, 114(2):798–811, 2000.

[36] P. A. Redhead. Thermal desorption of gases. *Vacuum*, 12(4):203–211, 1962.

[37] Deborah Holmes Parker, Mark E. Jones, and Bruce E. Koel. Determination of the reaction order and activation energy for desorption kinetics using TPD spectra: Application to D_2 desorption from Ag(111). *Surface Science*, 233:65–73, 1990.

[38] Francisco Zaera. Procedure for the deconvolution of TPD data, 2016.

[39] G. Binnig and H. Rohrer. Scanning tunneling microscopy. *Surface Science*, 126(1):236–244, 1983.

[40] G. Binnig, H. Rohrer, Ch. Gerber, and E. Weibel. 7 x 7 Reconstruction on Si(111) resolved in real space. *Physical Review Letters*, 50(2):120–123, 1983.

[41] Dawn Bonnel. *Scanning tunneling microscopy and spectroscopy, theory, techniques and applications*. VCH Publishers, New York, 1994.

[42] J. Bardeen. Tunnelling from a many-particle point of view. *Physical Review Letters*, 6(2):57–59, 1961.

[43] J.G. Simmons. Generalized formula for the electric tunnel effect between similar electrodes separated by a thin insulating film. *Journal of Applied Physics*, 34(6):1793–1803, 1963.

[44] Scott Price. *A Model Catalyst Investigation of Mass-Selected Vanadium and Vanadium Oxide Clusters Deposited on a Titanium Dioxide (110)-(1×1) Surface*. PhD thesis, University of California Santa Barbara, June 2011.

[45] Ulrike Diebold. The surface science of titanium dioxide. *Surface Science Reports*, 48(58):53–229, 2003.

[46] Stefan Wendt, Phillip T. Sprunger, Estephania Lira, Georg K. H. Madsen, Zheshen Li, Jonas Hansen, Jesper Matthiesen, Asger Blekinge-Rasmussen, Erik Lgsgaard, Bjrk Hammer, and Flemming Besenbacher. The role of interstitial sites in the Ti3d defect state in the band gap of titania. *Science*, 320(5884):1755–1759, 2008.

[47] Ulrike Diebold, J. F. Anderson, Kwok-On Ng, and David Vanderbilt. Evidence for the tunneling site on transition-metal oxides: TiO_2 (110). *Physical Review Letters*, 77(7):1322–1325, 1996.

[48] Ulrike Diebold, Jeremiah Lehman, Talib Mahmoud, Markus Kuhn, Georg Leonardelli, Wilhelm Hebenstreit, Michael Schmid, and Peter Varga. Intrinsic defects on a TiO_2 (110)(1×1) surface and their reaction with oxygen: a scanning tunneling microscopy study. *Surface Science*, 411(12):137–153, 1998.

[49] Xiao Tong, Lauren Benz, Steeve Chrtien, Horia Metiu, Michael T. Bowers, and Steven K. Buratto. Direct visualization of water-induced relocation of Au atoms from oxygen vacancies on a TiO_2 (110) surface. *The Journal of Physical Chemistry C*, 114(9):3987–3990, 2010.

[50] Yingge Du, Nathaniel A. Deskins, Zhenrong Zhang, Zdenek Dohnalek, Michel Dupuis, and Igor Lyubinetsky. Formation of O adatom pairs and charge transfer upon O_2 dissociation on reduced TiO_2 (110). *Physical Chemistry Chemical Physics*, 12(24):6337–6344, 2010.

[51] Hiroshi Onishi and Yasuhiro Iwasawa. Reconstruction of TiO_2 (110) surface: STM study with atomic-scale resolution. *Surface Science*, 313(1):783–789, 1994.

[52] M. A. Henderson, S. Otero-Tapia, and M. E. Castro. Electron-induced decomposition of methanol on the vacuum-annealed surface of TiO_2 (110). *Surface Science*, 412:252–272, 1998.

[53] S. P. Bates, M. J. Gillan, and G. Kresse. Adsorption of methanol on TiO_2 (110): A first-principles investigation. *The Journal of Physical Chemistry B*, 102(11):2017–2026, 1998.

[54] Loyd J. Burcham, Laura E. Briand, and Israel E. Wachs. Quantification of active sites for the determination of methanol oxidation turn-over frequencies using methanol chemisorption and in-situ infrared techniques. *Langmuir*, 17(20):6164–6174, 2001.

[55] Mohit Badlani and Israel E. Wachs. Methanol: A smart chemical probe molecule. *Catalysis Letters*, 75(3-4):137–149, 2001.

[56] Zhenrong Zhang, Oleksandr Bondarchuk, J. M. White, Bruce D. Kay, and Zdenek Dohnlek. Imaging adsorbate OH bond cleavage: Methanol on

TiO_2 (110). *Journal of the American Chemical Society*, 128(13):4198–4199, 2006.

[57] Jaime Oviedo, Roco Snchez-de Armas, Miguel ngel San Miguel, and Javier F. Sanz. Methanol and water dissociation on TiO_2 (110): The role of surface oxygen. *The Journal of Physical Chemistry C*, 112(46):17737–17740, 2008.

[58] Chi Lun Pang, Robert Lindsay, and Geoff Thornton. Chemical reactions on rutile TiO_2 (110). *Chemical Society Reviews*, 37(10):2328–2353, 2008.

[59] Jin Zhao, Jinlong Yang, and Hrvoje Petek. Theoretical study of the molecular and electronic structure of methanol on a TiO_2 (110) surface. *Physical Review B*, 80(23):235416, 2009.

[60] Zdenek Dohnlek, Igor Lyubinetsky, and Roger Rousseau. Thermally-driven processes on rutile TiO_2 (110)-(1$\times$1): A direct view at the atomic scale. *Progress in Surface Science*, 85(58):161–205, 2010.

[61] Umberto Martinez, Lasse B. Vilhelmsen, Henrik H. Kristoffersen, Jess Stausholm-Mller, and Bjrk Hammer. Steps on rutile TiO_2 (110): Active sites for water and methanol dissociation. *Physical Review B*, 84(20), 2011.

[62] Mingmin Shen and Michael A. Henderson. Identification of the active species in photochemical hole scavenging reactions of methanol on TiO_2 . *The Journal of Physical Chemistry Letters*, 2(21):2707–2710, 2011.

[63] Hui Shi, Ying-Chun Liu, Meng Miao, Tao Wu, and Qi Wang. Adsorption and dissociation of methanol on defective rutile TiO_2 (110) surface with bridging oxygen-vacancy pairs. *Chemical Physics Letters*, 584:98–102, 2013.

[64] Xiufeng Lang, Bo Wen, Chuanyao Zhou, Zefeng Ren, and Li-Min Liu. First-principles study of methanol oxidation into methyl formate on rutile TiO_2 (110). *The Journal of Physical Chemistry C*, 118(34):19859–19868, 2014.

[65] Shuo Liu, An-an Liu, Bo Wen, Ruidan Zhang, Chuanyao Zhou, Li-Min Liu, and Zefeng Ren. Coverage dependence of methanol dissociation on TiO_2 (110). *The Journal of Physical Chemistry Letters*, 6(16):3327–3334, 2015.

[66] Enrique Farfan-Arribas and Robert J Madix. Different binding sites for methanol dehydrogenation and deoxygenation on stoichiometric and defective TiO_2 (110) surfaces. *Surface Science*, 544(23):241–260, 2003.

[67] Michael A. Henderson, Sary Otero-Tapia, and Miguel E. Castro. The chemistry of methanol on the TiO_2 (110) surface: The influence of vacancies and coadsorbed species. *Faraday Discussions*, 114:313–329, 1999.

[68] U. Martinez, J. . Hansen, E. Lira, H. H. Kristoffersen, P. Huo, R. Bechstein, E. Lgsgaard, F. Besenbacher, B. Hammer, and S. Wendt. Reduced Step Edges on Rutile TiO2 (110) as Competing Defects to Oxygen Vacancies on the Terraces and Reactive Sites for Ethanol Dissociation. *Physical Review Letters*, 109(15):155501, 2012.

[69] Markus B Hugenschmidt, Lara Gamble, and Charles T Campbell. The interaction of H_2O with a TiO_2 (110) surface. *Surface Science*, 302(3):329–340, 1994.

[70] David Silber, Piotr M. Kowalski, Franziska Traeger, Maria Buchholz, Fabian Bebensee, Bernd Meyer, and Christof Wll. Adsorbate-induced lifting of substrate relaxation is a general mechanism governing titania surface chemistry. *Nature Communications*, 7, 2016.

[71] Yeohoon Yoon, Yingge Du, Juan C. Garcia, Zihua Zhu, Zhi-Tao Wang, Nikolay G. Petrik, Gregory A. Kimmel, Zdenek Dohnalek, Michael A. Henderson, Roger Rousseau, N. Aaron Deskins, and Igor Lyubinetsky. Anticorrelation between surface and subsurface point defects and the impact on the redox chemistry of TiO_2 (110). *ChemPhysChem*, 16(2):313–321, 2015.

[72] Estephania Lira, Stefan Wendt, Peipei Huo, Jonas . Hansen, Regine Streber, Sren Porsgaard, Yinying Wei, Ralf Bechstein, Erik Lgsgaard, and Flemming Besenbacher. The importance of bulk Ti^{3+} defects in the oxygen chemistry on titania surfaces. *Journal of the American Chemical Society*, 133(17):6529–6532, 2011.

[73] Lauren Benz, Jan Haubrich, Stephen C. Jensen, and Cynthia M. Friend. Molecular imaging of reductive coupling reactions: Interstitial-mediated

coupling of benzaldehyde on reduced TiO_2(110). *ACS Nano*, 5(2):834–843, 2011.

[74] Israel E. Wachs. Catalysis science of supported vanadium oxide catalysts. *Dalton Transactions*, 42(33):11762–11769, 2013.

[75] P. Cavalli, F. Cavani, I. Manenti, and F. Trifiro. Ammoxidation of alkylaromatics over V_2O_5/TiO_2 catalysts. *Catalysis Today*, 1(1):245–255, 1987.

[76] Geoffrey C. Bond and S. Flamerz Tahir. Vanadium oxide monolayer catalysts: Preparation, characterization and catalytic activity. *Applied Catalysis*, 71(1):1–31, 1991.

[77] N. Y. Topsoe, J. A. Dumesic, and H. Topsoe. Vanadia-titania catalysts for selective catalytic reduction of nitric-oxide by ammonia. *Journal of Catalysis*, 151(1):241–252, 1995.

[78] L. Lietti, P. Forzatti, and F. Bregani. Steady-State and transient reactivity study of TiO_2 supported V_2O_5/WO_3 De-NO_x catalysts: Relevance of the vanadium - tungsten interaction on the catalytic activity. *Industrial & Engineering Chemistry Research*, 35(11):3884–3892, 1996.

[79] G. S. Wong, D. D. Kragten, and J. M. Vohs. The oxidation of methanol to formaldehyde on TiO_2 (110)-supported vanadia films. *The Journal of Physical Chemistry B*, 105(7):1366–1373, 2001.

[80] G. S. Wong, M. R. Concepcion, and J. M. Vohs. Reactivity of monolayer V_2O_5 films on TiO_2 (110) produced via the oxidation of vapor-deposited vanadium. *Surface Science*, 526(3):211–218, 2003.

[81] Y. Fu and J. Shen. Selective oxidation of methanol to dimethoxymethane under mild conditions over V_2O_5/TiO_2 with enhanced surface acidity. *Chemical Communications*, 0(21):2172–2174, 2007.

[82] V. V. Kaichev, G. Ya. Popova, Yu. A. Chesalov, A. A. Saraev, D. Y. Zemlyanov, S. A. Beloshapkin, A. Knop-Gericke, R. Schlgl, T. V. Andrushkevich, and V. I. Bukhtiyarov. Selective oxidation of methanol to form dimethoxymethane and methyl formate over a monolayer V_2O_5–TiO_2 catalyst. *Journal of Catalysis*, 311:59–70, 2014.

[83] Robert J. Madix, Jrgen Biener, Marcus Bumer, and Andreas Dinger. The growth of vanadium oxide on alumina and titania single crystal surfaces. *Faraday Discussions*, 114:67–84, 1999.

[84] Hunter L. Neilson. *The Reactivity and Structure of Size Selected V_xO_y on a TiO_2 (110)-(1 x 1) Surface of Variable Oxidation State*. PhD thesis, University of California Santa Barbara, 2015.

[85] Henrik H. Kristoffersen, Hunter L. Neilson, Steven K. Buratto, and Horia Metiu. Stability of V_2O_5 supported on titania in the presence of water, bulk oxygen vacancies, and adsorbed oxygen atoms. *The Journal of Physical Chemistry C*, 2017.

[86] Enrico Tronconi, Ahmed S. Elmi, Natale Ferlazzo, Pio Forzatti, Guido Busca, and Paolo Tittarelli. Methyl formate from methanol oxidation over coprecipitated V-Ti-O catalysts. *Industrial & Engineering Chemistry Research*, 26(7):1269–1275, 1987.

[87] Qing Guo, Chenbiao Xu, Wenshao Yang, Zefeng Ren, Zhibo Ma, Dongxu Dai, Timothy K. Minton, and Xueming Yang. Methyl formate production on TiO_2(110), initiated by methanol photocatalysis at 400 nm. *The Journal of Physical Chemistry C*, 117(10):5293–5300, 2013.

[88] Elena Jakubikova, Anthony K. Rapp, and Elliot R. Bernstein. Density functional theory study of small vanadium oxide clusters. *The Journal of Physical Chemistry A*, 111(50):12938–12943, 2007.

[89] R. C. Bell, K. A. Zemski, K. P. Kerns, H. T. Deng, and A. W. Castleman. Reactivities and collision-induced dissociation of vanadium oxide cluster cations. *The Journal of Physical Chemistry A*, 102(10):1733–1742, 1998.

Appendix A

Surface contamination, anomalous ammonia production, and W_1 clusters

While investigating methane production from the clean TiO_2 surface, we looked into tracking m/z = 16 as well as m/z = 15, either of which are used in various reports in the literature to monitor methane. Shortly thereafter, we discovered production of mass 16 at low temperature that did not correspond to a desorption of mass 15. The following figures catalog our elimination of possible products to arrive at the conclusion that the TiO_2 surface was producing ammonia at temperatures just above room temperature (RT) and that is was caused by the sputter gun used to clean the surface by Ar^+. A blank run is defined by a TPD experiment following exposure of the clean surface to only the chamber background gases (H_2, N_2, CO, and CO_2) for approximately 12 hours. It should also be noted that the temperature scales indicated here are not calibrated and the reported values correspond to an actual surface temperature that is much higher.

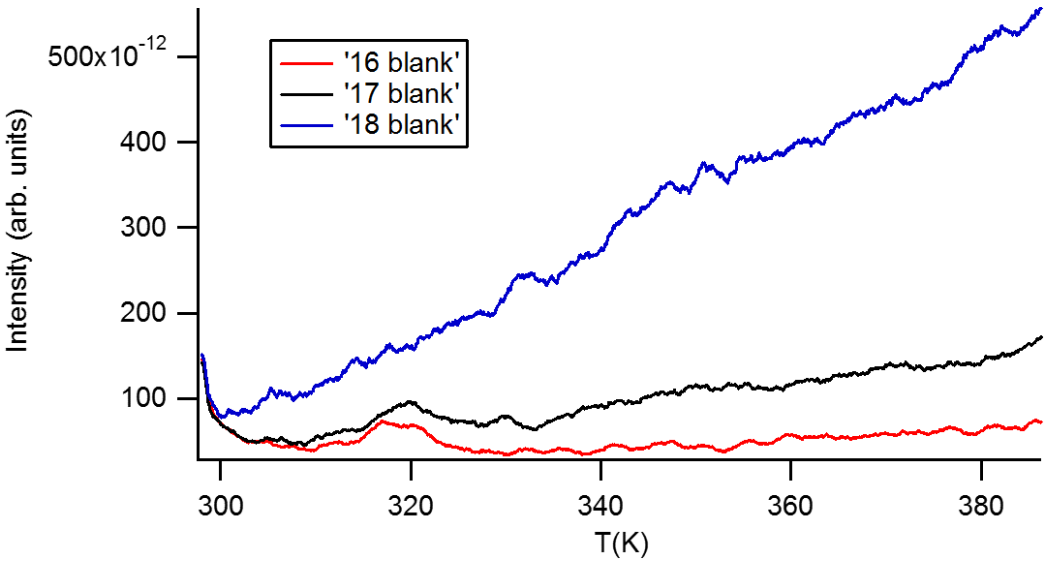

Figure A.1. Clean surface TPD blank run

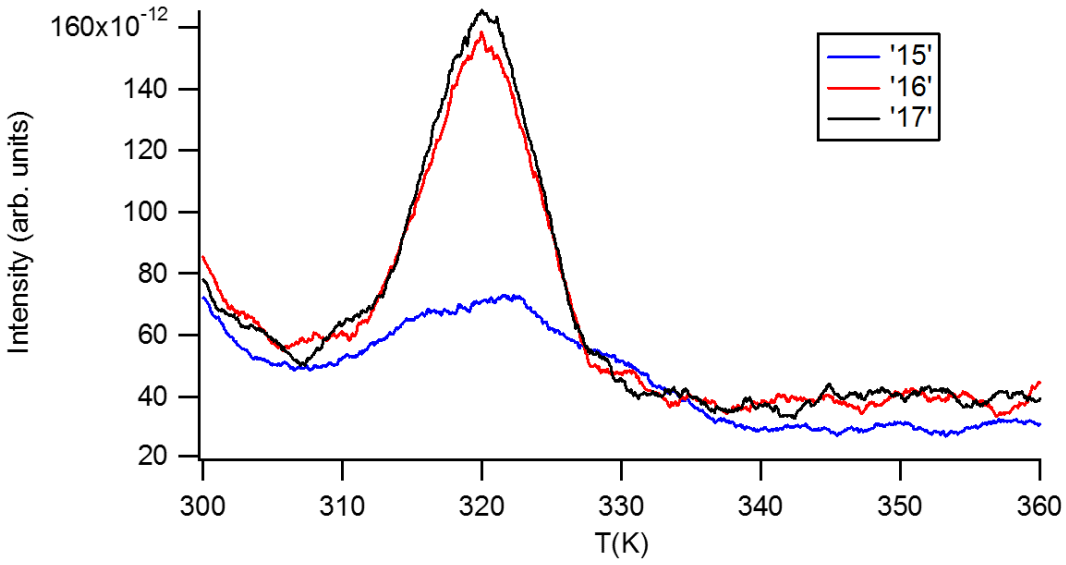

Figure A.2. Clean surface TPD after exposure to 10 L O_2

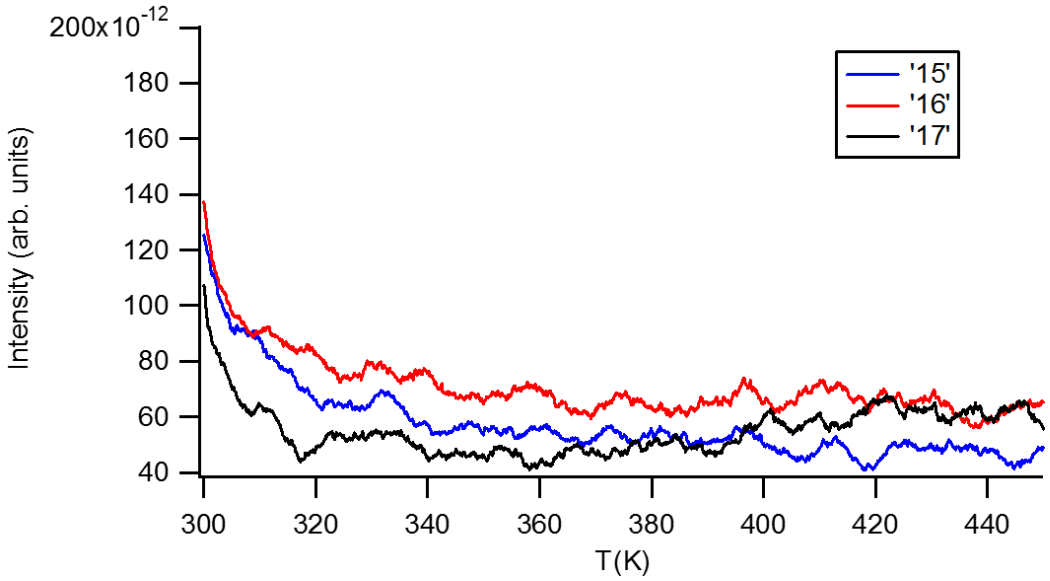

Figure A.3. TPD over the sample holder

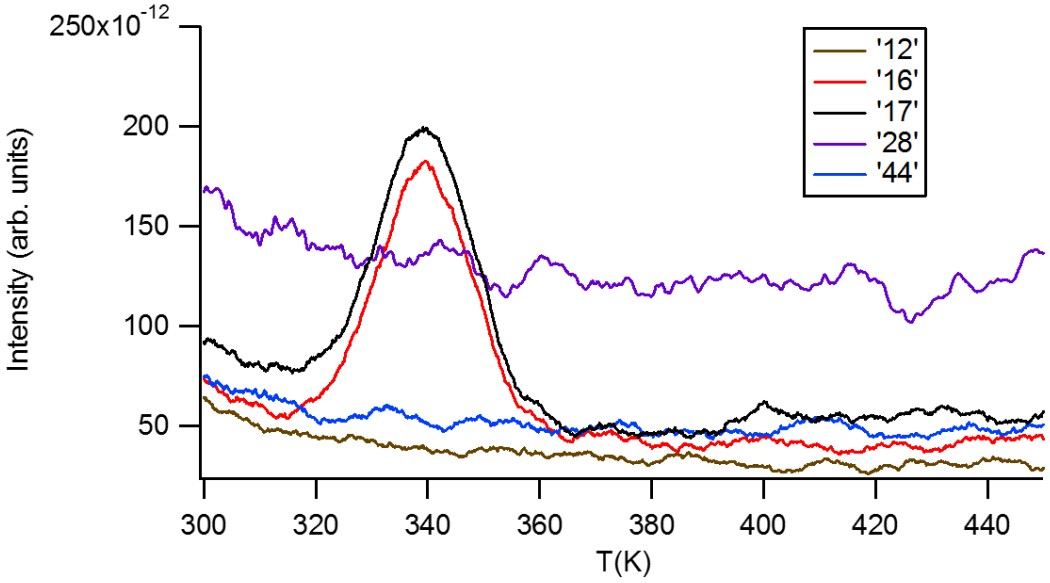

Figure A.4. Clean surface TPD after exposure to 10 L O_2 and tracking for carbon containing species

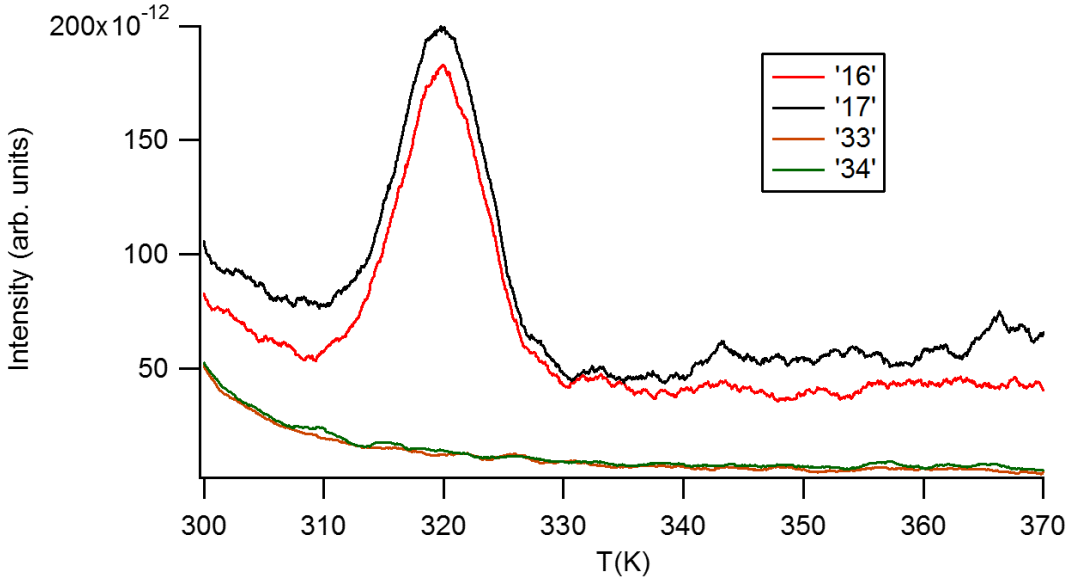

Figure A.5. Clean surface TPD after exposure to 10 L O_2 and tracking for hydrogen peroxide

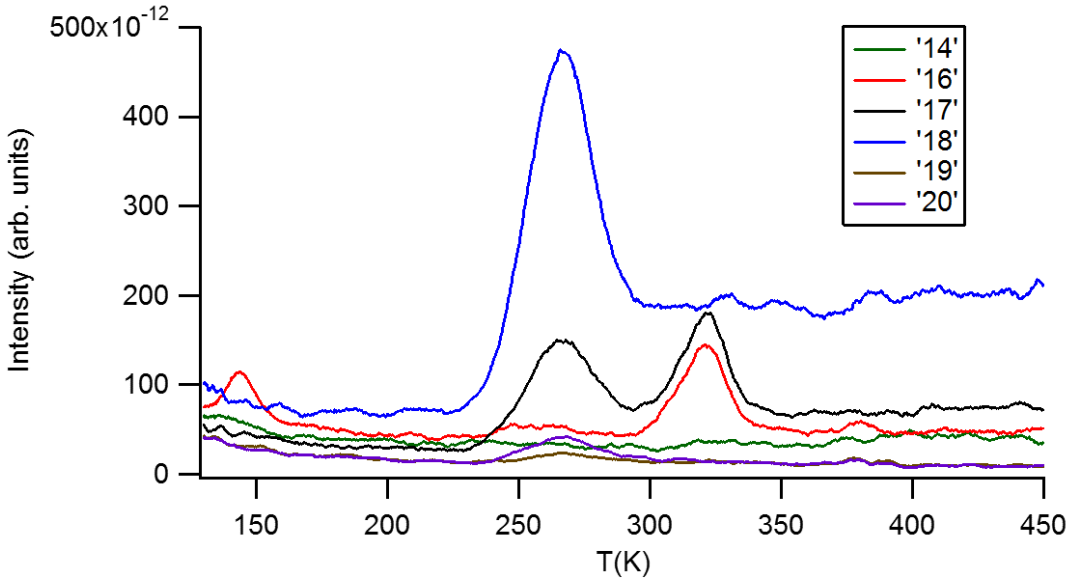

Figure A.6. Clean surface TPD after exposure to 10 L $^{18}O_2$ at 140 K

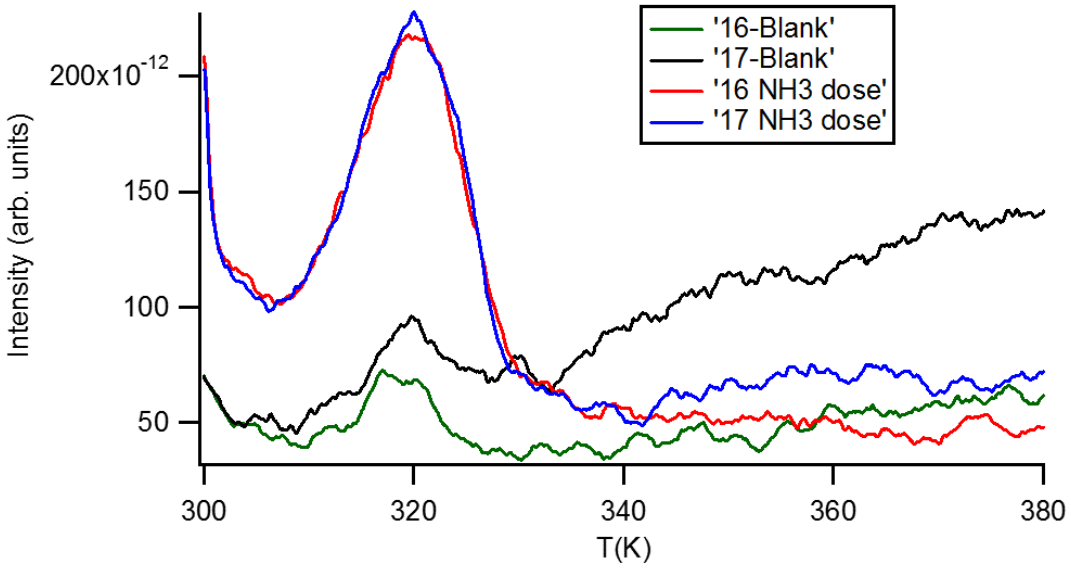

Figure A.7. Clean surface TPD after exposure to 1 L of a NH_3OH solution

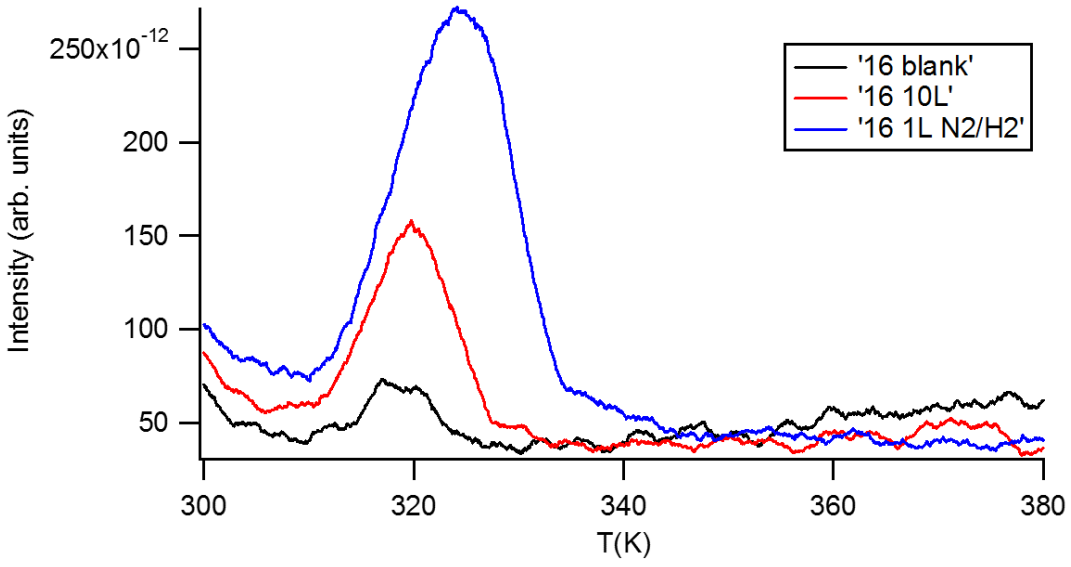

Figure A.8. Clean surface TPD after exposure to 1 L each N_2 and H_2

This series of TPD experiments demonstrated that the TiO_2 surface is in fact producing ammonia from adsorption of background gases under UHV by eliminating other possible desorption products as the cause of this mystery peak. We examined the surface by XPS to reveal that it did contain a measurable tungsten signal, a contaminant which was not detected by the crystal manufacturer. We found that the tungsten is localized near the surface by collecting XPS spectra as a function of sample angle relative to the incident x-rays in which a larger angle corresponds to a deeper sampling region.

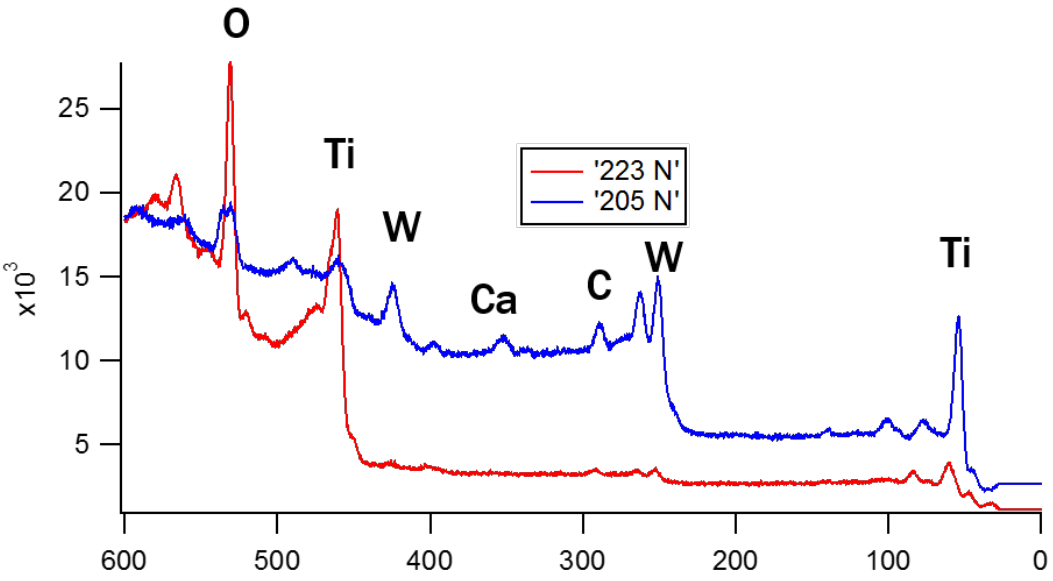

Figure A.9. XPS of the TiO_2 surface as a function of depth

The source of this tungsten was found to be the sputter gun, which has a tungsten filament to ionize argon in the chamber, by taking blank run TPD of a new crystal after 0, 1, and 3 sputter cycles. It is possible that this effect could simply be caused by surface roughness created by sputtering, but it remains even after annealing which should flatten the surface. Since the production of ammonia has never been observed before from this surface, we believe this is a substantial change brought on by tungsten contamination.

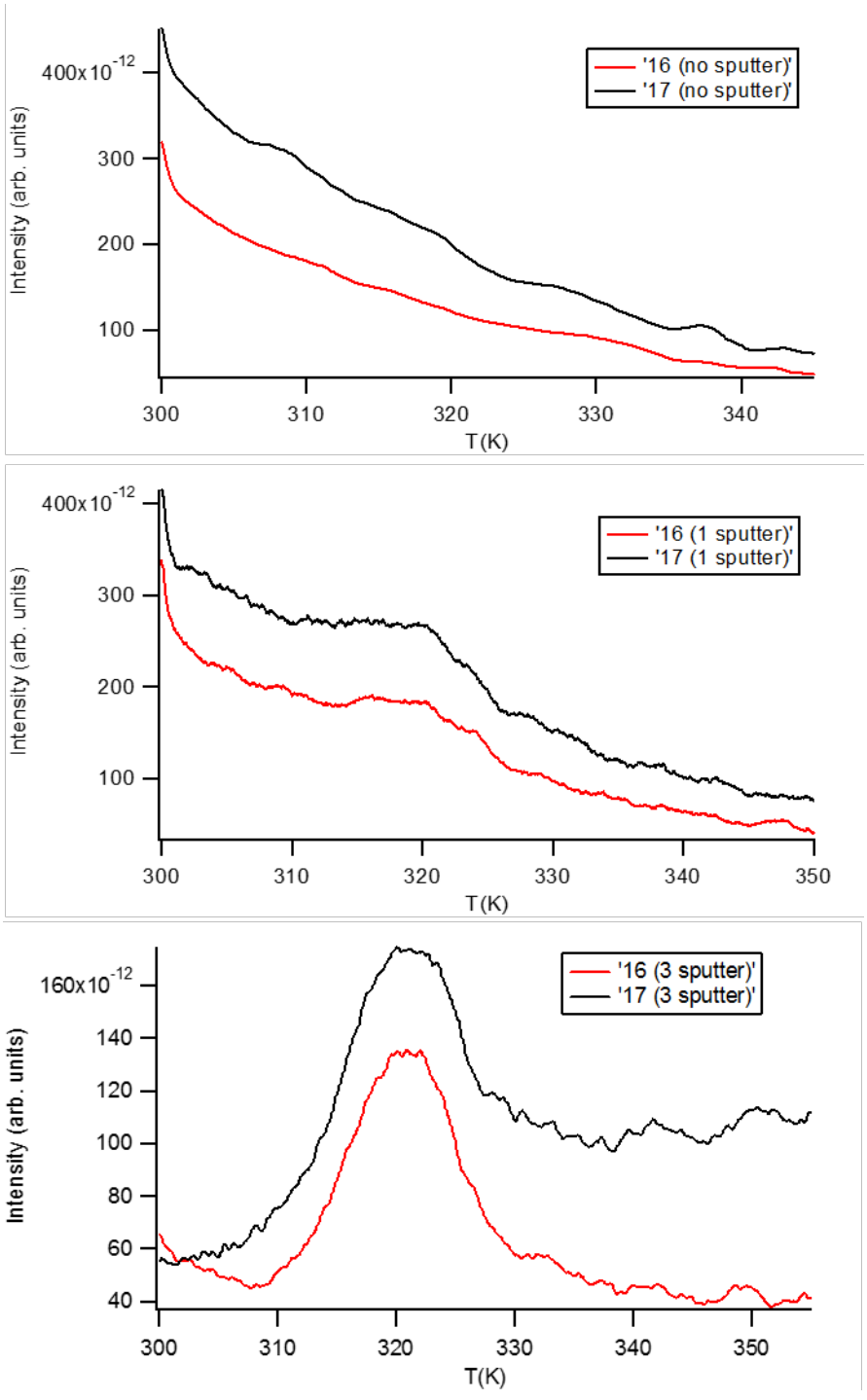

Figure A.10. Evolution of Blank Run TPD over three sputter/anneal cycles

To further demonstrate this connection, 0.20 ML tungsten monomers (W_1) were deposited on a clean reduced surface that showed no m/z = 16 or 17 desorption prior to deposition. A blank run TPD (no dosed gases) was taken after 12+ hours exposure to the UHV background to look for ammonia. A second blank run was done 24 hours later and showed an enhanced desorption signal indicating the the tungsten rearranged during the first run to a more active catalyst structure. There is a different temperature scale for this series of TPD experiments which likely represents the actual desorption temperature accurately to within 5% XPS of the clusters shows a very similar intensity for the W 4d peaks as seen on the sputter gun contaminated surface.

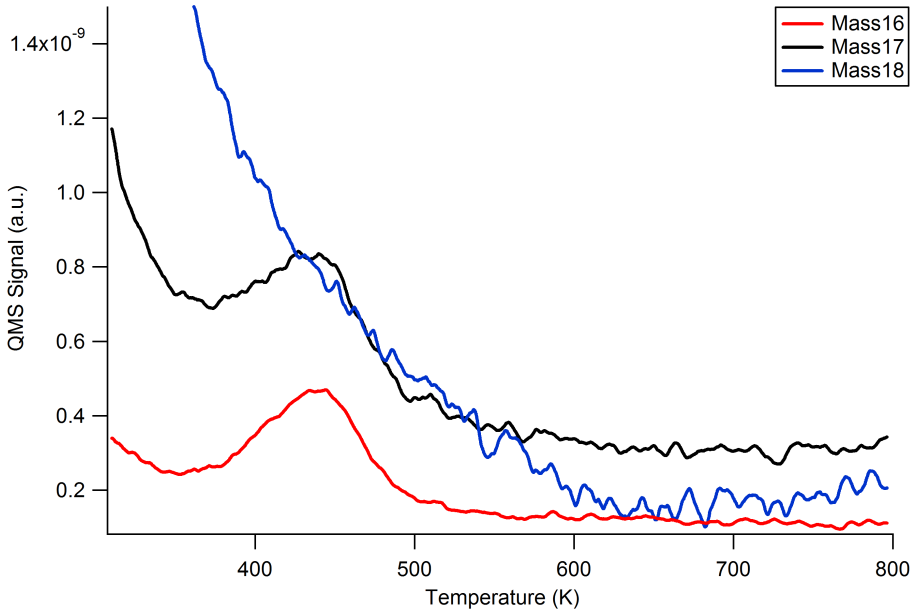

Figure A.11. Blank Run TPD after deposition of 0.20 ML W_1 clusters

Sputtering and annealing cycles from a sputter gun which was shown not to contaminate the sample has proved ineffective at removing tungsten from the surface as seen by ammonia desorption in TPD and tungsten XPS. While this result is unique and would be of great interest to the literature, it is hard to recommend further experiments as each would require a new substrate crystal and would be quite costly to carry out a complete investigation.

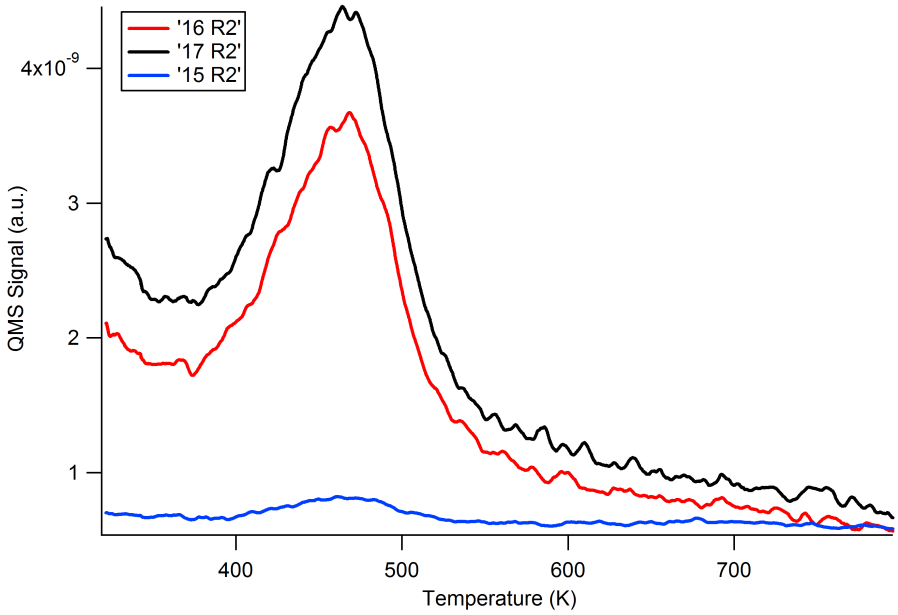

Figure A.12. Second blank Run TPD after deposition of 0.20 ML W_1 clusters

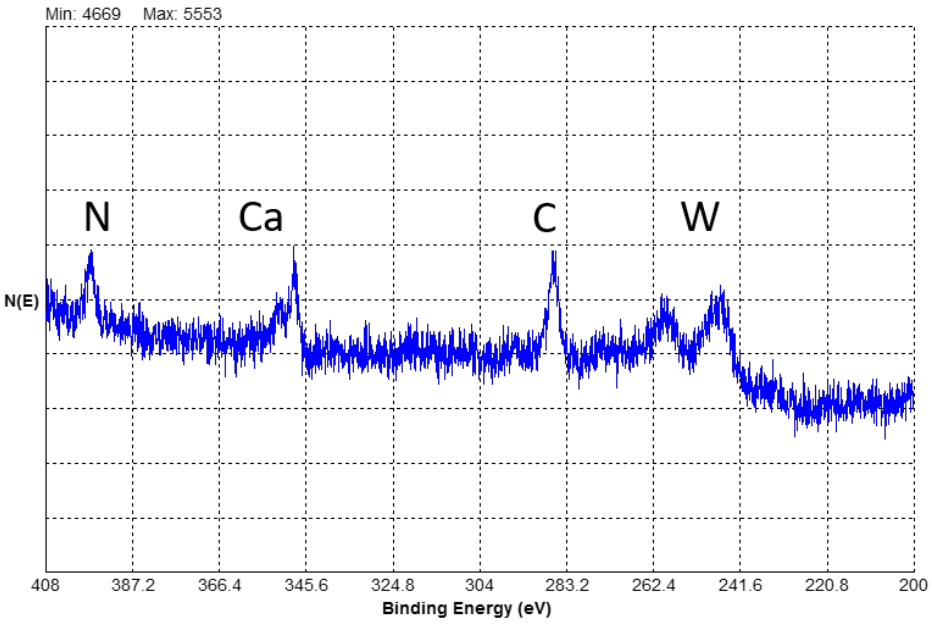

Figure A.13. Surface sensitive XPS after deposition of 0.20 ML W_1 clusters